UNIVERSIDADE DE LISBOA
FACULDADE DE CIÊNCIAS
DEPARTAMENTO DE FÍSICA

An Olfactory Virtual Reality System for Spatial Behaviors in Mice

José Miguel Gomes Teixeira

Mestrado Integrado em Engenharia Biomédica e Biofísica
Perfil em Sinais e Imagens Médicas

Dissertação orientada por:
Dr. Cindy Poo
Dr. Daniela Godinho

2022

Acknowledgements

To my parents who have always nurtured my curiosity,

To Mariana who has always provided me with the love and support that has made me keep going,

To Cindy for the opportunity and guidance in developing a state of the art neuroscience experimental system,

To Daniela for the kindness with which you accepted to supervise my thesis,

To Zach and my colleagues at the Systems Neuroscience Lab, with whom I've learnt so much over the last few years,

To the Champalimaud Research community for the amazing environment that fostered my personal and academic growth,

I sincerely thank you for making this possible!

Abstract

Animals have the ability of finding their way in their environments, being able to reliably visit known sources of food or water and return to their burrow or nest. Olfaction plays a major role in the spatial navigation behaviors of animals across phyla, however little is known about how olfactory and spatial information are actually combined in the brain in order to generate those behaviors. When studying spatial navigation in laboratory conditions, scientists typically design mazes where freely-moving rodents are provided with a rule for quickly navigating to rewards distributed in the environment, but investigating how olfactory information is processed in the brain is extraordinarily challenging if one cannot account for the olfactory properties of the environment a freely-moving animal is navigating in.

In order to more precisely control the spatio-temporal dynamics of olfactory stimuli in experiments involving freely-moving animals, these typically consist of odorized air flow pulses that are delivered at sparse locations in behavioral arenas, which require expensive instrumentation and increase the complexity in the physical construction of the mazes while also being inherently limited in the locations the stimuli can be provided.

Here, we have developed a virtual reality system that allows for the precise control of olfactory stimulus delivery properties in head-fixed navigating mice in both open an closed-loop conditions. By nature, it allows the parameterization of both the visual and olfactory dimensions of the environment, which potentiates the comparison of behavior and neural activity of mice navigating in environments containing different visual and olfactory scenes. In addition, the system is constructed mostly from standard laboratory equipment and draws from open source solutions, promoting its adoptability in different domains of research, and contributing to improve the replicability of experiments across institutions.

We validate this olfactory virtual reality system by designing a spatial navigation task where olfactory stimuli are predictive of reward location. Our results confirm the system is able to produce olfactory and visual virtual environments that are controlled by the movement of head-fixed mice in a closed-loop. Finally, to complement the behavioral data, we also present data demonstrating the compatibility of our system with cutting edge neural population recording techniques.

Keywords: behavior; olfaction; olfactory virtual reality; spatial navigation;

Resumo

Comportamentos de navegação espacial como filopatria são observados em diversas espécies animais. A capacidade de navegar no espaço, percorrendo localizações de interesse como fontes de alimento ou água, e posteriormente retornar a 'casa', requer uma representação cognitiva do ambiente - um mapa mental - que permite a um animal calcular trajetórias entre a sua localização e um objetivo espacial, permitindo-lhe assim navegar de forma eficiente mesmo que por percursos não conhecidos. A função olfactiva é fundamental para as capacidades de aprendizagem espacial e navegação de espécies de múltiplos filos, no entanto não é claro onde no cérebro e como as informações olfactivas e espaciais são integradas para produzir esses comportamentos.

O estudo da navegação espacial em condições laboratoriais classicamente tem-se baseado na construção de labirintos nos quais roedores navegam livremente em busca de recompensas distribuídas no ambiente. Neste tipo de experiências comportamentais, tipicamente os investigadores associam a localização das recompensas às de outros objetos ou estímulos no ambiente, fornecendo assim uma regra espacial que os animais apreendem de tal modo que, após um período de aprendizagem, são capazes de rapidamente navegar ao encontro de localizações de interesse. Por outro lado, não é possível caracterizar com precisão a dimensão olfactiva de todo o ambiente em tempo ou espaço visto que as moléculas odorantes se difundem em suspensão na atmosfera de forma caótica, pelo que o estudo da função olfactiva tipicamente requer algum grau de restrição dos movimentos do animal de forma a que as propriedades dos estímulos olfactivos (principalmente a duração e a intensidade) sejam comparáveis entre múltiplas apresentações de cada estímulo.

Assim, o estudo simultâneo da navegação espacial e da função olfactiva em animais livres requer que os estímulos olfactivos sejam produzidos em localizações específicas do ambiente e apenas quando o animal se encontra perto delas, de forma a reduzir a difusão dos odores pelo ambiente. No entanto, a adição da dimensão olfactiva aumenta a complexidade da construção dos labirintos e requer instrumentação específica; também, como as localizações dos estímulos olfactivos são fixas no labirinto, este tipo de experiências é limitado por natureza pelo *design* físico do labirinto, sendo pouco prático senão impossível alterar as propriedades espaciais da dimensão olfactiva do ambiente a partir do momento em que o animal inicia a sessão experimental.

Verifica-se, assim, uma tensão entre a validade ecológica de um paradigma experimental e o controlo do experimentador sobre as propriedades (por exemplo sensoriais) do ambiente: cenários naturalísticos evocam comportamentos e respetiva atividade neuronal naturalísticos, mas devido à sua complexidade torna-se difícil perceber a relação entre as observações experimentais e os estímulos que as produziram; por outro lado, o controlo preciso das propriedades do ambiente permite a quantificação/parametrização dos estímulos, facilitando a caracterização do comportamento ou atividade neuronal por eles elicitada, mas habitualmente impõe limitações e assunções na interpretação dos resultados.

Perante isto, desenvolvemos um sistema de realidade virtual para murganhos (*Mus musculus*) capaz

de controlar com precisão as propriedades dos estímulos olfactivos. Neste sistema, o murganho encontra-se fixo em cima de uma roda na qual pode correr livremente, e o movimento da roda é usado para atualizar a cena visual que é renderizada num ecrã parabólico que cobre a maioria do campo visual do animal, promovendo a imersão do mesmo na realidade virtual. Desta forma, a manipulação do sinal de movimento determina a interatividade do sistema, permitindo tanto regimes de ciclo fechado, onde todas as alterações no ambiente virtual resultam das ações do próprio animal, ou regimes de ciclo aberto, em que os eventos (por exemplo, estímulos) acontecem de forma independente do comportamento do animal.

Este sistema permite a parametrização completa das dimensões visual e olfactiva do ambiente, oferecendo ao experimentador a possibilidade de manipular o ambiente sensorial dos animais, potenciando assim a replicabilidade de protocolos científicos e a comparação do comportamento e atividade neuronal de animais navegando em diferentes ambientes virtuais. A possibilidade de manipulação do sinal de movimento usado para calcular o deslocamento no ambiente virtual permite a realização de investigação sobre propriocepção e integração sensorimotora. Adicionalmente, o sistema é construído por materiais de laboratório comuns de forma modular e beneficia de tecnologia de licenciamento livre (*open source*), permitindo a fácil adição e remoção de componentes mediante as necessidades experimentais - por exemplo, a adição de uma dimensão auditiva pode ser concretizada com a incorporação de uma coluna de som na qual os estímulos são reproduzidos tanto em ciclo aberto como fechado, extendendo assim a usabilidade deste sistema a domínios de investigação não diretamente relacionados com a navegação espacial, como percepção sensorial ou tomada de decisão. Equipamento de estimulação neuronal também pode ser incorporado no sistema e controlado pelo mesmo em ciclo fechado, abrindo a porta a estudos de perturbação de função.

A principal vantagem de um paradigma de realidade virtual é que oferece ao experimentador controlo absoluto sobre o ambiente sensorial do animal. Desta forma, o grau de realismo do ambiente virtual (do ponto de vista do animal) é definido pelo experimentador em função dos seus objetivos. Adicionalmente, a implementação de um paradigma de realidade virtual baseada em computação gráfica determina uma latência muito reduzida na responsividade do sistema, oferecendo assim ao experimentador a liberdade de realizar manipulações no ambiente (por exemplo trocando a localização de determinados objetos) de forma imediata e em qualquer momento durante a sessão experimental, de acordo com o comportamento do animal (ciclo fechado), ou a mando de um experimentador que arbitra sobre quais e quando essas manipulações devem acontecer (ciclo aberto). Em último lugar, devido à natureza da implementação baseada em computador, as experiências podem usufruir de um número enorme de ambientes virtuais em simultâneo, sendo esse número limitado apenas pela capacidade de memória do computador utilizado, por oposição a experiências usando labiritos clássicos cujo número é limitado pelo espaço físico disponível no laboratório.

Naturalmente, é impossível determinar quantitativamente o grau de imersão dos animais na realidade virtual, isto é, o quão eles percebem o ambiente virtual como um espaço físico ('real'), mas uma avaliação qualitativa é possível caracterizando o comportamento dos animais e a sua semelhança com o de animais navegando livremente em labirintos clássicos - se os animais demonstrarem comportamentos naturalísticos, é verossímil a conclusão de que eles se sentem, de facto, imersos na realidade virtual. Também, os murganhos são uma espécie na qual os comportamentos de fuga (*flight*) e congelamento (*freezing*) são facilmente evocados por estímulos/contextos aversivos, pelo que a ausência destes comportamentos após a fixação dos animais no sistema de realidade virtual olfactiva é reveladora de que os animais não sentem desconforto ou medo.

Para determinar o grau de imersão dos animais e a usabilidade deste sistema na investigação da

aprendizagem espacial mediada pela função olfactiva, desenvolvemos uma tarefa de navegação espacial em ciclo fechado em que a dimensão olfactiva do ambiente virtual é informativa da presença e localização de recompensas no ambiente, fornecendo assim aos animais uma regra de aprendizagem espacial à semelhança de abordagens mais clássicas. Os resultados revelam algumas assinaturas comportamentais de aprendizagem espacial, sugerindo que os murganhos entendem o ambiente virtual como real, sendo capazes de aprender as localizações de interesse e navegar entre elas de forma livre, e validando assim este sistema de realidade virtual olfactiva para os objetivos propostos. Finalmente, para complementar os resultados comportamentais, mostramos também dados da atividade de populações de neurónios de murganhos no sistema de realidade virtual olfactiva, demonstrado a sua compatibilidade com modernas técnicas de aquisição.

Palavras-chave: comportamento, navegação espacial, olfacto, realidade virtual, realidade virtual olfactiva

Contents

Acknowledgements **i**

Abstract **iii**

Resumo **v**

List of Figures **xi**

List of Tables **xiii**

List of Abbreviations **xv**

1 Introduction **1**
- 1.1 Navigating through space . . . 2
- 1.2 Olfaction . . . 6
- 1.3 Olfactory-cued spatial navigation . . . 8
- 1.4 Olfactory Virtual Reality . . . 12

2 Methods **13**
- 2.1 OVR System Development . . . 14
  - 2.1.1 VR engine . . . 14
  - 2.1.2 Behavioral interface . . . 16
  - 2.1.3 Experimental rig . . . 21
- 2.2 OVR System Validation . . . 22
  - 2.2.1 Training Regime . . . 22
  - 2.2.2 Experimental Regime . . . 23
  - 2.2.3 Neural recordings: Electrophysiology . . . 26
  - 2.2.4 Neural recordings: Photometry . . . 27

3 Results & Discussion **29**
- 3.1 Mouse training . . . 29
- 3.2 Mouse behavior . . . 32
- 3.3 Mouse neural activity: electrophysiology . . . 39
- 3.4 Mouse neural activity: photometry . . . 41

4 Conclusion **43**

Bibliography **45**

Appendices **50**
.1 OVR system design . . . 51
.1.1 Behavioral interface . . . 51
.1.2 Enclosure assembly design . . . 55
.2 Mouse behavior . . . 58
.2.1 Natural behaviors . . . 58
.2.2 Additional analyses . . . 65
.3 Mouse neural activity . . . 65
.3.1 Recording rig . . . 65
.3.2 Neuropixels probe implantation . . . 66
.3.3 Electrophysiology signal analysis . . . 67
.3.4 Photometry signal analysis . . . 67
.4 List of equipment . . . 68
.5 Supplementary visualizations of behavior . . . 71
.5.1 Behavioral summaries of the mice not shown in the main text . . . 71
.5.2 Running behaviors of the mice not shown in the main text . . . 75

List of Figures

1.1 A place cell in the rat hippocampus . . . 3
1.2 Place, head-direction and grid cell activities and approximate locations in the mouse brain 4
1.3 Odorant molecules can differ along many chemical dimensions . . . 7
1.4 Preferred axonal targets of PCX cells along the anterior-posterior axis . . . 8
1.5 Odor-cued navigation task design . . . 9
1.6 Behavioral performance of mice in the odor-cued navigation task . . . 10
1.7 Spiking activity of three PCX neurons in the odor-cued navigation task . . . 11
1.8 Selectivity of the recorded population of PCX neurons . . . 11

2.1 The developed OVR system . . . 14
2.2 Schematic of the initial system design . . . 15
2.3 Schematic of the presented system design . . . 15
2.4 Screen Assembly and optical path of the visual projection. . . . 16
2.5 Geometry of the screen assembly and mouse positioning . . . 17
2.6 Raw rotary encoder signal . . . 18
2.7 Breathing signal . . . 19
2.8 Mouse and OVR behavioral interface . . . 20
2.9 PID signal of stimulus presentations . . . 21
2.10 Perspective of the VE used in the OVR experiment . . . 24
2.11 Point-of-view of a mouse navigating in OVR . . . 26
2.12 Coronal view of the approximate recording coordinate . . . 27

3.1 Time spent on each session during the training regime . . . 29
3.2 Distance traveled on each session during the training regime . . . 30
3.3 Average distance traveled between consecutive reward presentations during the training regime . . . 31
3.4 Average duration of each lap of the corridor (each trial) during the training regime . . . 32
3.5 Behavioral summary of the first session of mouse #1 in the experimental regime . . . 33
3.6 Behavioral summary of the first session of mouse #2 in the experimental regime . . . 34
3.7 Breathing rate aligned to odor presentations . . . 35
3.8 Mouse velocity respective to stimuli . . . 36
3.9 Mouse velocity respective to rewards . . . 36
3.10 Mouse velocity respective to stimuli (sorted) . . . 38
3.11 Mouse velocity profile on the length of the VR corridor . . . 39
3.12 Characterization of spiking activity . . . 40
3.13 Characterization of spiking amplitude . . . 41

3.14 Photometry signal of a neuron population recorded in a mouse operating the OVR system 42

1 3D render of the running wheel . . . 51
2 Detail of wheel surface . . . 52
3 Camera positioning . . . 53
4 Acrylic holder design . . . 55
5 The developed enclosure assembly . . . 56
6 Demonstration of system retraction in the training box . . . 57
7 A closed training box . . . 58
8 Mouse behaving in OVR . . . 59
9 Mouse licking behavior . . . 61
10 Characterization of casting behavior . . . 63
11 Casting behavior . . . 64
12 Mouse velocity respective to omissions . . . 65
13 The recording rig used for electrophysiology recordings . . . 66
14 Sagittal view of the approximate recording coordinate . . . 67
15 Behavioral summary of the first session of mouse #3 in the experimental regime . . . 71
16 Behavioral summary of the first session of mouse #4 in the experimental regime . . . 72
17 Behavioral summary of the first session of mouse #5 in the experimental regime . . . 73
18 Behavioral summary of the first session of mouse #6 in the experimental regime . . . 74
19 Behavioral summary of the first session of mouse #7 in the experimental regime . . . 75
20 Mouse #1 velocity respective to stimuli . . . 76
21 Mouse #1 velocity respective to stimuli (sorted) . . . 76
22 Mouse #3 velocity respective to stimuli . . . 77
23 Mouse #3 velocity respective to stimuli (sorted) . . . 78
24 Mouse #4 velocity respective to stimuli . . . 78
25 Mouse #4 velocity respective to stimuli (sorted) . . . 79
26 Mouse #5 velocity respective to stimuli . . . 79
27 Mouse #5 velocity respective to stimuli (sorted) . . . 80
28 Mouse #6 velocity respective to stimuli . . . 80
29 Mouse #6 velocity respective to stimuli (sorted) . . . 81
30 Mouse #7 velocity respective to stimuli . . . 81
31 Mouse #7 velocity respective to stimuli (sorted) . . . 82
32 Mouse #1 velocity respective to rewards . . . 82
33 Velocity profile of mouse #1 on the length of the VR corridor . . . 83
34 Mouse #3 velocity respective to rewards . . . 83
35 Velocity profile of mouse #3 on the length of the VR corridor . . . 84
36 Mouse #4 velocity respective to rewards . . . 84
37 Velocity profile of mouse #4 on the length of the VR corridor . . . 85
38 Mouse #5 velocity respective to rewards . . . 85
39 Velocity profile of mouse #5 on the length of the VR corridor . . . 86
40 Mouse #6 velocity respective to rewards . . . 86
41 Velocity profile of mouse #6 on the length of the VR corridor . . . 87
42 Mouse #7 velocity respective to rewards . . . 87
43 Velocity profile of mouse #7 on the length of the VR corridor . . . 88

List of Tables

2.1 OVR task trial types 25

1 Parameters used for running the KiloSort algorithm on the electrophysiology data 67
2 OVR computer specifications 68
3 OVR system components 69
4 Enclosure assembly components 70

List of Abbreviations

CCU Champalimaud Centre for the Unknown

Hipp Hippocampus

OB Olfactory Bulb

OSN Olfactory Sensory Neuron

OVR Olfactory Virtual Reality

PCX Piriform cortex

ECX Entorhinal cortex

VE Virtual Environment

VR Virtual Reality

Chapter 1

Introduction

The purpose of the brain is, first and foremost, to control behavior (Krakauer et al., 2017), and the ability to move and act on the world in response to environmental stimuli is of chief importance in maximizing the chances of survival. There are incredibly detailed descriptions of the numbers, types and connections of neurons in some animal species, for which the *Caenorhabditis elegans* is a great example (White et al., 1986), and despites this knowledge, explanations for natural behavior have remained elusive, especially for more complex animals such as mammals. How is information about the environment represented in the electrical activity of the brain? And how does the brain generate appropriate behavior from that neural activity?

Systems neuroscience attempts to bridge the gap between stimulus and behavior by studying the organization of neural circuits and how they integrate internal and external information to form representations of environmental and bodily properties that can be used to generate appropriate behavior. Since the works of Cajal and Golgi, who have meticulously studied the structure and physiology of neurons in the late 19th century, neuroscientists have described the organization of dendritic trees and axonal projections, and the biophysics of the neuronal membrane and synapses, having produced a biophysically inspired mathematical model for neural activity at the single cell level as early as 1952 (Hodgkin & Huxley, 1952). This fundamental knowledge of structure and function is independent of animal behavior, and the cytology of nerve cells doesn't differ significantly between organisms: the major changes between species and even phylogenies regard the organization/architecture of the types of neurons. Considering this, the diversity of behaviors produced by animals must result from different circuit architectures, and the degree of evolutionary refinement of sensory and cognitive functions.

Animals and many other life forms have evolved to survive in different environments and are generally able to move through them, be it by water, land or air. Bacteria do so by chemotaxing, a biochemical process that influences the bacterial cell body orientation in regard to the gradient of chemical substances of the environment. Chemoreceptors on the cell's membrane can detect the concentration of beneficial or harmful substances, thus allowing a form of navigation towards or away from regions of space that have higher concentration values of these substances (Wadhams & Armitage, 2004). Animals have developed more sophisticated chemosensing mechanisms, namely olfaction and gustation, that allow to characterize the chemical properties of locations and objects in the environment, contributing to cognitive descriptions of said locations and objects in order to segregate which are ethologically relevant or not, thus supporting navigation. A prime example of olfactory-cued navigation can be observed in forensic dogs that are trained to navigate through a previously unvisited environment to a goal location relying chiefly on olfactory cues.

What sensory and cognitive mechanisms support these behaviors? How does olfaction participate

in learning spatial features and navigating through known and unknown environments? Precisely how olfaction contributes to spatial learning and navigation is one of the research focuses of the Systems Neuroscience Lab in the Champalimaud Neuroscience Programme at the Champalimaud Centre for the Unknown (CCU) in Lisbon, where researchers use a combination of ethology and electrophysiology approaches in an attempt to uncover the functioning of these mechanisms in mice (*Mus musculus*), a species for which olfaction is of the utmost importance not only for navigation but also for social interaction and other natural behaviors.

When studying spatial navigation in rodents, neuroscientists generally design mazes or arenas that the animals can explore and that provide them with rewards at specific sites (Vorhees & Williams, 2014). On the other hand, when studying the olfactive function, animals are usually anesthetized or otherwise restrained in order to precisely control odorant stimulus timing and intensity. Because of this tradeoff between experimental control and ecological validity of the results, there is a great challenge in experimental design in order to not only comprise olfactory and spatial aspects of behavior simultaneously, but to study how olfactory and spatial representations converge at the neural level. To tackle this challenge, a virtual reality (VR) setting seems adequate as it allows the experimenter to have precise control of the spatial and odorant characteristics of the environment while providing the advantages of body fixation for neural signal acquisition: a better quality of signal due to the reduction of movement related noise or artifacts and the use of a wider range of recording techniques, such as intracranial electrode implants or optical approaches.

In this section, knowledge of spatial and olfactory representations and the Systems Neuroscience Lab's research into the convergence of those representations will be reviewed first, as it allows positing some of the requirements for a VR implementation.

1.1 Navigating through space

Being able to remember locations in space and efficiently navigate between them increases the probability of survival of an animal, for example by allowing it to reliably return to shelter or food and water sources. Species of homing pigeons have been bred specifically to promote the capacity of reliably returning 'home' even when navigating huge distances. Diverse animal species such as bats, elephants and pythons can also show goal-oriented behavior over great distances (Grieves & Jeffery, 2017). Additionally, animals that are familiar with an environment are able to navigate quickly and efficiently between target locations within it, even when traveling through unexperienced routes.

Complex navigation behaviors such as these can only be achieved if animals have a cognitive representation of space - a form of spatial memory - that they can access in order to draw trajectories between the self and a goal's location. Building this representation - spatial learning - requires that the animal experiences the environment, using its senses to characterize locations in the environment and movement information to define distance and direction relationships between those locations. This mental map of space should be continuously updated as animals explore familiar and unfamiliar areas to reflect new or improved knowledge of the environment, therefore improving its accuracy. A mental representation of this nature permits an animal to use local and distal cues present at any location in the environment to draw efficient trajectories to locations of interest at the level of the neural activity, which can inform motor planning areas and execution of navigation, without having to rely on the memorization of specific routes. In addition, it should also support quicky learning to navigate to new ethologically relevant sites as they are laid on a preexisting mental map, which inherently features the relationship between mapped locations.

The first major neurophysiological evidence supporting the existence of a cognitive representation of space, or map, appeared about fifty years ago by the hands of John O'Keefe (O'Keefe, 1976) in a series of works where he described neurons in the hippocampus (Hipp) of freely behaving rats for which their activity was selective for spatial locations in the environment - place cells (Figure 1.1). Interestingly, the Hipp had already become the focus of particular attention in spatial memory and learning research since the controversial case of patient HM (Henry Molaison), who, in 1953, underwent bilateral surgical excision of his hippocampi in an attempt to attenuate seizure episodes. Although successful in that aspect, patient HM became unable to form new episodic memories or navigate in new environments despites having intact childhood memories and cognitive capabilities, which lead to the belief that the Hipp played an important role in spatial learning and memory (Squire et al., 2008; Moser et al., 2015). Diverse posterior studies assessing navigational skills before and after hippocampal lesion suggest this structure is fundamental for spatial memory formation, *ie*, spatial learning (Eichenbaum, 2017; Knierim & Hamilton, 2011; Matthews & Best, 1995).

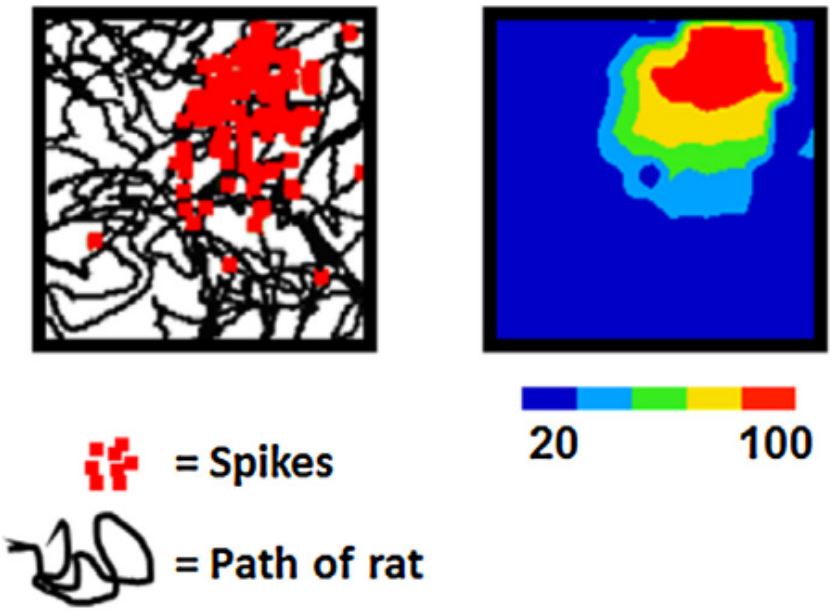

Figure 1.1: A place cell in the rat hippocampus. A rat's hippocampal activity is recorded while it navigates a square arena. **Left:** rat trajectory through the environment (black trace) and locations at the moment a place cell fired a spike (red dots). **Right:** That place cell's spatial firing rate - the cell fires the highest the closer the rat is to a specific location in the environment. (Figure adapted from Grieves & Jeffery (2017))

As rats become familiar with an environment, place cells in the Hipp are recruited in succession and become selective to particular locations of the environment such that the entire environment can be represented by a subset of the pyramidal cells in the Hipp. As each cell fires action potentials - 'spikes', due to their high amplitude and short duration - with a maximum rate at a point defined in the 2D cartesian plane and given that the population activity covers the entirety of the experimental arena, the conjunctive activity of this cell population can be used to successfully predict an animal's position in the environment, which effectively shows that the hippocampus encodes all possible spatial locations in a familiar environment, especially goal or reward locations.

Since then, neurons modulated by diverse spatial aspects of the environment have been described in the hippocampus and neighboring structures (Grieves & Jeffery, 2017; Hartley et al., 2014), namely grid cells in the entorhinal cortex, boundary cells in the subiculum and entorhinal cortex, and head-direction cells in the entorhinal and retrosplenial cortices and other cortical and thalamic areas (Figure

1.2); populations of cells in these areas can also be modulated by task demands (Bittner et al., 2017; Radvansky et al., 2021; Gauthier & Tank, 2018).

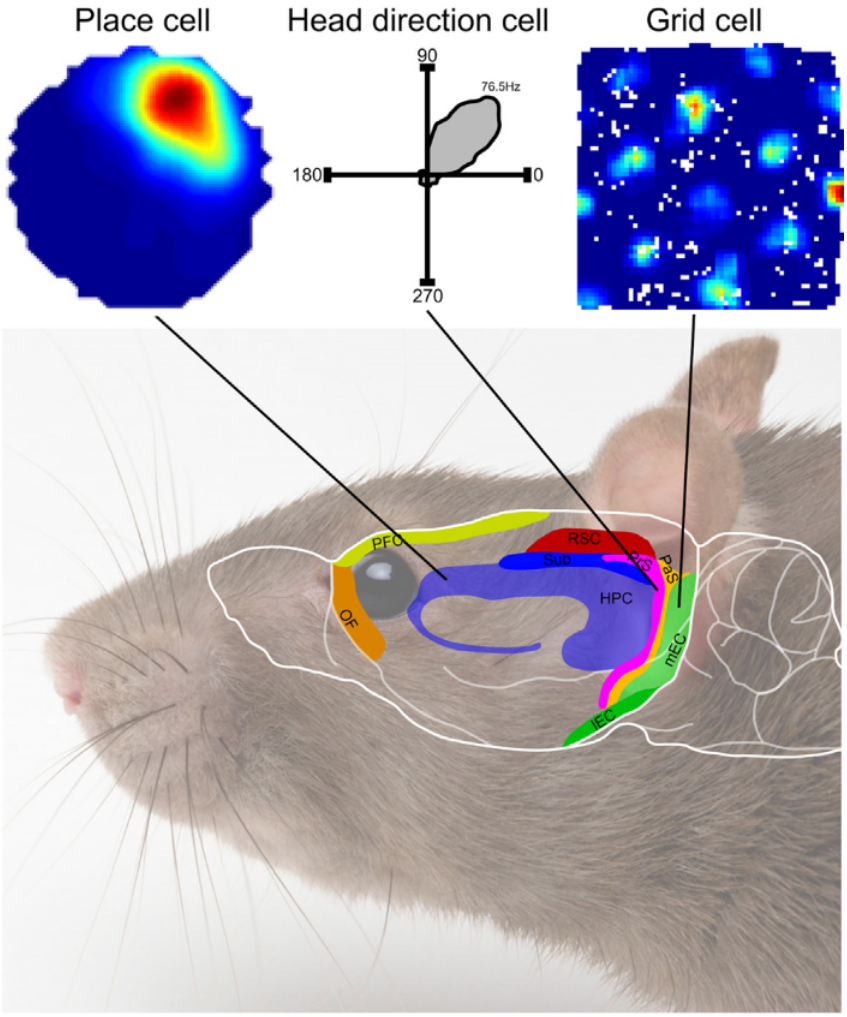

Figure 1.2: Place, head-direction and grid cell activities and approximate locations in the mouse brain. Place cells fire more strongly at specific locations of the environment. Head-direction cell activity is modulated by the direction an animal is facing. Grid cells have place-cell 'like' activity but they are selective for multiple equally-spaced locations, composing a triangular lattice. (Figure adapted from Grieves & Jeffery (2017))

Head direction cells are modulated by the direction an animal faces and their preferred direction seems to be anchored to the distal-most cues available in the environment, thus their conjunctive activity can function as an internal compass that can contribute to the formation of a map by informing about the directional relationships between locations in the environment as the animal transverses it (Grieves & Jeffery, 2017). Similarly to place cells, grid cells selectively fire at specific locations in the environment, however, their firing is not restricted to a single point in the plane - instead, each cell fires maximally at locations forming a triangular lattice (Figure 1.2). The spatial frequency of this lattice increases along the ventro-dorsal direction of the cortical surface and its orientation is informed by distal landmarks, possibly through input from the head direction population activity, such that the collective grid population activity can represent the position of the animal on the environment with great accuracy.

Interestingly, also in the entorhinal cortex, boundary/border and object cells have been observed. Boundary cells are more active near walls or barriers in the environment while object cells show diverse object-related activity. The activity of these neurons is controlled mostly by visual cues in the environment ('landmarks') that serve as anchoring points for the representations. The diversity of spatial and

context signals in the hippocampal vicinity, together with the dense interconnectivity between these regions and the aforementioned observations regarding the hippocampal role in spatial memory formation, collectively suggest that the hippocampal cognitive map is possibly not only a map of space, instead containing abstract information of objects or locations of interest that supports memory formation.

Map-less navigation strategies purely relying on egocentric information such as path integration, where animals estimate their current position by integrating self-motion information with their previous position estimation, are possible. In fact, they should be necessary as an animal is exploring a previously unvisited environment because it can't yet have a cognitive map supporting the navigation behavior. In path integration, an animal combines self-motion movement information likely coming from motor, proprioceptive and vestibular areas with visual information related to movement through the environment - the optic flow signal - which collectively can provide velocity information in the vectorial form (magnitude and direction). This information allows the animal to draw a trajectory from its previous known position in order to estimate its current position, in a process similar to dead reckoning performed by sailors (Etienne & Jeffery, 2004), and is potentially computationally more efficient than map-based navigation strategies (Savelli & Knierim, 2019).

For example, homing behaviors can be generated solely by path integration as when animals explore the environment, they can use the spatial trajectory built-up from the successive increments of positional estimation to quickly and accurately home, effectively retracing their steps, being only limited by their capacity to remember the sequence of those 'steps'. Not only, when allothetic (external) cues such as visual landmarks on the environment are not stable or accessible, idiothetic (internally generated) information can gain control of the activity of spatial (place, grid, boundary) and directional (head direction) representing neurons, suggesting that navigation strategies based on egocentric or allocentric work in complementary fashion depending on the availability of learned cues or the accuracy of the cognitive map of space.

Current theories posit that place cell activity is not purely reflecting space, instead their preferred firing location is informed by the activity of the grid population, which is modulated by head direction and boundary cell firing (Knierim & Hamilton, 2011), and information about context that likely derives from the combination of sensory derived information with object cell activity. Spatial goals are also encoded by the place population (Sato et al., 2017; Gauthier & Tank, 2018), potentially by means of postsynaptic modulation mechanisms from goal or reward areas, and the behavioral relevance of sensory stimuli modulates hippocampal spatial representations (Radvansky et al., 2021).

Hence, the place population activity potentially reflects not only spatial but contextual maps of the environment (Priestley et al., 2022), thus supporting spatial memory and navigation. Not only, the cognitive abstract map in the Hipp likely reflects episodic memory formation by binding abstract information about events with the places where those events happen (Knierim & Hamilton, 2011; Nieh et al., 2021; Eichenbaum, 2017). Path integration can help build this cognitive map when an animal is learning an environment, by providing it with an internally generated signal carrying information of distance and direction between locations in space that is computationally efficient. In fact, when animals explore new environments, they usually adopt a 'base' near a visual landmark and take exploratory bouts radially from that location in succession, in a way that covers most of the environment and that has been shown to be associated with the emergence of place cells (Savelli & Knierim, 2019).

Classical spatial learning and navigation tasks take place on physical mazes that need to be built and that are generally not easily modifiable, especially if the modifications imply changes to the dimensions or the structure of the maze. In addition, available laboratory space is a major constraint not only to the shape and size of a maze, but also to the number of different mazes that could be simultaneously used

for experimental purposes.

Over the past forty years, multiple maze layouts have been designed for studying spatial learning and navigation that have greatly contributed to our insight of these mechanisms as they allow to segregate between strategies of navigation biased towards allocentric cues or egocentric cues, depending on specific configurations or task design, chiefly the Morris Water Maze, variations of the Radial Arm Maze and the T-Maze (Vorhees & Williams, 2014). The goal with these designs is to repetitively present the animals to an environment containing salient local and/or distal spatial cues that enable them to compose a memory representation of the relationships between locations in the environment, especially the locations where stimuli and rewards are presented, hence building a cognitive map. Animals that are experienced in these environments are able to navigate quickly and with low error rates to reward locations, thus by manipulating the presence or location of different cues one can probe into the relative contribution of local and distal cues to learning and navigation, and whether the animals navigate in map-based or self-motion based strategies. Behavioral and neural activity data from experiments using these designs have illuminated the mechanisms of spatial navigation based on local and distal stimuli and action-reward associations and navigation mediated by a cognitive representation of the environment.

1.2 Olfaction

Animal life forms have evolved complex sensory systems that allow the characterization of chemical and physical properties of the environment, potentially contributing to the richness of a cognitive spatial map by adding dimensions of sensory information. Olfaction in particular seems to play a role in spatial awareness as scent marking, a behavior in which animals urinate or defecate in specific locations in order to mark their territory or their paths in the environment, is seen across many animal species. The domestic dog can be trained for searching point-source odors (Hepper & Wells, 2005), eg cadavers, which is fundamentally an olfactory-guided navigation task. In fact, in addition to mammals olfactory-cued navigation behaviors seem to be present in fish (DeBose & Nevitt, 2008), birds (Gagliardo, 2013) and even insects (Steck, 2012; Chin et al., 2018). Recent works have also revealed olfactory-guided navigation capabilities in humans (Jacobs et al., 2015), a species that has significantly less olfactory sensitivity than dogs or rodents.

The human genome contains just under 400 olfactory receptor gene families, while the mouse and dog genomes contain about 1200 and 1400, respectively. The proteins encoded by these gene families are expressed in the membranes of olfactory sensory neurons (OSNs) distributed on the surface of the olfactory epithelium. In mammals, the olfactory epithelium is located inside the nasal or vomeronasal cavity and each OSN expresses a single receptor gene. The differential expression of receptor genes leads to selectivity in the binding of odorant molecules to OSNs - some OSNs bind only to ketones, some are selective to aldehydes, other OSNs bind to certain functional groups that can be present the odorant molecules (Leon & Johnson, 2003). Any arbitrary odorant molecule therefore binds only to a subset of all OSNs.

OSNs expressing the same gene project their axons to the same targets in the olfactory bulb (OB) - the glomeruli, regions of the OB where thousands of axonal projections converge and synapse into mitral and tufted (M/T) cells. The activity of these cells thus reflects molecular features of the odorants as it results from the convergence of OSNs with equal molecular selectivity. Moreover, OSNs selective for similar molecular features project to neighboring glomeruli within the OB such that the correlation of stimulus-evoked patterns of activity of M/T cells in a glomerulus to different odors increases in proportion to the chemical similarity of the odorants. Because the axonal projections from OSNs selective for similar

molecular properties synapse in neighboring regions of glomeruli in the OB, different molecules will evoke different localized (in the glomeruli tissue) patterns of neuronal firing no matter the chemical dimension along which the molecules are different (Figure 1.3). Thus, the OB contains chemotopy, this is, an anatomical mapping between molecular properties (chemistry) and the organization of cells along the tissue surface (topology) (Johnson & Leon, 2007).

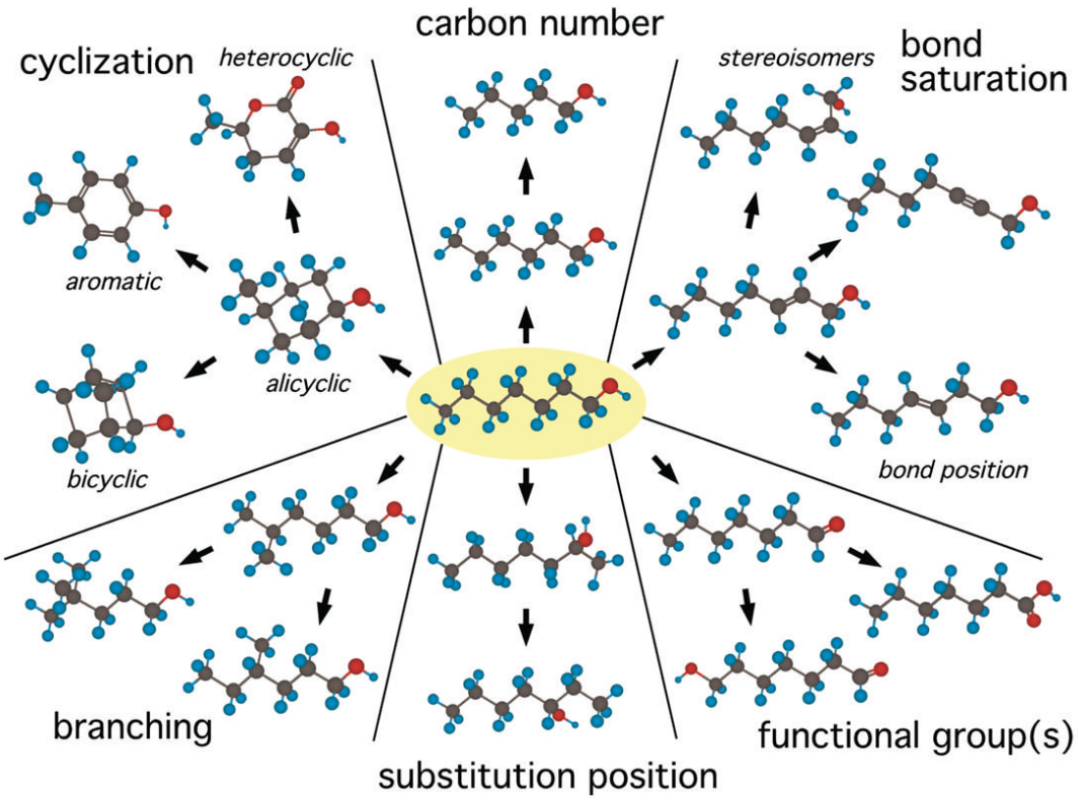

Figure 1.3: Odorant molecules can differ along many chemical dimensions. The odorant 1-heptanol's (center) structure can be varied incrementally along any dimension, resulting in incrementally dissimilar molecules. The degree of similarity is encoded in OB activity. (Figure adapted from Johnson & Leon (2007))

Therefore, odor identity is encoded in the population activity of M/T cells in the OB, which enables the existence of neural mechanisms for odor identification and discrimination that could produce olfactory-mediated behaviors.

M/T cell axons project to several cortical areas collectively designated as olfactory cortex. The largest of which is the piriform cortex (PCX), where M/T axons synapse in a spatially distributed matter that does not seem to conserve the chemotopy observed in the OB organization (Isaacson, 2010). The lack of spatial organization in the neuronal activity of PCX cells is in striking contrast with neocortical representations of other sensory information, namely in the somatosensory cortex, where spatial relations of activated cells are conserved between sensory and cortical cells (Stettler & Axel, 2009). In addition, individual PCX neurons don't appear to be selective to an odor or molecular feature, instead responding to dissimilar odors whereas auditory or visual cortical neurons show more specificity to stimulus properties. Interestingly, the piriform cortex is phylogenetically older than the neocortex, having a 'primitive' three layered cellular organization that is similar to the hippocampal architecture and typical of the allocortex.

Moreover, odors are represented sparsely in the PCX, with only 3-15% of the cells responding to individual odorant molecules, and the proportion of nonresponsive cells greatly increases along the anterior-posterior axis of this region (Litaudon et al., 2003). In fact, along the anterior-posterior axis

of the piriform cortex, there is also a gradient in the proportion of the preferred axonal targets of the cells in the population (Figure 1.4). Most significantly, cells in the anterior-most part of the cortex project mostly back to the OB, while in the posterior-most part cells project mostly to the lateral part of the entorhinal cortex (ECX). This structural organization suggests that the anterior part of the PCX is mostly involved in olfactory processing per se, supporting odor learning and odor discrimination by means of its autoassociative circuitry (Barnes et al., 2008), while in the posterior part the circuit is essentially feedforward and bidirectionally connected to neighboring structures like the perirhinal and entorhinal cortices, an architecture ideal for learning and recalling associations between olfactory information coming from the OB and anterior piriform cells and information represented in the connected structures (Haberly, 2001; Haberly & Bower, 1989), in order to support behaviors such as olfactory-cued spatial navigation.

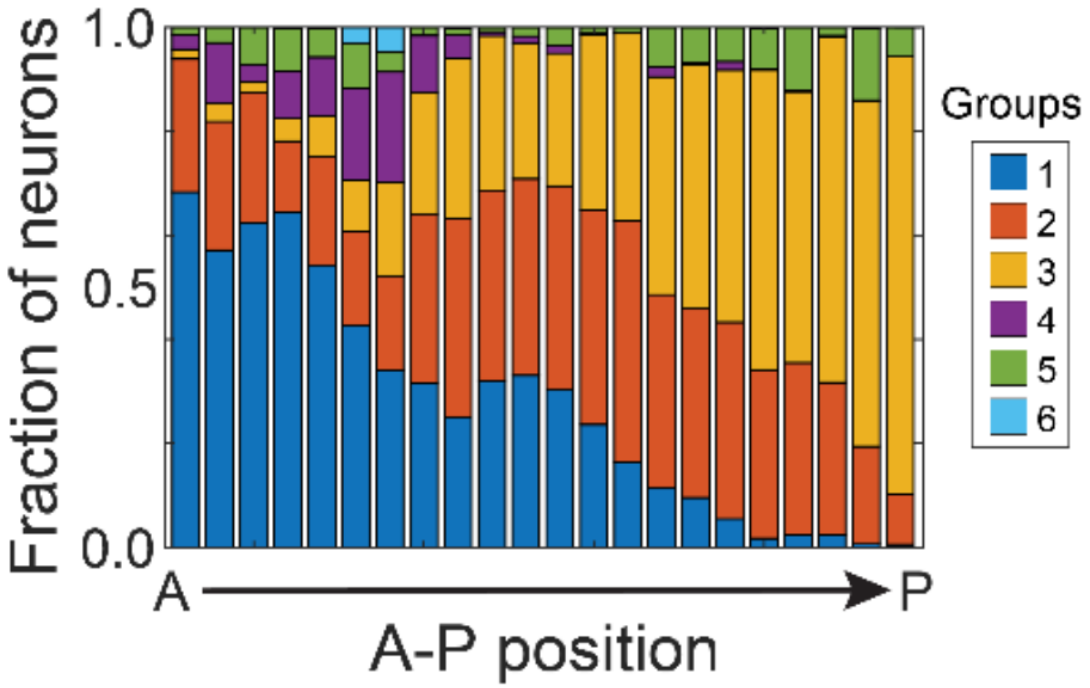

Figure 1.4: Fraction of PCX neurons projecting to a specific brain region as a function of their position on the anterior-posterior axis of the piriform cortex. Groups are **1)** OB, **2)** olfactory tubercle, **3)** (lateral) ECX, **4)** orbitofrontal cortex, **5)** caudate putamen, **6)** thalamus. (Figure adapted from Chen et al. (2021))

1.3 Olfactory-cued spatial navigation

Given the widespread presence of olfactory-cued navigation behaviors across taxa in the animal kingdom and that organizational principles of the olfactory function are well conserved across evolution and species (Ache & Young, 2005; Aboitiz & Montiel, 2015), the hypothesis that the role of olfaction is mostly to support spatial navigation by using odors to chemically characterize spatial locations in the environment rather than simply detecting and discriminating odors in airborne mixtures has gained traction over the recent years (Jacobs, 2012). Evidently, this hypothesis implies that olfactory and spatial streams of information must converge in the brain. Where and how are these combined?

The piriform cortex-entorhinal cortex-hippocampus circuit emerges as a major candidate for performing this function. In the first place, as previously discussed, both the PCX and Hipp circuitries are adequate to perform associative functions. In the second place, as just mentioned, the posterior part of

the PCX is massively connected to the lateral part of the ECX, where most of the object-associated activity can be found, suggesting that the PCX-ECX chain of the circuit provides the hippocampal cognitive map with odor-object information. Lastly, considering that odor identification can be performed at the level of the OB where, due to the existence of chemotopy, spatially distributed neural representations encode the molecular properties of the odorants (Johnson & Leon, 2007), it is reasonable to assume that piriform's activity is not redundant - it should be doing something else than just 'translating' or relaying the activity patterns coming from the OB (Stettler & Axel, 2009).

To assess the role of the PCX in olfactory-cued navigation behaviors, researchers at the Systems Neuroscience Lab in the Champalimaud Centre for the Unknown (CCU) have developed a spatial navigation task where rats are trained to navigate to a specific location contingent on olfactory stimulus identity while neuronal activity in the posterior part of PCX and Hipp are simultaneously recorded through electrophysiological methods (Poo et al., 2022). In this task, researchers used an elevated four arm version of a radial arm maze that will be from now onwards referred to as the 'plus-maze'.

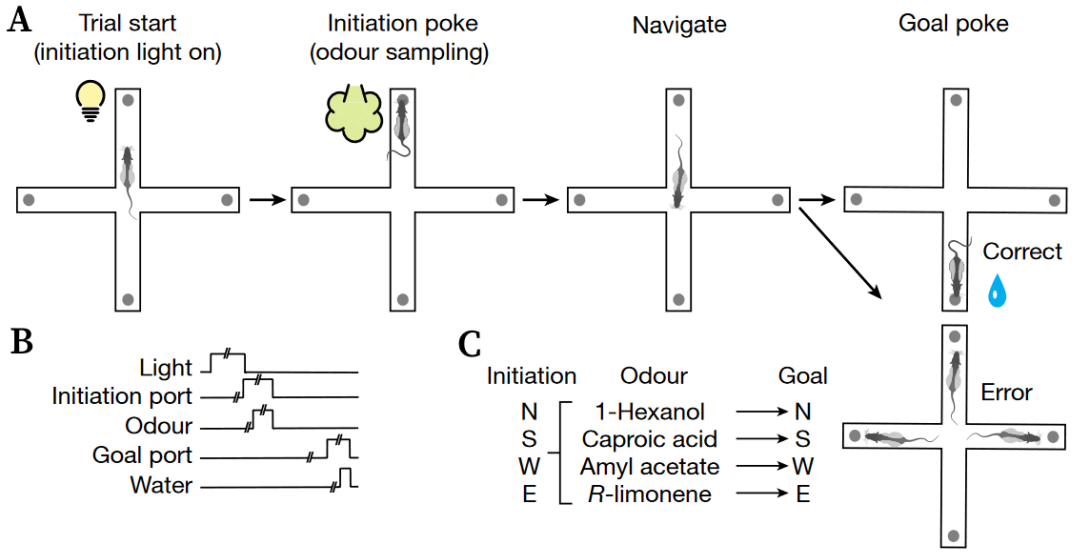

Figure 1.5: Task design. (**A**) Diagram of the trial structure. A light cue indicates the port the rat must approach in order to receive an odorant stimulus and must navigate to the correct port in order to receive a liquid reward. (**B**) Temporal organization of the trial and behavioral events in each trial (**C**) Stimulus to goal location mapping. At each port, the rat can receive one of four possible stimuli - 1-hexanol, caproic acid, R-limonene or amyl acetate - and must navigate to the corresponding location. (Figure adapted from Poo et al. (2022))

This plus-maze is located at the center of a room with rich distal visual cues and has four identical $1\,\mathrm{m}$ long arms spanning from a centerpoint into the four cardinal directions. At the end of each arm there is a small port where the rat can receive either one of four possible odorant stimuli or a water reward. At the beginning of each trial, a light cue indicates which port the rat should approach to sample one of four possible odorant stimuli, the identity of which determines to which port it has to subsquentially navigate in order to be rewarded (Figure 1.5). If the rat failed to approach the correct (rewarded) port, it would have to wait before the next trial started. This task promotes an allocentric strategy of navigation since it would be more efficient to use a representation of absolute space in order to estimate the quickest trajectories between stimulus and reward locations than to learn the sixteen possible trajectories for a given trial (four stimulus sampling locations $\times$ four goal locations). The rats learn the task and performance reaches 75% of correct navigation choices within a week and show no preference to individual odors or reward locations (Figure 1.6).

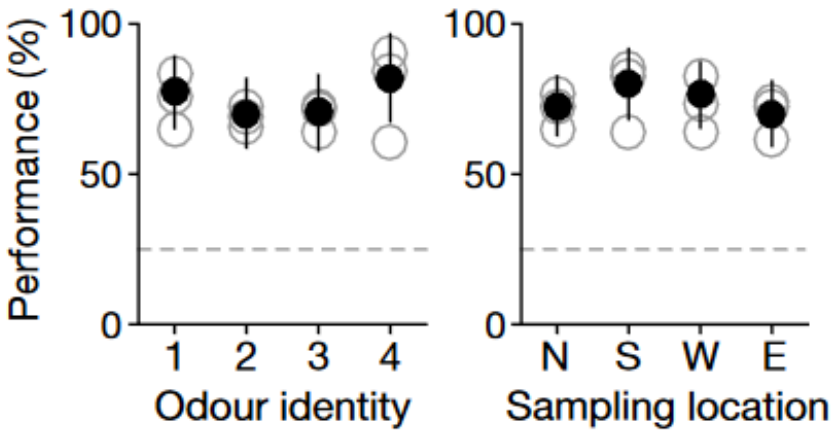

Figure 1.6: The behavioral performance of the rats across the four odorant stimuli (**left**) and rewarded locations (**right**) is similar and significantly superior to chance-level (25%). (Figure adapted from Poo et al. (2022))

The stimulus-evoked activity of recorded PCX neurons was analyzed in both the temporal and spatial dimensions, as shown in Figure 1.7, allowing the characterization of their selectivity to both odor identity and sampling locations. Example cell 1 fires more strongly at the 'West' port, regardless of the sampled odor, showing place-cell 'like' activity; example cell 2 responds only to odor 4, regardless of the sampling location; finally, the activity of example cell 3 peaks when Odor 1 is sampled at the 'North' port, showing conjunctive selectivity for stimulus identity and location. From all the recorded PCX cells in this experiment there was observed a bigger proportion of cells selective to location, than to odor identity or to their conjunction (Figure 1.8). A lower proportion of odor responsive cells could be somewhat expected as the recording probe was located in the posterior part of the piriform cortex which, as previously described, contains less odor responsive cells (compared to the anterior part), however the large amount of spatially modulated cells in the piriform cortex is intriguing.

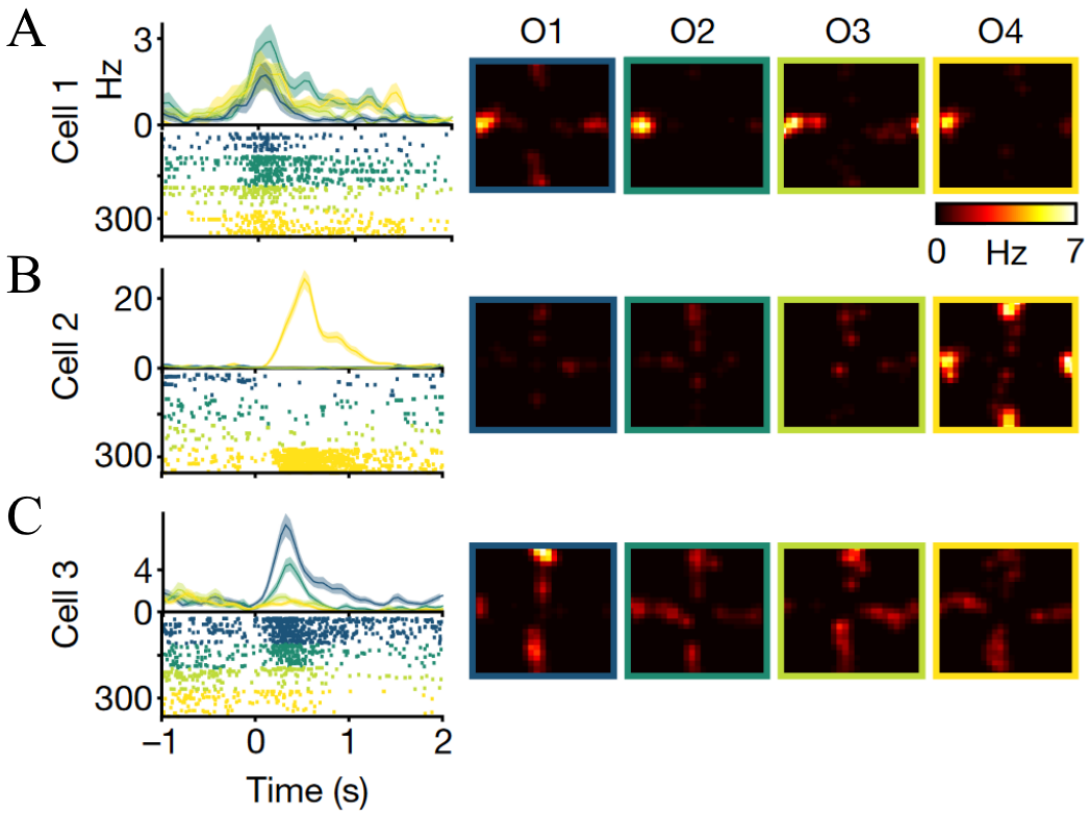

Figure 1.7: (**Left**) Spiking activity of three PCX neurons aligned to delivery onset of the four odorant stimuli (O1-O4). (**Right**) Firing activity of the same neurons aligned to the spatial position of the rat. Cell 1 is not selective to odors but fires more strongly at the 'West' port. Cell 2 is selective to O4 regardless of sampling location. Cell 3 fires more strongly when the rat samples O1 at the 'North' port. (Figure adapted from Poo et al. (2022))

These results potentially suggest that spatial and olfactory information are somehow combined in the posterior part of the PCX. However, the cells' apparent preference for the goal/reward locations reflects that this activity is modulated by task demands, potentially mediated through object-associated activity in the ECX. To further investigate what signals are contributing to the activity observed in the PCX, it would be fundamental to be able to present olfactory stimuli at locations that are different than the goal (reward) locations, which is not possible in the described plus-maze design.

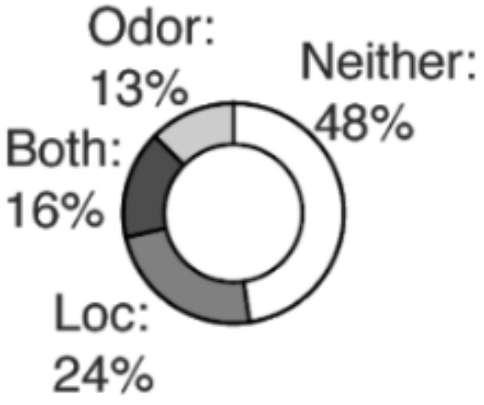

Figure 1.8: Selectivity of the recorded population of PCX neurons. 'Loc' stands for Location (Figure adapted from Poo et al. (2022))

1.4 Olfactory Virtual Reality

There is a fundamental tradeoff in animal research between ecological validity and experimental control. On one hand, naturalistic experimental scenarios elicit natural behavior and neural activity, but because these are generally complex and highly dynamic it is difficult to uncover precise relationships between observations and the stimuli that produced them. On the other hand, controlled experimental environments allow the quantification of neural activity and behavior and potentiate the study of these relationships, as the stimuli space is greatly reduced and generally parametrized; however, results from such experiments are constrained by the experimental design, its assumptions, limitations and heuristics, and therefore cannot be interpreted as what one would expect to observe in more naturalistic settings.

Assessing the contribution of olfaction to spatial learning and behavior demands that **1)** the odorant stimuli are precisely controlled in space and time, and **2)** the mouse can freely explore the environment in order to learn the reward contingencies that engage it in the task. The plus-maze task aforementioned attends these requirements as mice are free to roam and explore the maze while only providing odorant stimuli at specific locations, however, apart from manipulations to reward rules or stimuli statistics, introducing changes to the environment during an experimental session is not practical, namely changes to the maze's physical aspect such as the length of the arms. This can be somewhat countered by simultaneously using interconnected mazes that the animal can navigate in-between either freely or in accordance to an experimental criterion, but available laboratory space greatly limits this possibility.

Taking this into consideration, a virtual reality (VR) paradigm could contribute to circumventing some of the adversities related with experimental design for the presented purposes. In the first place, the virtual environment (VE) can be designed to seem (and 'feel') as naturalistic as desired while still allowing for full control of environmental, stimulus and rewards parameters and statistics. Also, because the experimental environment itself is virtual, generally implemented as a computer program, modifying any aspect of the environment is as simple as changing lines of code. The power that VR offers to experimentalists is well described in Sherman & Craig (2003): VEs are "subject only to the rules of their human creators. The creator has total dominion".

The deity-like power of freely designing and manipulating the aspect and physical rules of the environment is perhaps the greatest advantage a VR approach can offer. It not only allows the design of an almost unlimited number of environments that the animal can experience, it also allows full control of its sensory information, enabling the production of unrealistic or un-naturalistic stimuli and the co-occurrence of stimuli that doesn't happen in the natural world. These possibilities have inspired the Systems Neuroscience Lab to develop an olfactory virtual reality (OVR) system that could extend their research possibilities, and that motivated the research project here reported.

VR has been used in neuroscience research profusely in recent years in zebrafish (Huang et al., 2020; Bianco et al., 2011), flies (Reiser & Dickinson, 2008), nonhuman primates (Matsumura et al., 1999), humans (Astur et al., 2005) and rodents (Thurley & Ayaz, 2017; Lopatina et al., 2020; Dombeck & Reiser, 2012). Animals are generally head or body restrained, which increases the amount of applicable neural signal recording techniques (in particular optical techniques as these are very sensitive to signal artifacts resulting from motion of the imaged tissue, (Thurley & Ayaz, 2017)) without significantly disrupting proprioceptive signals, and enables the use of optogenetic techniques for introducing perturbations to neural activity while animals perform a task. In fact, olfactory-cued navigation behavior has been observed in mice performing VR tasks that contain visual and olfactory information (Radvansky & Dombeck, 2018; Harvey et al., 2012) as well as exclusively olfactory information (Fischler et al., 2021) and place cells in mice navigating virtual environments have been recorded multiple times (Harvey et al., 2009).

Chapter 2

Methods

In this chapter, the developed olfactory virtual reality (OVR) system is described and validation procedures are posited. The main requirement for this system is the feature of precise olfactory stimulus controllability while mice navigate in VR environments in a closed-loop manner, so that it can be used in the research of olfactory-cued spatial learning and navigation. Additional requirements are that the system is based as much as possible on open-source tools and that it is modularly designed in order to accommodate additional sensory modalities if required. Also, the hardware assembly should allow incorporation of electrophysiologic or optical fluorescence instrumentation in order to enable recording the neural activity of behaving animals.

In summary, the system is constituted by a screen assembly where the visual aspect of the VE is displayed, a behavioral interface that provides olfactory stimuli and liquid rewards to the animal while simultaneously recording its behavioral output, which is fed into the computer that is generating the experience by means of a VR engine. In addition, an enclosure assembly was designed that fits two OVR systems into two training 'boxes', allowing for conveniently training two animals simultaneously and independently while minimizing the required laboratory space.

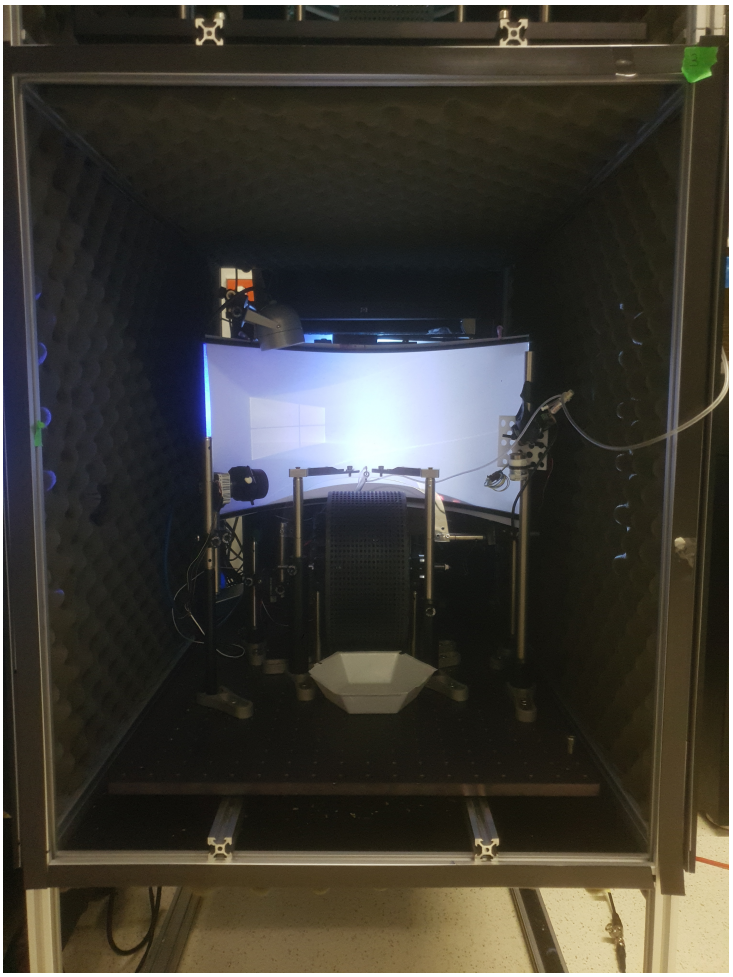

Figure 2.1: The developed OVR system.

2.1 OVR System Development

2.1.1 VR engine

Considering that the VR engine's latency in processing the animal's movement signals to update the visual scene should be smaller than that animal's reaction time (100 ms for a mouse), a computer-based VR implementation is naturally the most powerful and flexible one (Dombeck & Reiser, 2012), especially considering the increase in the number of tools designed for ethology experiments in VR settings, such as Bonvision (Lopes et al., 2021), ViRMEn (Aronov & Tank, 2014) or MazeMaster (https://github.com/BRAINLab-Aachen/MazeMaster#readme); also behavioral and neural data acquisition devices require the use of a computer. We initially based our VR system on the ViRMEn engine, as it was designed as a MatLAB package by researchers at the University of Princeton specifically for mice neuroethology and offered a convenient user interface for VE design. VR engine interfacing with recording devices was assured via a miniDAQ device (National Instruments), while HARP, an in-house developed acquisition device (Champalimaud Hardware Platform) was used in conjunction with a custom Bonsai routine for recordings destined for post-hoc analysis (Figure 2.2).

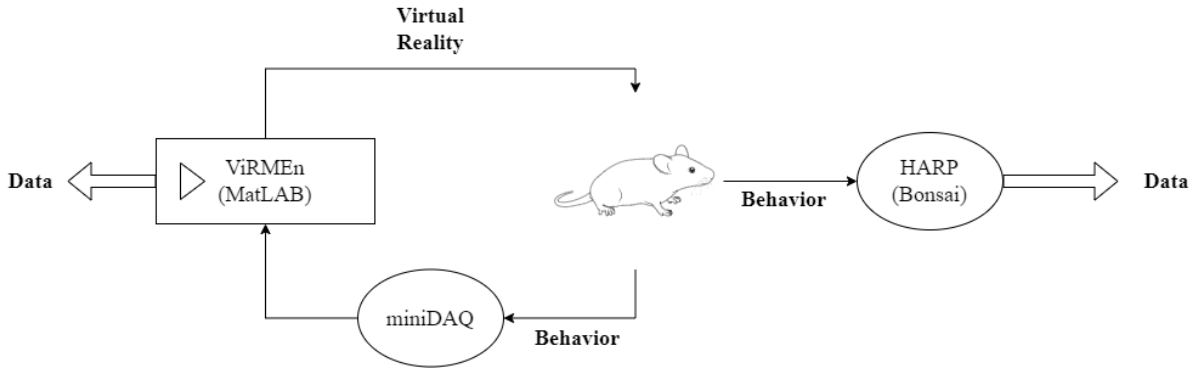

Figure 2.2: Schematic of the initial system design based on ViRMEn.

The posterior release of BonVision prompted forsaking this somewhat convoluted design for one where both the VR experience and data acquisition are handled exclusively by Bonsai (Figure 2.3). Bonsai is an open-source visual programming language designed to handle the acquisition and processing of simultaneous asynchronous data streams (Lopes et al., 2015), which is why it was used in our initial implementation to sample analog signals for behavioral analysis. Being able to generate the VR experience in the same software that's acquiring the behavioral data not only reduces the number of software dependencies and hardware necessary to implement the system, thus reducing its complexity, it also greatly facilitates time alignment of data streams coming from different sources - such as the mouse and the VR engine - as they now originate from the same Bonsai routine.

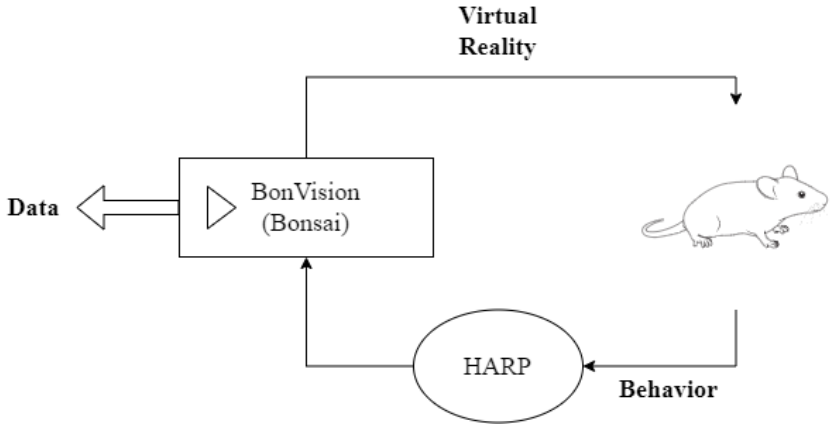

Figure 2.3: Schematic of the presented OVR system design based on BonVision

BonVision is a Bonsai library that uses OpenGL to render 2D and 3D visual stimuli that can be used in scientific settings due to the low level interactivity possibilities it offers, allowing users to customize many parameters of the visual rendering pipeline for their specific purposes. This library was developed by a collaboration of researchers from the University College London and NeuroGEARS Ltd. (lead developers of Bonsai) specifically for scientific research in humans and animals (Lopes et al., 2021). Because of the low-level nature of BonVision, VEs and experimental protocols can be used independently of particular elements of hardware, which allows the replication of tasks with different model animals and contributes to the modularity of the OVR system.

In order to render a 3D VE in a screen of an arbitrary shape, BonVision defines the VR user as a point at the geometric center of a 3D cube wherein the VE is displayed on the cube's faces using cube mapping, a popular computer graphics rendering technique. In this retinotopic reference frame, an arbitrary display device can be defined according to its position relative to the user (the origin of the frame) and its own

geometry, becoming a virtual 'window' that sifts which portion of the 3D cube to render by calculating, for each pixel of the screen, a vector that originates at the origin of the frame, passes through that pixel, and terminates at a point in the cube's surface. In this way, each pixel of the display device is naturally mapped to the pixel in the 3D cube that it renders.

Within the BonVision framework, VEs are implemented as custom Bonsai scripts depicting the locations of visual objects in the retinotopic frame of reference and that are accessed by a main Bonsai routine that runs the VR experience, including behavioral and environmental events, and that handles both translating the movement of the subject into a change in the visual aspect of the VR and recording the needed behavioral signals. In this way the VE is independent of experimental protocols, which enables different visual and olfactory VEs to be used interchangeably with different behavioral tasks.

2.1.2 Behavioral interface

Profiting from a screen assembly design from the Harvey Lab at Harvard University (Minderer et al. (2019), https://github.com/HarveyLab/mouseVR/blob/master/README.md), an in-house designed 3D printed wheel (Champalimaud Hardware Platform, Appendix .1.1) and I/O electronic boards (HARP), we first sought to align the video projector and wheel to the center of the screen and incorporate a rotary encoder (US Digital) on the wheel axis that measures its absolute position and feeds its signal to the PC via an analog signal recorded by the HARP board. The visual aspect of the VE is rendered onto an elevated parabolic screen spanning $210°$ around the mouse, covering a big portion of the mouse's field of view. The assembly consists of a hollow acrylic 'box' supported by metal rails (ThorLabs) where a $61\,\mathrm{cm}$ x $122\,\mathrm{cm}$ translucent white film screen is fitted. A high-definition laser projector (Laser Beam Pro) is mounted centered on top of the assembly and two mirrors are used to reflect the image such that it covers the entirety of the screen (Figure 2.4). This assembly covers a significant portion of the mouse's field of view while greatly limiting optical noise in the projection.

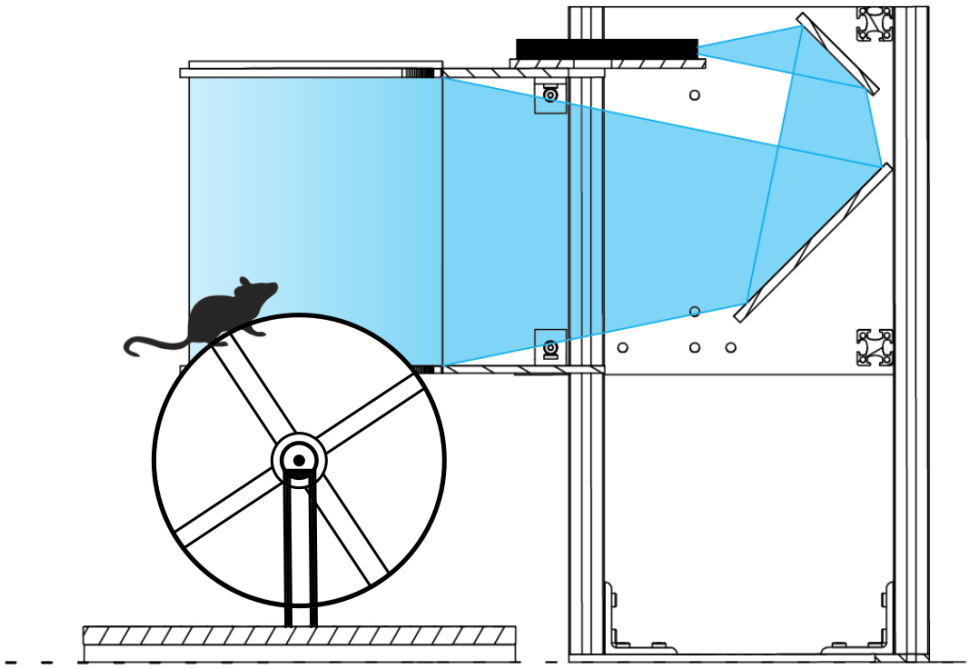

Figure 2.4: Screen Assembly and optical path of the visual projection. Optical noise is reduced as the optical path of the projection is enclosed to the acrylic box, and the projection covers a significant amount of the mouse's view. (Figure adapted from `https://github.com/HarveyLab/mouseVR/blob/master/README.md`)

The parabolic screen geometry used in the OVR system was therefore implemented as a 3D mesh file that is used by BonVision's rendering pipeline and that was produced according to Equation 2.1 (as defined in https://github.com/HarveyLab/mouseVR/blob/master/README.md), which defines the shape of the screen's curvature, and the screen's dimensions.

$$y = -0.125x^2 + 5 \tag{2.1}$$

The mouse is head-fixed on top of a 3D printed plastic wheel (r = 10 cm, width = 10 cm) aligned with the center of the screen, at a distance of 12.7 cm and at a height of 2.5 cm from the wheel's surface (Figure 2.5). The wheel's surface is perforated by a grid of $\sim$1 mm holes that enhances the mouse's grip of the wheel and allows draining of urine. This reduces the sensory noise contributed from self-deposited odors by the animals (Figure 2.8, Appendix .1.1). Naturally, this implementation only allows for the mouse to navigate in one spatial dimension (1D), however the use of 1D VEs simplifies the training process of the animals and provides for increased stability of neural recordings (Thurley & Ayaz, 2017). It is also a simpler implementation of a VR engine that suffices for a proof of concept.

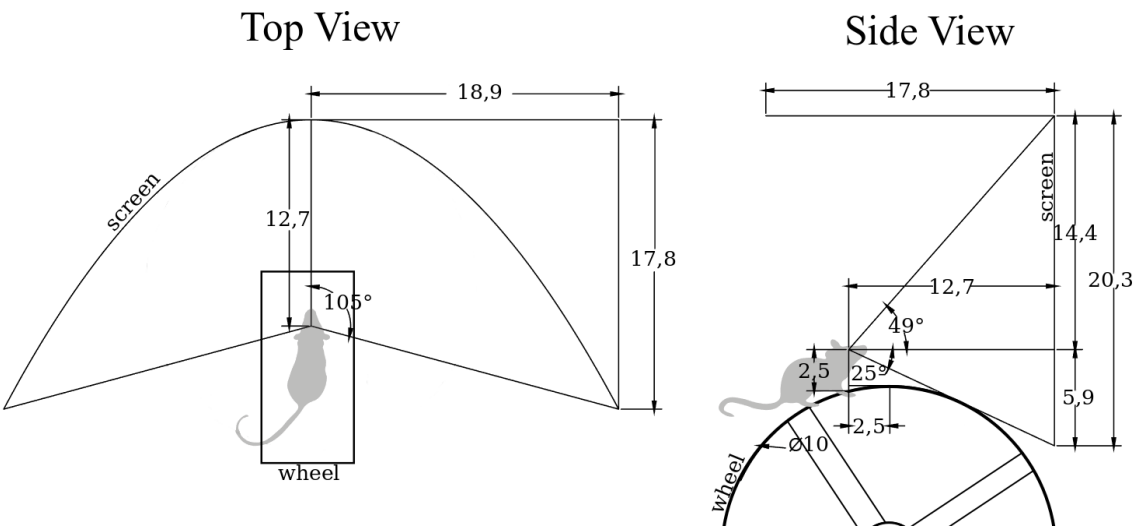

Figure 2.5: Top (**Left**) and Side (**Right**) views of the positioning of the mouse relative to the screen and its geometry. Units are approximate, in centimeters. (Figure adapted from `https://github.com/HarveyLab/mouseVR/blob/master/Guide/mouse_positioning_on_the_ball.png`

The 0° to 360° range of positions of the wheel are mapped linearly on the rotary encoder's output analog signal ranging from 0 V to 5 V with a positional sensitivity of $\sim$0.35°. A mouse running on the wheel will rotate it by a certain angle θ that corresponds to an arc length that is given by definition by $\theta \times r$ and which the mouse has run in the real world. As the sensor encodes the position of the wheel in degrees, one can handily determine the distance traveled in the virtual world by calculating the arc length respective to any value θ of total rotation.

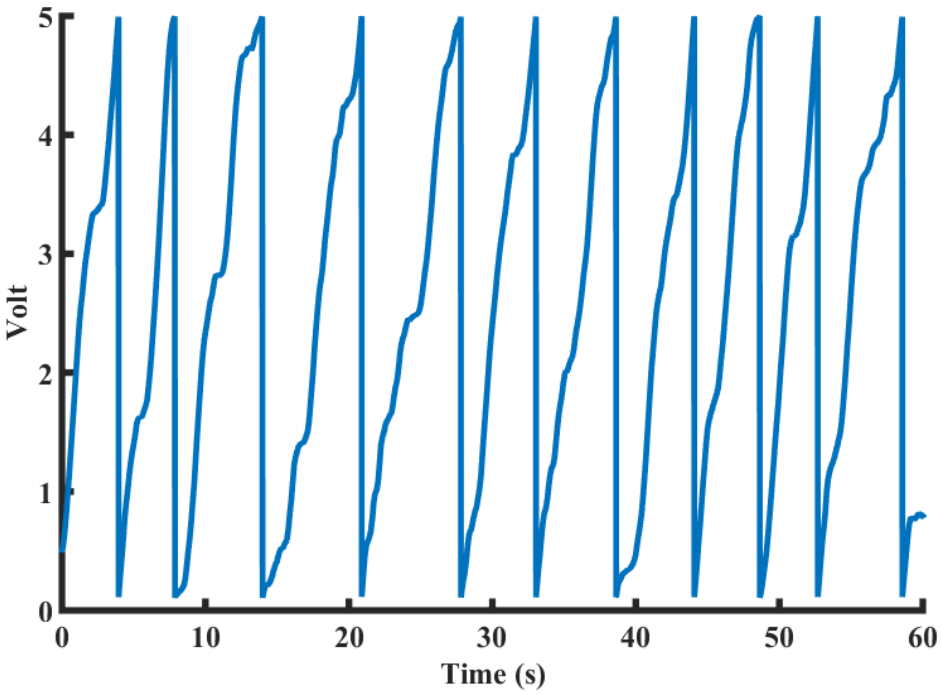

Figure 2.6: Raw rotary encoder signal.

However, because the sensors' signal does not monotonically increase with the rotation of the wheel, containing discontinuities where the signal warps around its maximum output of $5\,\mathrm{V}$ (Figure 2.6), this calculation is implemented by detecting high amplitude *extrema* in the derivative of the encoder signal, as those points correspond to the discontinuities in its signal. In that manner, one can keep track of the amount of complete rotations of the wheel in both directions (the direction is given by the sign of the derivative) since the start of the VR session, which multiplied by the wheel perimeter (arc length of $\theta = 2\pi$) and added to the arc length corresponding to the wheel position measured in any iteration of the VR engine, result in the total distance ran by the mouse at that moment.

A custom Bonsai script processes the raw rotary encoder signal as just described and returns an absolute virtual position value based on the wheel geometry, in accordance to the aforementioned mathematical principles. The main Bonsai routine running the OVR experience uses this virtual position value at each iteration to update the visual aspect of the VE and trigger experimental events (*eg* rewards) as the animal runs on the wheel in a trial-based, closed-loop manner. In addition, a gain parameter was included to adjust the magnitude of the rotary encoder signal on the virtual position calculation as it facilitates manipulating the virtual velocity of the animal, opening a new domain of experiments by allowing to dissociate self-motion and optic flow signals.

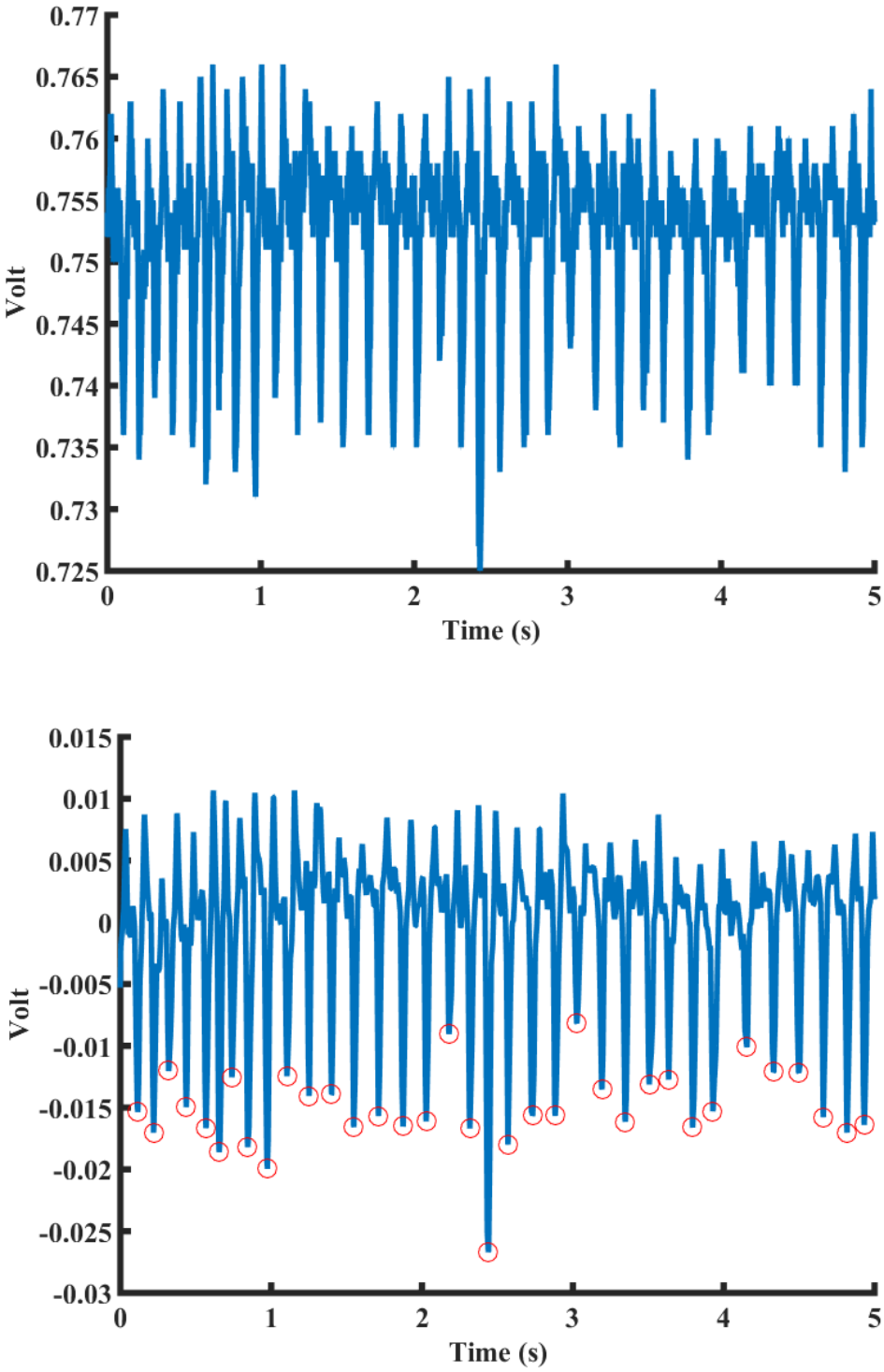

Figure 2.7: Raw (**Top**) and lowpass filtered (**Bottom**) air flow sensor signal of a mouse breathing while operating the VR system. Circles denote automatically labeled individual inhalation events.

A transparent acrylic holder was designed to secure in front of the mouse's rostrum a liquid reward spout, an odorant stimulus tube and a breathing sensor tube (Figure 2.8, Appendix .1.1), which can be optimally positioned for each mouse's rostrum as the holder is bilaterally mounted on manual tridimensional microcontrollers (ThorLabs). This allows for small adjustments between experimental sessions, thus reducing the effects of variance in mouse anatomy to accessibility of rewards and stimulus percep-

tion.

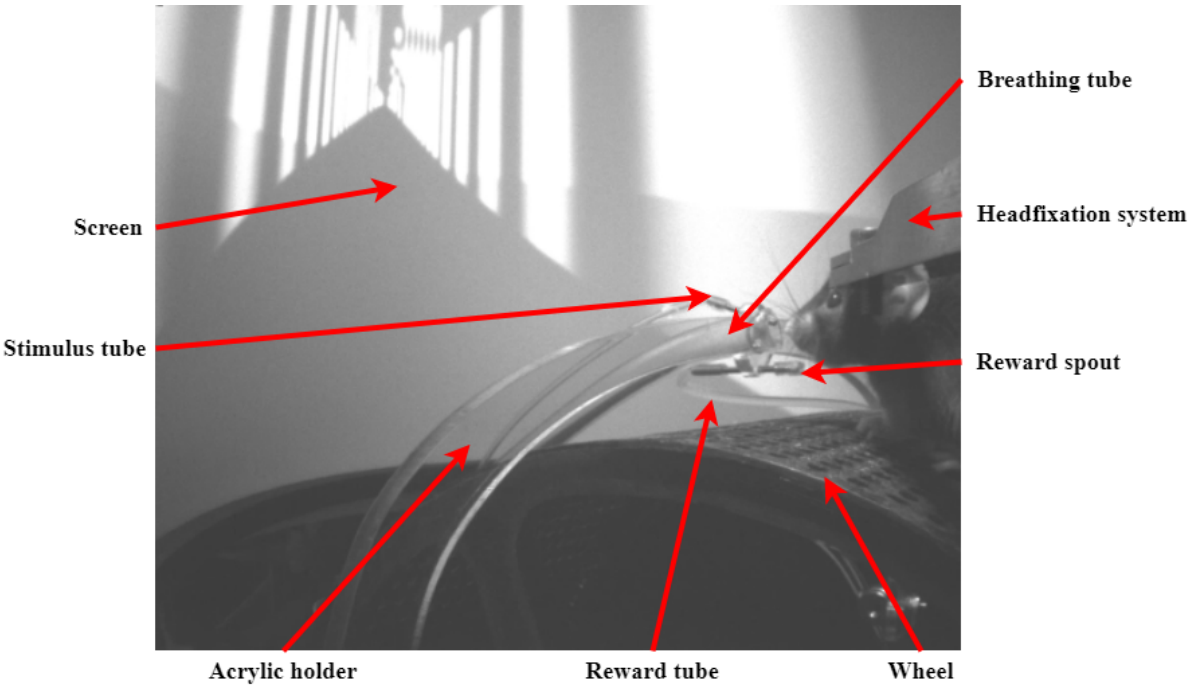

Figure 2.8: Identification of the behavioral interface's components. An unannotated version of this image is included in Appendix (8).

A key ethological signal to assess if an animal is being attentive to the olfactory stimuli is its breathing rate (Kepecs et al., 2007). In order to record the breathing signal, a tube is connected to a highly-sensitive air flow sensor (Honeywell) that is installed anterior to the mouse position on the system, below the screen assembly. The open end of the tube is held in front of the animal's nose by the acrylic holder and the sensor's output signal is recorded by the HARP board. The viability of this implementation was assessed by measuring the sensitivity of the sensor to mouse respiration in an anesthetized animal as a function of the distance between the mouse's nose and the sensor, which consequently informed the design and geometry of the acrylic holder.

The breathing rate is derived *a posteriori* from the breathing signal recorded by the airflow sensor. The sensor's output signal is low-pass filtered at a frequency of 30 Hz and local *minima* in the filtered signal are automatically labeled using MatLAB's $findpeaks()$ method as these points correspond to inhalation events (Figure 2.7); the breathing rate is then defined by a sliding time window count of the labeled points.

Olfactory stimuli are delivered to the mouse by means of an olfactometer (Island Motion). This device manipulates and directs the airflow coming from a pressurized source through different output valves, which allows the use of multiple odorants simultaneously in order to provide airborne odor mixtures with short latency, and is controlled via TCP/IP communication. When the mouse reaches a stimulus location, the VR engine prompts the olfactometer to switch its output air valve from one containing a dry paper filter to one where the airflow permeates an odorized paper filter. The odorized paper filters are prepared by applying 12 µL of an odorant solution (Appendix .1.1 to syringe filters (Whatman).

This output air-stream then merges with an air-stream of constant flow rate - a carrier stream ($0.4\,\mathrm{L\,min^{-1}}$) - that flows to the mouse's nose through a fine tube. This carrier stream guarantees that the airflow reaching the mouse is constant, odorized or not, thus reducing variability in olfactory stimulus presentation that could be a source of variance in the behavioral or neural data. To ensure this, we used a photoion-

ization device to measure the dynamics of stimulus presentation (Figure 2.9). As can be observed from these measurements, the temporal dynamics of all stimuli events is identical, while the amplitude slowly decays over consecutive stimuli events due to depletion of the odorant solution. This effect can be reduced by using multiple odorized filters at the different olfactometer output ports, and looping over them whenever a stimulus is produced. In addition, these measurements allow to estimate the latency between the stimulus being triggered on and it reaching the mouse due to the length of tubing ($\sim$50 ms).

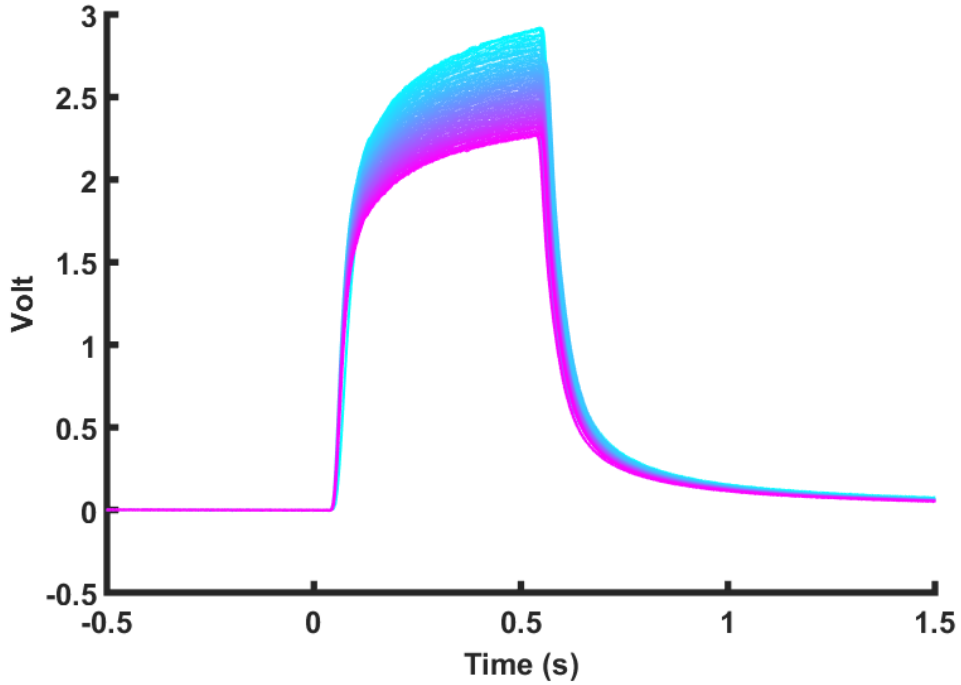

Figure 2.9: Photoionization detection (PID) signal of 100 olfactory stimulus presentations. This signal conveys the concentration of odorant molecules in filtered atmospheric air as the olfactory stimulus is toggled on/off, measured at the air flow outlet in the mouse's behavioral interface. The stimuli are toggled on at $Time = 0$ (zero) and have a duration of 0.5 s. The color code represents the ordering of stimulus presentations, with the first presentation in blue, and the last (hundredth) in magenta.

In similar fashion to stimuli, when the mouse reaches a reward location, the engine triggers the opening of a solenoid valve (NResearch) by providing it with a digital signal through the HARP board. A liquid reservoir containing water is suspended above the animal location in the system, such that water flow rate is controlled exclusively by gravity once the valve is opened, hence the volume of reward is defined only by the amount of time it stays open (Appendix .1.1). The output of the valve is connected to thin tubing (Cole-Parmer) ending near the mouse's mouth.

2.1.3 Experimental rig

Each OVR system is mounted on a breadboard (ThorLabs), allowing for portability and interchangeability between training boxes. The breadboard is equipped with wheel gantry assemblies (OpenBuilds) that allow its retraction out of the box for ease of access to components or for introducing or removing a mouse by rolling the breadboard on horizontally placed metal rails (Appendix Figure 6). The training boxes are made of metal rails (ThorLabs) and custom manufactured acrylic panels that are covered by soundproof foam (McMaster-Carr), and are closed while animals are running such that sources of light or sound external to the training box are greatly reduced, contributing to the concentration of the animals (Appendix .1.2.

As the system is fitted inside the training box during experimental sessions, the animal is illuminated by an infrared light source (CMVision) and monitored by a video camera (FLIR) equipped with an infrared filter (LEE Filters), which provides a video recording that is clean of eventual differences in the light intensity of the visual projection. The camera is positioned laterally to the mouse so that not only experimentally relevant behaviors like licking, sniffing, casting, whisking, grooming and running can potentially be recorded, the visual scene presented to the mouse at the moment of each frame acquisition is also recorded (Appendices .1.1 and .2.1). In addition, pupil size seems to be related to behavioral state variables (Cazettes et al., 2021), so the ability to record pupil position and size was taken into account when positioning the camera in the system, thus enabling a new scope of analysis. In order to facilitate alignment of the video stream to the remaining of the recorded signals and each frame of the VE, the camera is not freely shooting; instead, frame capture is controlled by the HARP board at a prespecified frame rate (30 Hz) via the camera's digital I/O feature, and each frame is automatically timestamped by means of a built-in digital clock in the HARP device.

To enable electrophysiological recordings of animals navigating in VR, this system can be set up in a Faraday cage instead of the presented training box. In this case, a motorized micromanipulator should also be installed posterior-laterally to the mouse's location on the system to control the position of an acute recording probe during the experimental session and the remaining necessary recording instrumentation properly placed on or near the system.

2.2 OVR System Validation

Subjects experiencing a perfect VR simulation shouldn't be able to distinguish it from experiencing the real world. Hence, the fundamental features for producing this illusion are immersiveness and interactivity (Sherman & Craig, 2003). Immersiveness is related to the feeling of presence in an environment and is determined mostly by the sensory richness of that environment as well as the quality of sensory feedback. Interactivity is associated with the feeling of agency on an environment, this is, a non-interactive VR system will most likely disrupt the illusion of belonging on the VE even if the system provides a rich sensory experience, since the user would effectively be a 'spectator' of the VE and not an 'actor' in it. Thus, interactivity is the key element determining the 'closed-loopness' of the system, as any changes in the virtual environment should result from the subject's actions.

To assess the quality of the OVR simulation, a group of seven mice was trained to operate the wheel and their behavior recorded while they navigated in OVR. If the mice are apprehending the VR experience as navigating through real space, they should display naturalistic behavior and events such as spatially discrete stimuli and rewards should elicit brain activity and behavior in line to what is been observed in mice freely navigating. In this section, stimulus delivery properties will be characterized, the used training and experimental protocols will be described, and procedures for recording the neural activity of mice in the OVR system will be presented.

2.2.1 Training Regime

After recovery from the surgical implantation of a prosthetic headbar for head-fixation in the OVR system, the animals go through a habituation and training regime designed to habituate them to the experimenter, head fixation in the experimental rig, and exposure to the OVR experience, and to motivate them to learn the reward contingencies of the environment. Head-fixation is a common-use technique that allows neural recording from behaving rather than anesthetized animals without the necessity of

chronic implantation of recording probes.

Mice are individually assessed every day from the day before the implantation surgery. This process consists of a general health assessment, including weighing, initially to evaluate if an animal is healthy and can undergo the surgical procedure, and then to follow the recovery of each mouse to surgery until they can be used in experimental conditions, meaning they show no signs of pain or discomfort, and show stereotypical healthy adult rodent behaviors, which typically happens three to five days after implantation. At this time they are submitted to a regime of water restriction.

In order for lab animals to be trained to perform tasks in experimental circumstances, many times under stressful conditions, reinforcement learning mechanisms are generally used to motivate the animal to participate in the experiment. Positive reinforcement strategies rely on providing pleasing events, namely rewards consisting of sweet water or food, motivating the animals to be engaged in the task, while negative reinforcement strategies opt to use unpleasant or painful stimuli such as an air puff to the animal's rostrum. While naturally more stressful for the animals, these stimuli are also more salient to the animal and promote quicker learning.

The presented regime of water restriction breaks this dichotomy as animals are able to get water only during the experimental session and don't have *ad libitum* access to it on their homecage. Hence, water rewards have the property of positive reinforcement in the sense that they are pleasing events that the animals are motivated to experience, while ongoing deprivation has an unpleasant and possibly stressful effect on the animal. The daily assessments of these animals include investigating for signs of dehydration, and the regime is stopped if an animal's body weight drops below 80% of their baseline (pre-water deprivation) weight. This heuristic measure is designed to make the animals motivated to seek sources of water while maintaining a level of dehydration that is not harmful to the overall health of the animal, in accordance to the institution's veterinary practices.

In the first two to three days of water deprivation, mice are not allowed to drink water, but interact with the experimenter's hands while in their home cage. At this point, mice are provided with a daily amount of $\sim 0.7\,\mathrm{mL}$ of water at regular times in the day and only in the experimental room. They become progressively habituated to receiving their daily water intake initially in the hands of the researcher, then freely-moving on the OVR apparatus, and ultimately head fixed on the system. Water is manually provided in a sparse manner for about twenty to thirty minutes each time.

The mice need around seven days to complete this part of the training protocol. After this, reward delivery becomes yoked to each animal's running behavior while head-fixed on the apparatus, experiencing the projection of a VE consisting of a $500\,\mathrm{cm}$ long linear corridor, and animals quickly learn the closed-loop reward condition. Individual reward events happen each time the animal runs a certain distance, which is drawn from an uniform distribution for which the range increases over training sessions, until the point where only one reward event is present at every transversal of the corridor. The aim of this strategy is to motivate the animals to run for longer distances between individual rewards, thus staying engaged in the VR experience for longer periods of time and completing more transversals of the corridor. The whole training regime lasts for about fifteen to twenty days.

2.2.2 Experimental Regime

Animals that conclude the training regime are able to run through a virtual corridor and collect a liquid reward, and therefore should be ready for exposure to olfactory virtual reality without being overwhelmed by the experience. For this, a new VE was designed by modification of the linear corridor used in training to a sufficient degree that it was not familiar to the animals. Animals still only have

access to drinking water while on the apparatus, and they are introduced to it once a day at regular times.

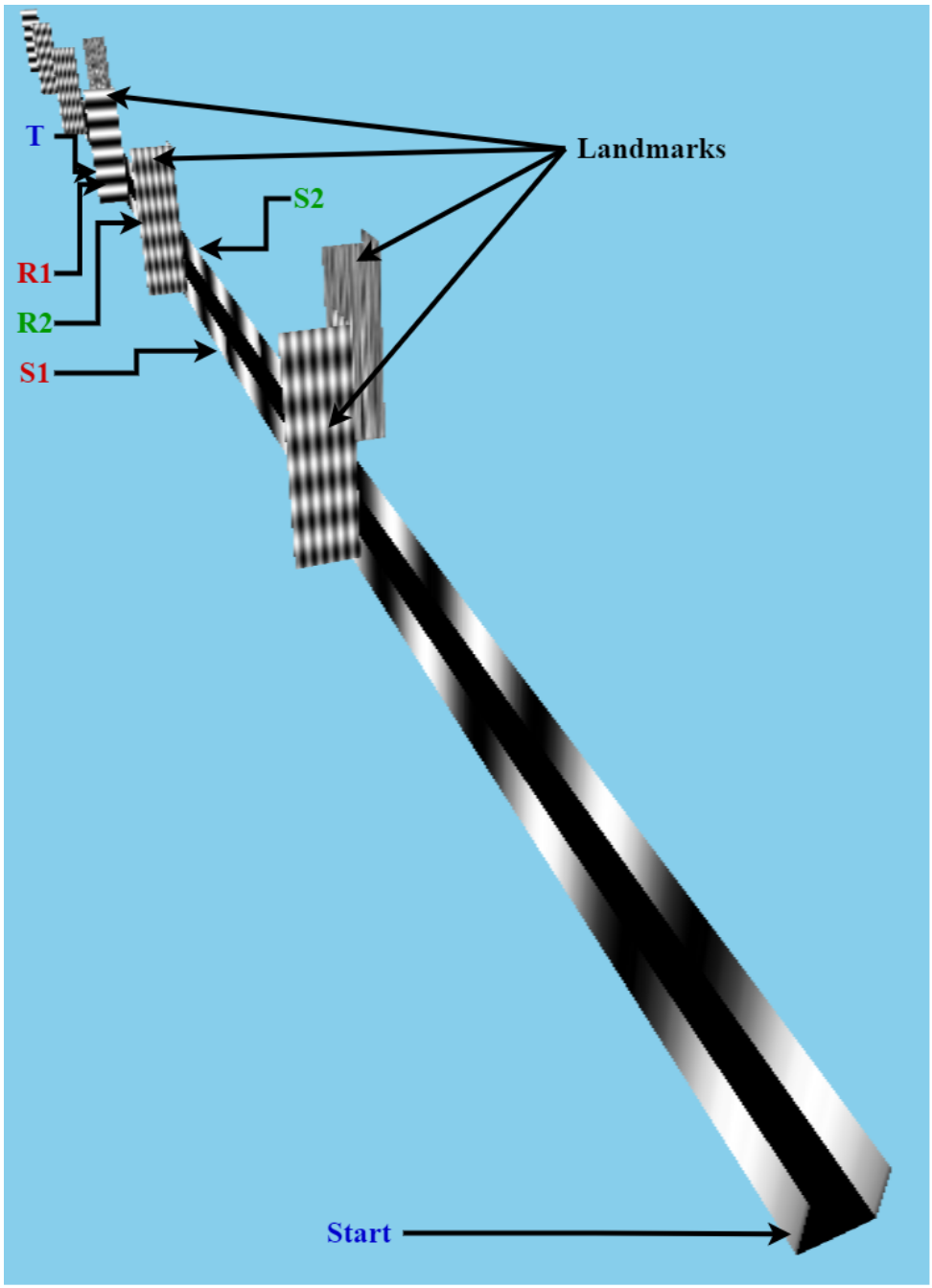

Figure 2.10: Perspective of the VE used in the OVR experiment. The locations of events are labeled (**T** stands for the teleportation location). This image was generated with BonVision.

On each lap of the corridor - each trial - the animal is probabilistically subject to one of three reward contingencies (Figure 2.10, Table 2.1): **40%** of the time, an olfactory stimulus is provided at a location S1 in the corridor, with a reward provided at another location further along the corridor, R1 - trial type **S1R1**; **40%** of the time, the same olfactory stimulus (the same odorant molecule delivered in similar concentration and dynamics) is provided at a different location S2, and reward also being provided at another location, R2 - trial type **S2R2**; the remaining **20%** of the time, no stimulus or reward events happen in the transversal of the corridor - **probe trial**. At the moment the animals arrive at the teleportation location, the animal is moved back to the starting position in the virtual corridor instantly, in order to

Frequency	Trial type	Stimulus Location	Reward Location
40%	S1R1	200	420
40%	S2R2	290	320
20%	probe	-	-

Table 2.1: OVR task trial types. Values are in cm.

start a new trial.

In this design, the stimulus and reward locations can be different, but are associated, as the mouse can only experience S1 paired with R1, and S2 paired with R2 for the nonprobe trials. Thus, not only the olfactory stimulus is informative about the presence of reward, it is also informative about its location. Also, as the corridor the mouse is navigating is identical for all trial types, the only environmental variable the mouse can use in order to efficiently navigate to rewards is the location of the odor stimulus presentation.

In addition, for both nonprobe trial types, a velocity threshold criterion is used to condition reward presentation such that if a mouse runs at an average velocity of more than $30\,\mathrm{cm\,s^{-1}}$ in the $50\,\mathrm{cm}$ of corridor preceding reward location, it is not presented (omission). Velocity is calculated as the difference in value between consecutive virtual positions divided by the difference in the timestamps of those positions. If such criterion would not be used, and rewards were always available at their designated locations, the animals wouldn't need to pay attention to the olfactory dimension of the corridor and could just run at high speeds between individual reward events, thus maximizing their temporal reward rate. In this manner, optimal behavior demands that animals pay attention to the olfactory stimuli as they inform them of reward presence and location, thus reducing the probability an animal learns a non olfactory-cued navigation strategy. Animals that have learned the contingency should show decreased velocity when approaching a reward location, which is a behavioral biomarker of spatial learning.

The VE is designed to resemble a linear track/corridor, where high lateral walls would prevent the animal - if it wasn't head fixed - such that it can run only forward in the environment. Distal cues constituted by textured visual objects much taller than the walls are placed outside the corridor which, together with patterned textures on the lateral walls (local cues), constitute a visual cue rich environment, contributing to optic flow mechanisms and for the animal to learn the metric of the environment (Figure 2.11). Since animals are teleported in the VE instantly when a trial ends, the visual aspect of the corridor is replicated at the end of the track, such that as the animal is teleported to the beginning of the track its perspective is maintained from the preceding moments when it was approaching the teleportation location.

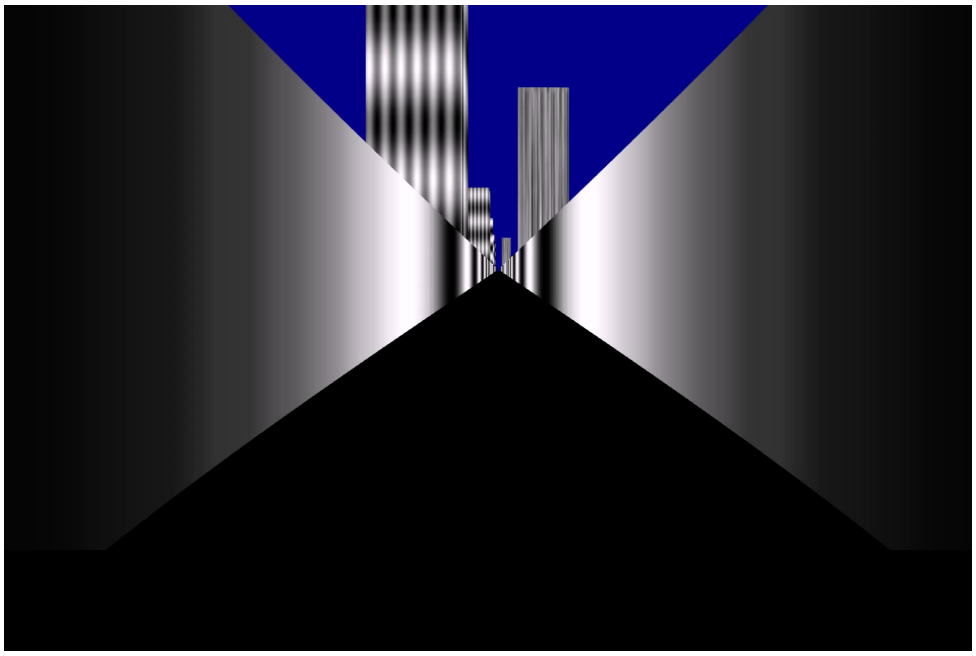

Figure 2.11: Point-of-view of a mouse navigating in the OVR system.

2.2.3 Neural recordings: Electrophysiology

Despites the fact that behavioral data is rich in revealing aspects of spatial learning, the ultimate purpose for this system is to allow neural recordings in behaving animals, as only that allows to uncover the neural mechanisms involved in olfactory-cued spatial learning and navigation. To assess the viability of using intracranial recording techniques in behaving animals operating this system, it was set up in an air table inside a Faraday cage and an electronic micromanipulator (National Instruments) was fitted laterally to the running wheel to secure a Neuropixels 1.0 probe (imec). Acquisition hardware (National Instruments) was installed and a second computer was used exclusively to run the acquisition software (SpikeGLX, (https://github.com/billkarsh/SpikeGLX/blob/master/README.md). The behavioral data recorded in the same computer that runs the OVR experience and the neural data are synchronized via TTL signals produced and timestamped by the HARP board that are recorded in the second computer simultaneously with the neural data, with the recording instrumentation achieving a sampling rate of $30\,\mathrm{kHz}$.

After the previous experiments, an additional mouse that was not trained in the OVR system was placed on the rig while anesthetized in order to avoid subjecting the animal to a stressful and potentially overwhelming setting it hasn't experienced previously. Nonetheless, all the equipment in the system was turned on and the OVR task described was running during the acquisition in order to control for sources of electrical noise, thus assessing usage of this system in proper experimental scenarios. Conveniently, the breathing sensor in the system allows for online monitoring the level of anesthesia of the mouse.

The recording probe was then acutely implanted on the mouse at the following anatomical coordinates relative to Bregma: $2.1\,\mathrm{mm}$ posterior, $1.5\,\mathrm{mm}$ lateral, $2.5\,\mathrm{mm}$ ventral (Figure 2.12 for a coronal view, Appendix .3.2 for a sagittal view). As the neuropixels probe has hundreds of electrodes spanning a $10\,\mathrm{mm}$ long shank, this would ensure that we could record cells from Hipp, which is a very active brain region even under anesthesia, by vertical implantation of the probe.

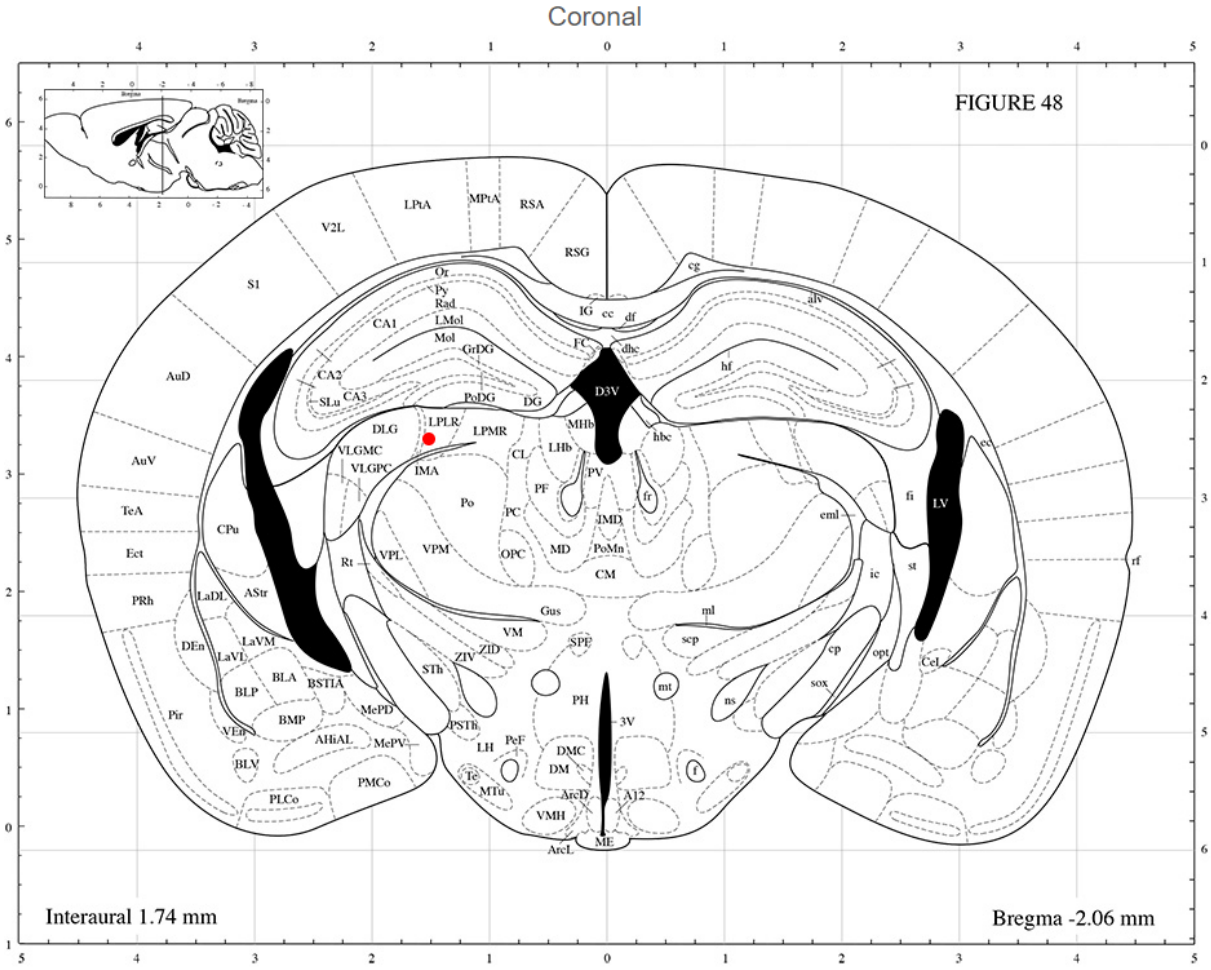

Figure 2.12: Coronal view of the approximate recording coordinate. This figure was generated using `http://labs.gaidi.ca/mouse-brain-atlas/`

2.2.4 Neural recordings: Photometry

A final experiment was carried out in the context of a different research project at the Systems Neuroscience Lab that aims to uncover the neural mechanisms by which serotonin could modulate certain aspects of cognition such as expectation; the aim of this prototype experiment was to investigate whether this OVR system was suitable for research investigating such processes.

A transgenic mouse deriving from a SERT-Cre line expressing GCaMP7f was trained to operate the OVR system. Mice from this genetic line express the fluorescent protein GCaMP7f only in neurons that contain the SERT gene (serotonin transporter gene) by means of Cre-Lox recombination. This protein binds to calcium ions that transverse the neuron's membrane, becoming fluorescent, such that the fluorescence of a neuron is proportional to the flow of calcium ions through its transmembrane channels - the dynamics of calcium flow through the neuronal membrane are mechanistically involved in firing an action potential. Hence, by subsequently implanting an optical fiber in a SERT neuron population, one can record the neuronal population activity by means of photometry (Li et al., 2019), as opposed to electrophysiology techniques.

This mouse was allowed *ad libitum* access to a running wheel inside its homecage until the headbar implantation surgery; at that moment the running wheel was removed. After recovering from the surgery, this mouse was handled by the experimenter and was habituated to the OVR system for five days. The mouse was trained to run on a virtual linear corridor identical to the corridor shown in Figure 2.11, but

that did not contain visual distal landmarks (as identified in Figure 2.10) nor stimulus or reward events. Thus, the only metric of space that this VE provides to the mouse is the frequency of the texture in the walls of the virtual corridor. This training protocol leverages the rodent's innate propensity for running without the necessity of depriving the animal's access to drinking water.

In this prototype experiment, after the posited training schedule this mouse was head-fixed in the OVR system and the implanted optical fiber connected to recording hardware, and its neural activity was recorded at $100\,\mathrm{Hz}$ while the mouse navigated the VE just described. However, for this experimental session a stimulus was introduced consisting of manipulating in a non-cued, unpredictable manner the gain factor that translates the rotary encoder signal to movement in the VE . This was achieved by automatically setting the gain factor to a value of $1\times$, $0.3\times$ or $3\times$, which would remain in effect for an amount of time T drawn from the following distribution, in seconds (during the training regime the mouse experienced only a gain factor of $1\times$): $T \sim U(90, 180)$

Chapter 3

Results & Discussion

3.1 Mouse training

The group of seven mice required 7-10 training sessions to achieve the desired behavior. During the course of this period, they became able to stay engaged on the VR experience for longer amounts of time, hence running for increasingly larger distances in each session (Figures 3.1 and 3.2). Also, as defined by the training regime, they learn to run for increasing distances between consecutive reward presentations (Figure 3.3).

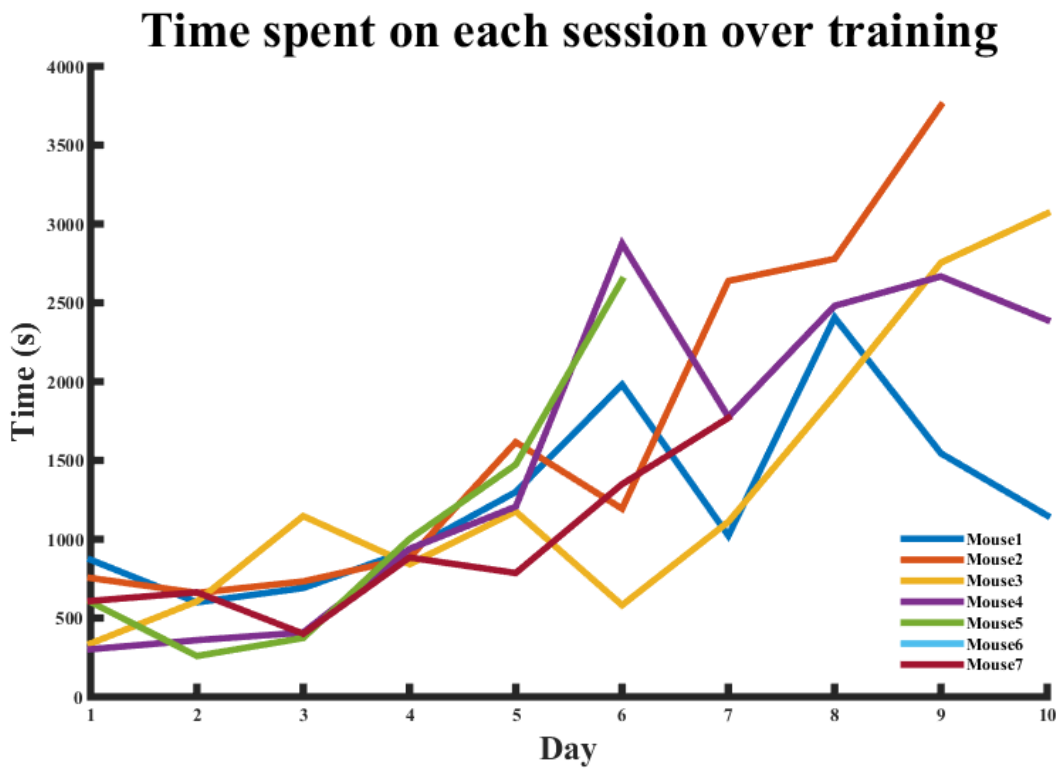

Figure 3.1: Time spent on each session during the training regime. Different lines represent different mice, the unit is seconds.

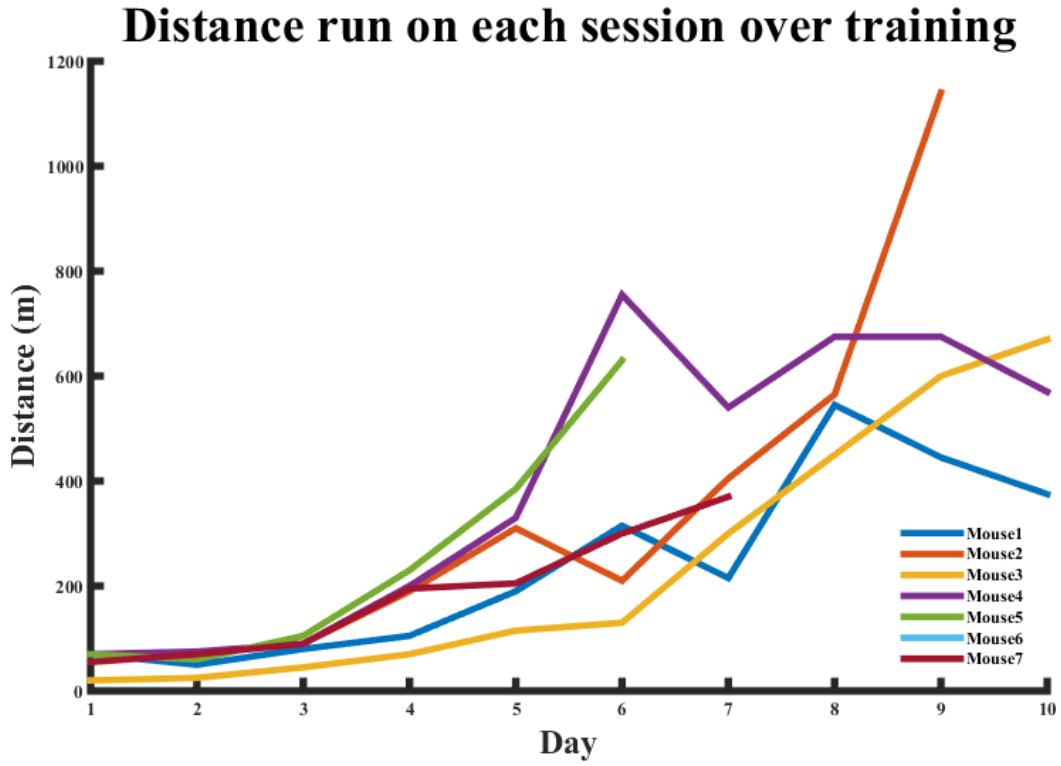

Figure 3.2: Distance traveled on each session during the training regime. Lines represent the same mice as the previous figure, the unit is meters.

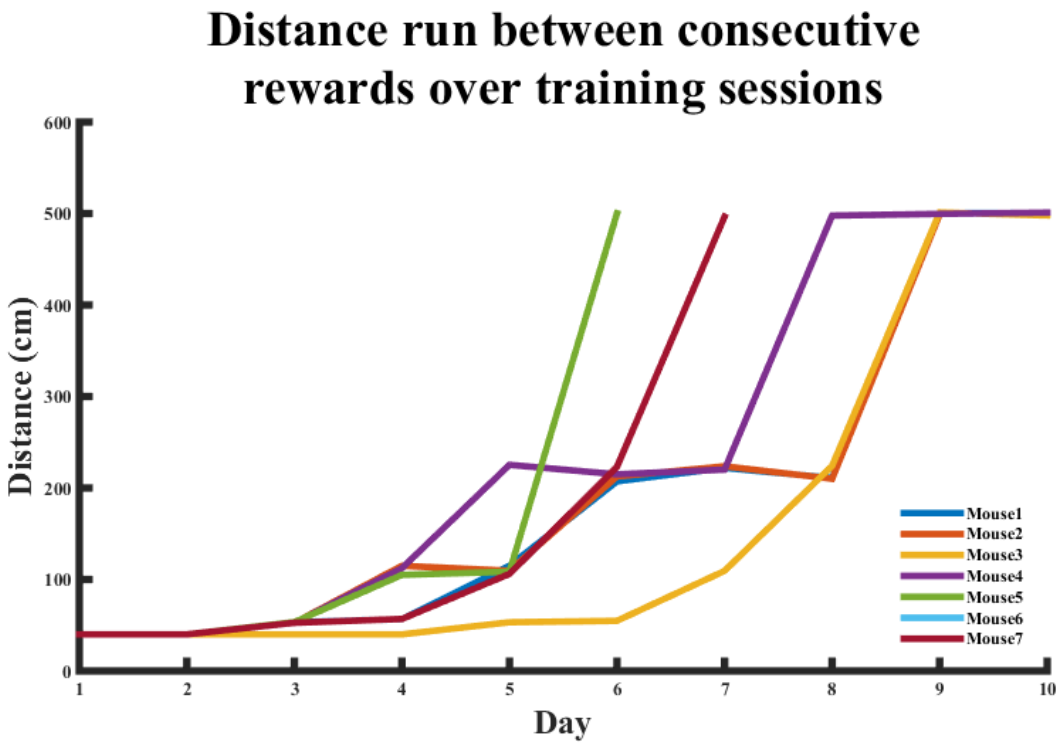

Figure 3.3: Average distance traveled between consecutive reward presentations during the training regime. Lines represent the same mice as the previous figures, the unit is centimeters.

Most importantly, most mice require decreasing amounts of time to complete a single transversal of the VR corridor, showing not only that the animals are comfortable being head-fixed in the OVR system and motivated to engage in the VR experience, but also that they become increasingly more apt in navigating in VR to collect increasingly sparser water rewards (Figure 3.4).

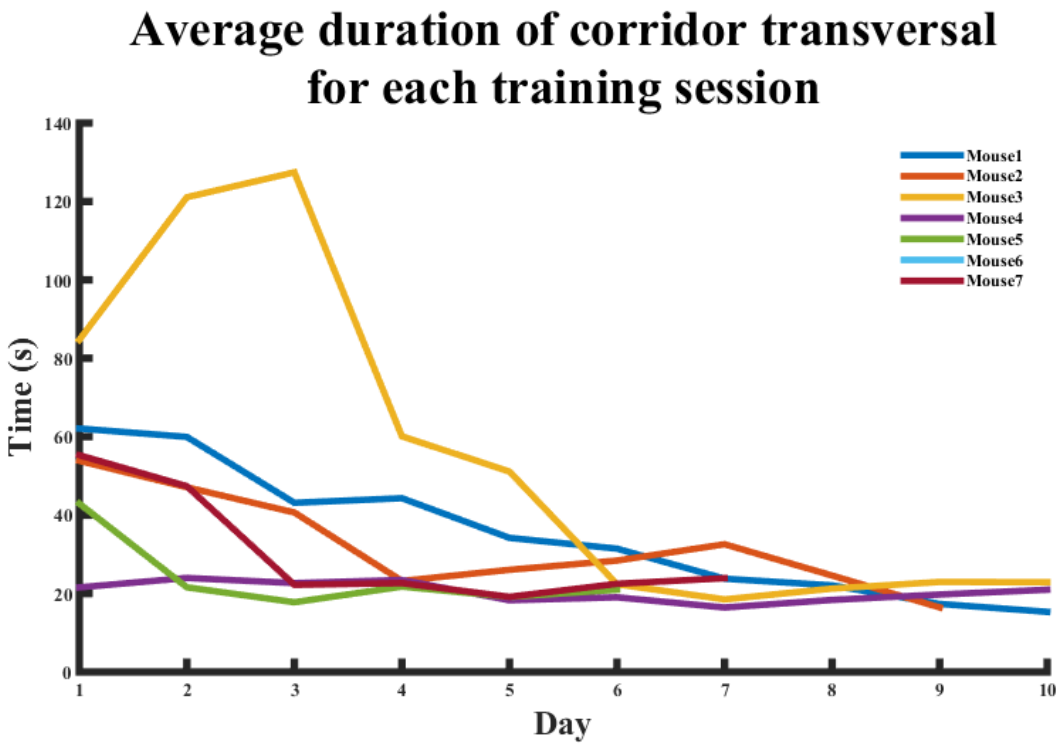

Figure 3.4: Average duration of each lap of the corridor (each trial) during the training regime. Lines represent the same mice as the previous figures, the unit is seconds.

3.2 Mouse behavior

At the time the mice show they are capable to run on the OVR while experiencing a single reward event per corridor transversal (*ie*, per trial), as can be noted of Figure 3.3, they are considered trained and are introduced to the described experimental regime.

On their first session in this regime, the animals should maintain the acquired behavior, being able to run for large distances in the VR at naturalistic speeds. The behavior of two of the mice is shown on Figures 3.5 and 3.6 (and in Appendix .5 for the remaining mice). In addition, the introduction of reward events conditioned by olfactory stimuli should elicit behavioral signatures of learning. Mice are known to be able to quickly learn the location of rewards in spatial tasks, sometimes only after experiencing a couple trials in both real (Vorhees & Williams, 2014) and virtual environments (Chen et al., 2018), so trial-based visualizations of the behavior can reveal the dynamics of learning.

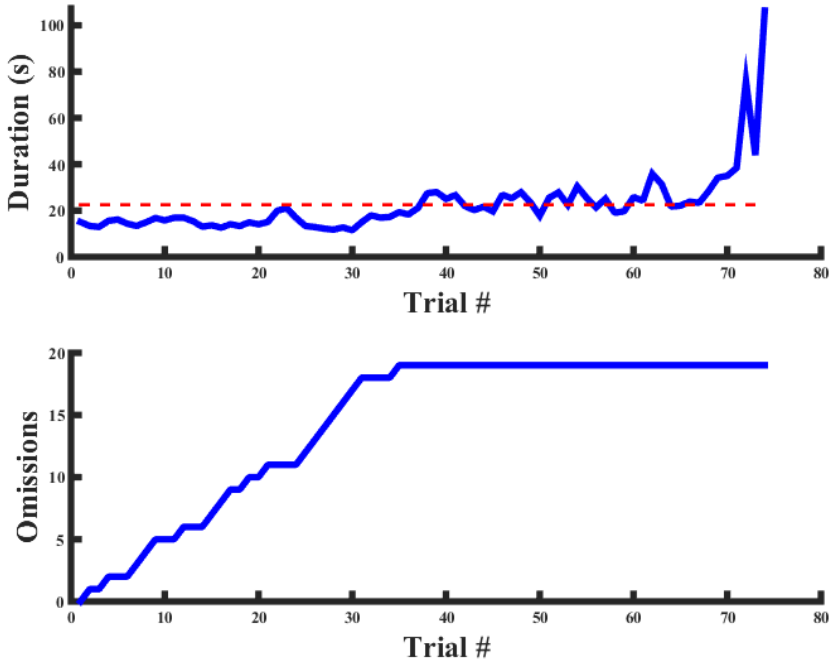

(a) (**Top**) Trial durations (blue solid trace) and average trial duration (red dashed line), in seconds. (**Bottom**) Number of reward omissions during the session.

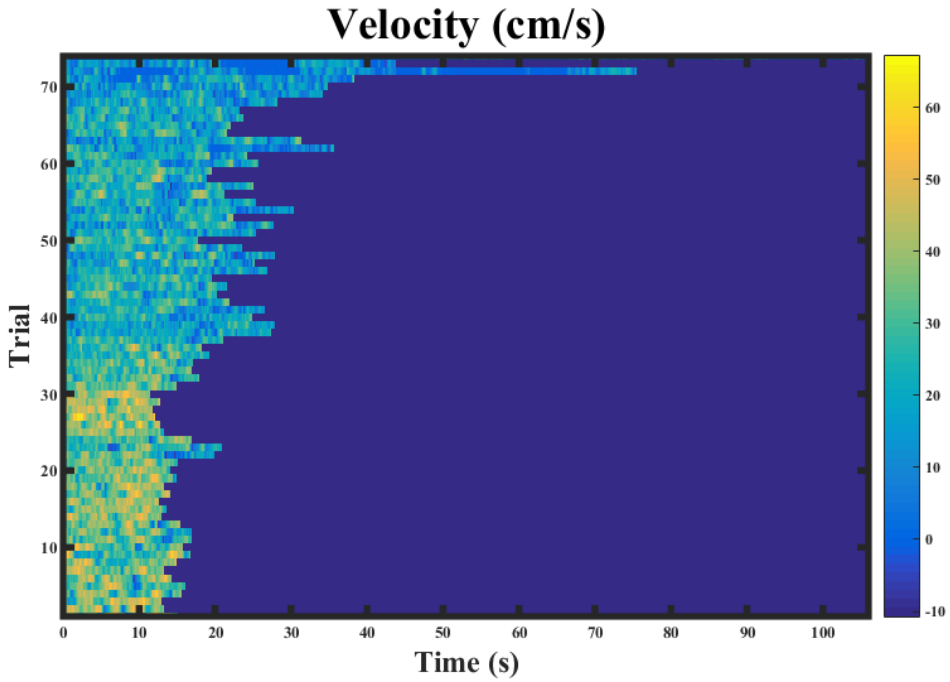

(b) Duration and mouse velocity for each trial. Shorter trials are associated with higher average velocities or less periods of immobility during the session.

Figure 3.5: Behavioral summary of the first session of mouse #1 in the experimental regime.

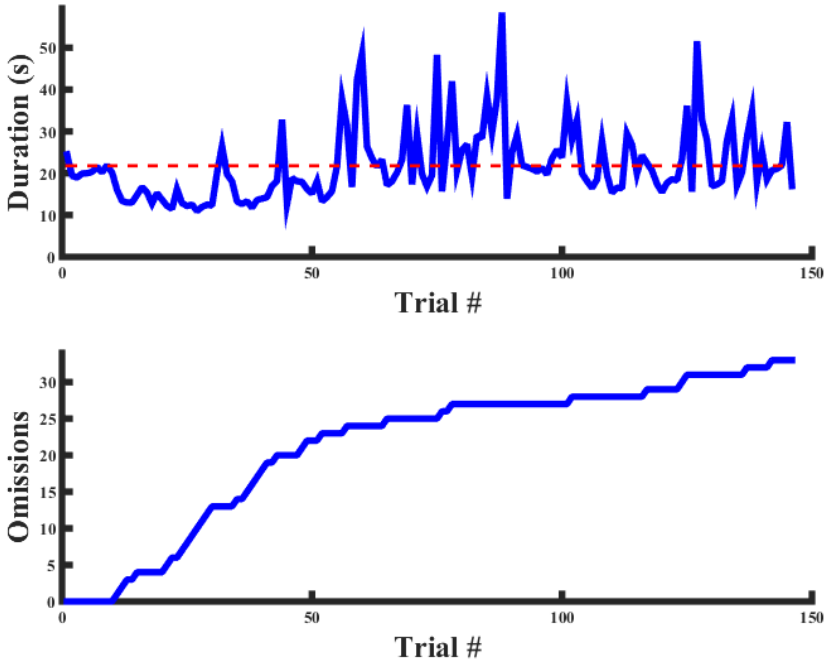

(a) (**Top**) Trial durations (blue solid trace) and average trial duration (red dashed line), in seconds. (**Bottom**) Number of reward omissions during the session.

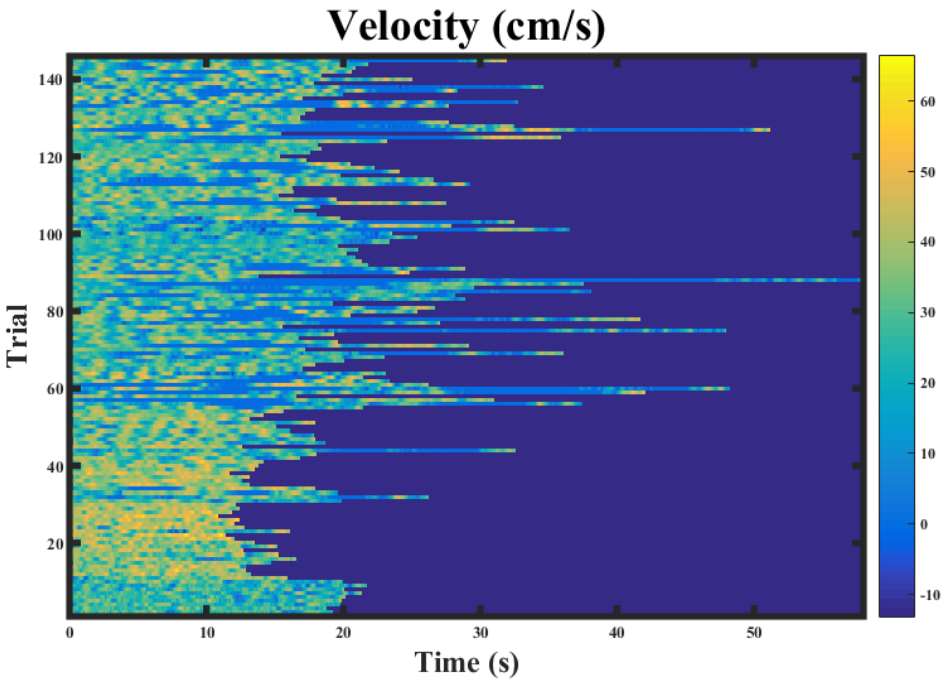

(b) Duration and mouse velocity for each trial. Shorter trials are associated with higher average velocities or less periods of immobility during the session.

Figure 3.6: Behavioral summary of the first session of mouse #2 in the experimental regime.

If the mice are learning the stimulus-reward associations during the course of the session, they should show, after some trials, an increased breathing rate in response to olfactory stimulus presentation as it is informative of reward location (Figure 3.7, and their velocity should decrease as they are arriving at the reward location in order to minimize reward omissions triggered by the previously mentioned velocity criterion.

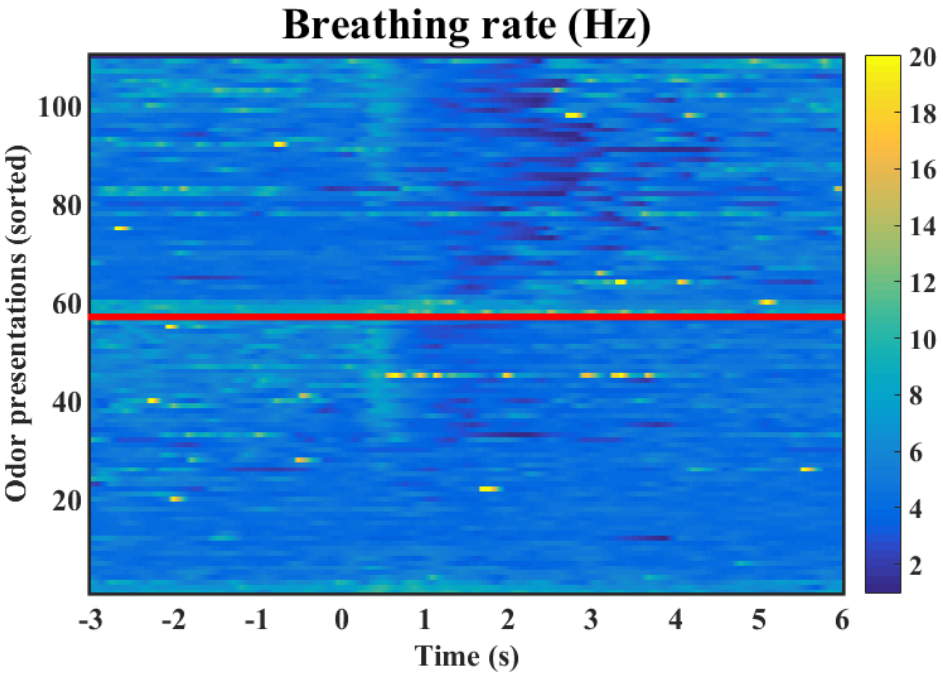

Figure 3.7: Breathing rate of mouse #3 aligned in time to individual odor presentations (stimuli) for the two non-probe trial types. Trial types are separated by the red line and are sorted in increasing order for each type. Odors are presented at $Time = 0$ (zero).

In order to better describe the running behavior of the animals, their velocity is analyzed in both time and space. Time based visualizations allow to estimate the duration of and latency between running bouts, and are especially useful when the visualization is aligned to events of interest such as stimulus or reward presentations, while space based visualizations better capture their behavior respective to locations of interest (Figures 3.8, 3.9 and 3.11).

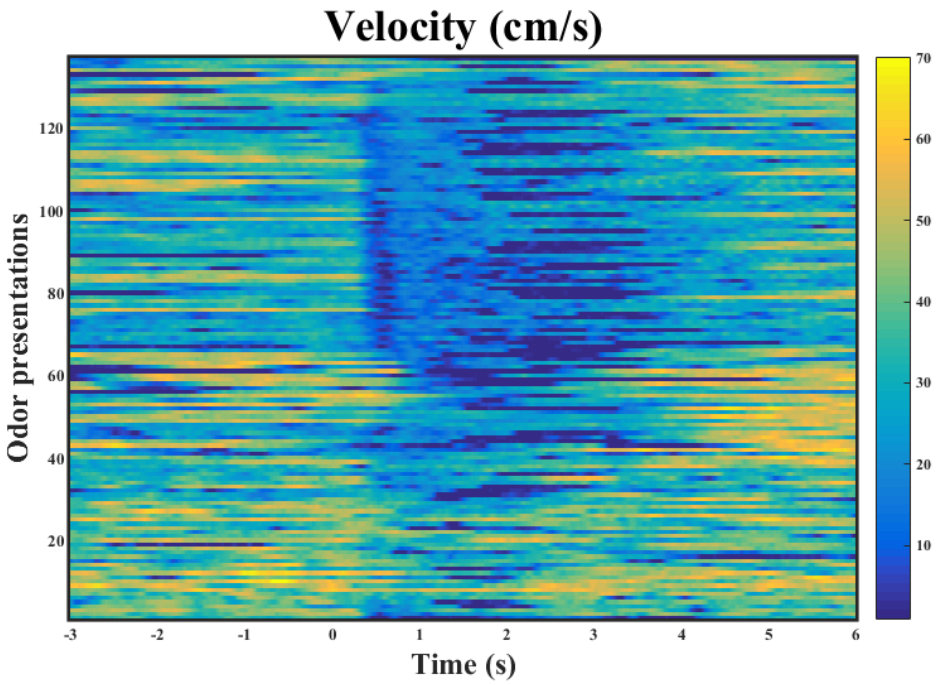

Figure 3.8: Velocity of mouse #2 aligned in time to individual odor presentations (stimuli). Odors are presented at $Time = 0$ (zero).

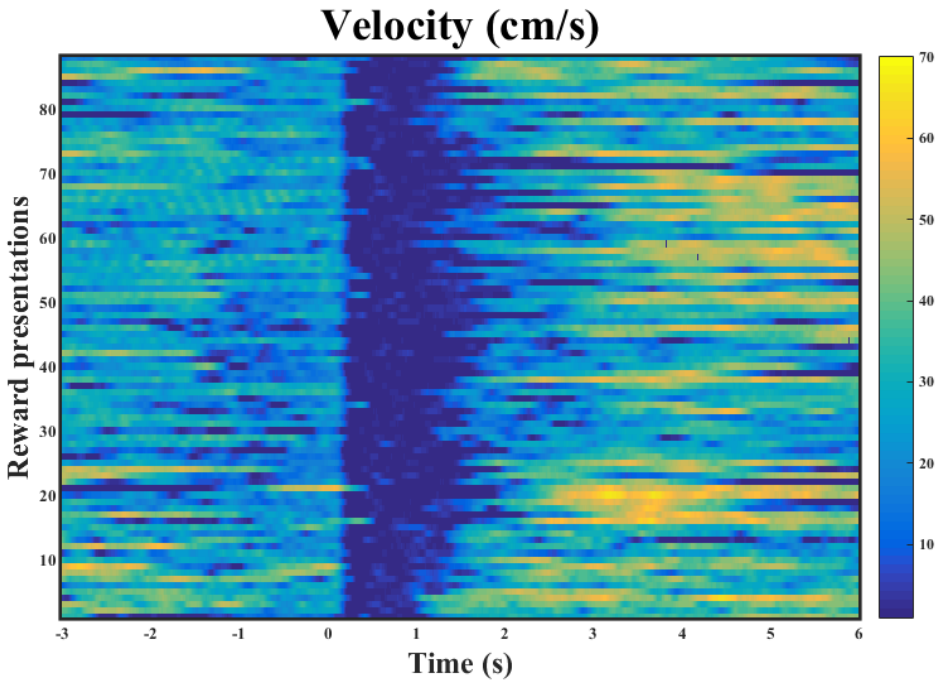

Figure 3.9: Velocity of mouse #2 aligned in time to individual reward presentations. Rewards are presented at $Time = 0$ (zero).

On their first session in the complete OVR experience, ie, when olfactory stimuli are introduced, mice display diverse behaviors as can be seen on the two exemplary mice shown on Figures 3.5 and 3.6. Mouse #2 initially runs at generally high velocities, but then reduces its overall velocity and starts stopping for greater amounts of time at some point in the session, just before trial 60 (Figure 3.6b). It

seems that it also starts running at high velocities only at specific moments in the trials, maintaining a generally reduced velocity otherwise, and engages in this behavior for some trials. In similar manner, mouse #1 also runs at generally high velocities for the initial portion of the session, until around trial 30, and then reduces its overall velocity (Figure 3.5b). However, it maintains a reduced variance in its corridor transversal, and does not stop for long amounts of time, in contrast to the previous exemplary mouse, as can be seen in Figure 3.5a. Also in contrast with that animal, after trial 30 this mouse is able to collect almost all possible rewards.

Although these mice show different variances in the amounts of time they need to transverse the OVR corridor, their average duration of transversal is similar, and also the slopes of their omission curves are identical (Figures 3.5a and 3.6a), possibly reflecting similar learning rates despite varying behavioral strategies. However, a low omission rate doesn't show by itself successful learning of the odor-cued reward contingency, as maintaining an overall low velocity through the length of the corridor effectively leads to reward presentation.

In order to analyze if mice are actually paying attention to the olfactory dimension of the VR experience, their breathing signal is recorded and processed as previously described. In Figure 3.7, the breathing rate of mouse #3 is shown aligned in time to individual odor presentations. As there are two possible locations for odor presentation (two non-probe trial types, S1R1 and S2R2), individual stimuli presentations are sorted in sequential order into the two groups separated by the red trace, in order to compare possible effects of the location of stimulus presentation in learning and behavior. It should be noted that the latency between the olfactory stimulus being triggered on by the olfactometer and it reaching the end of the stimulus tube by the mouse's rostrum is $\sim 50\,\mathrm{ms}$ (Figure 2.9).

It can be observed that this mouse did not display changes in the breathing rate specific to odor presentations in the initial half of the session, and then started increasing its breathing rate in response to the stimuli in similar manner for both trial types. The bouts of reduced breathing rate that can be seen on the top half of the figure are respective to reward consumption in the S2R2 trial type, where the stimuli and reward events are separated by a small distance. This increase in breathing rate from a baseline value of around $4\,\mathrm{Hz}$ to 6-$10\,\mathrm{Hz}$ in response to odor presentation is inline with the breathing dynamics that can be observed in freely-moving rodents performing olfactory discrimination tasks (Kepecs et al., 2007).

Finally, if mice have learned the reward contingency, they should show in their running behavior signs of the expectation of odors and/or rewards at their respective locations, which should translate into reduced velocities as the animals reach those locations, and higher velocities otherwise (Figure 3.9). A decrease in the running velocity of the mouse accompanied by an increase of its breathing rate is a definite behavioral marker of odor sampling and reward consuming behaviors.

Similarly to the breathing rate visualization, the velocity signal can also be aligned to events of interest to observe the animal's running behavior as they approach and leave the locations of these events. In Figure 3.8, it can be observed that the mouse maintains general high velocities both before and after individual stimulus events, however, it begins stopping for a moment when stimuli are presented after trial 60, potentially showing the animal is learning that it should pay attention to the olfactory stimulus. Sorting the trials by trial type reveals there are no significant differences in this behavior regarding stimulus location (Figure 3.10).

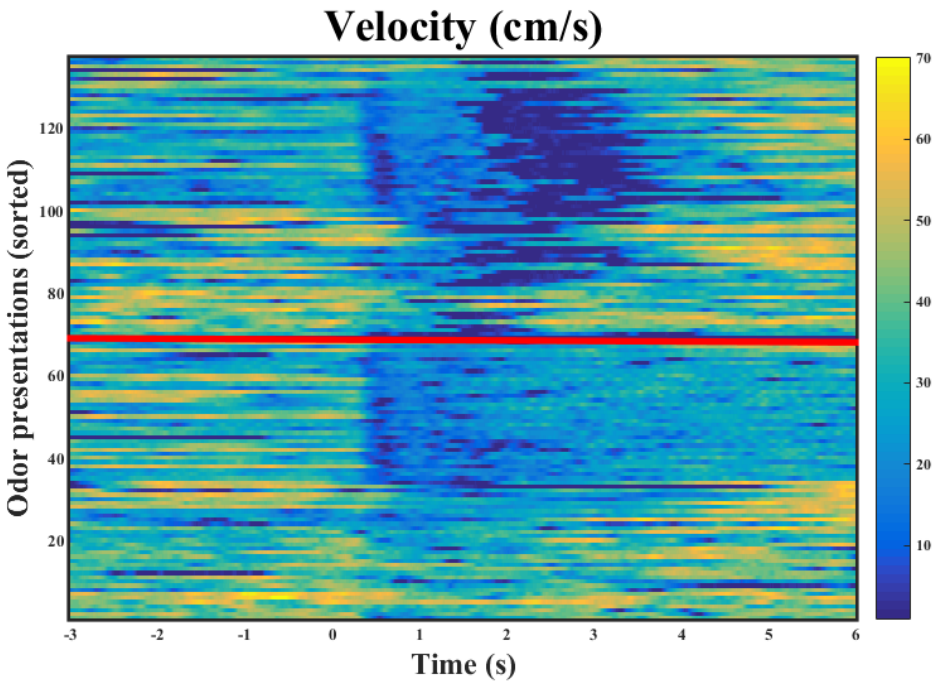

Figure 3.10: Velocity of mouse #2 aligned in time to individual odor presentations (stimuli), sorted by trial type. Trial types are separated by the red line and are sorted in increasing order for each type. Odors are presented at $Time = 0$ (zero).

Grouping the trials according to the location of the stimulus presentation allows the comparison of the two odor-cued trial types (Table 2.1), and reveals the animal does not show a bias for one stimulus location over the other. As for reward events, it can be seen in Figure 3.9 that the mouse has an initial high velocity approaching the reward location, but stops doing so at around trial 25, and maintains a generally high velocity leaving the reward location throughout the whole session. In trials 25-50, the mouse showed an overall reduced velocity approaching the reward location.

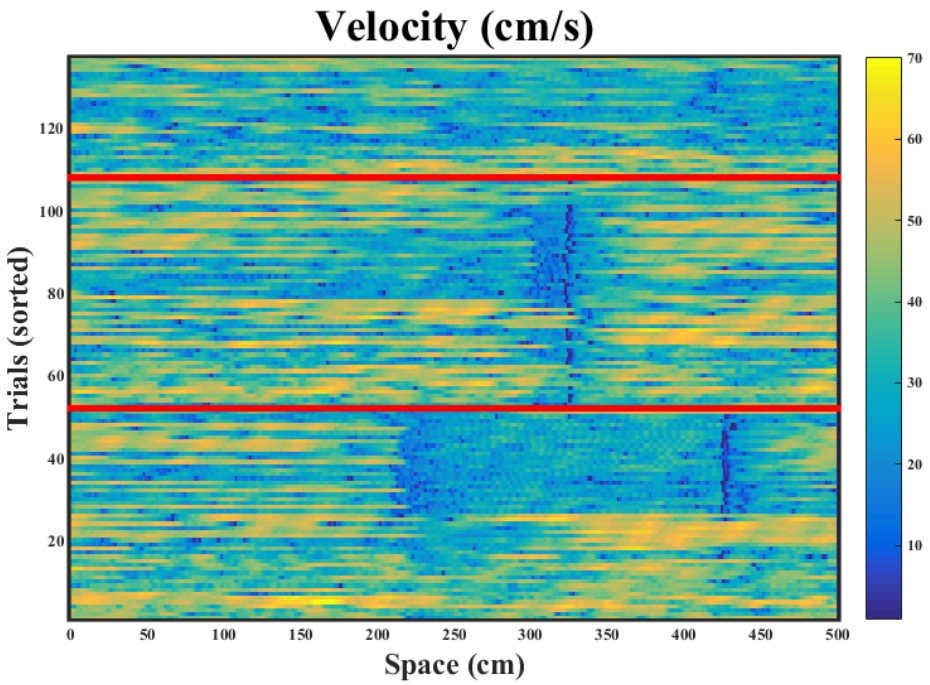

Figure 3.11: Velocity profile of mouse #2 on the length of the VR corridor. Trial types are separated by the red lines and are sorted in increasing order for each type. Bottom: S1R1 trials; middle: S2R2 traials; top: probe trials

Due to the length of the virtual corridor, the presence of visual landmarks at different locations of the environment, and the set of different locations for stimulus and reward presentations, a spatial visualization of the running behavior can be useful to analyze how specific spatial locations, even if not cued, can potentially be used by the mouse to more efficiently navigate. Also, as the experimental task is simple, the animals' running behavior in the different trial types should be stereotyped once they learn a rewarded navigation strategy. In Figure 3.11, the running behavior of mouse #2 is shown for the three trial types. It can be observed that the mouse initially run at high velocities through the corridor. However, at around trial 25 of the S1R1 condition, it started slowing down at the stimulus location, and maintained a reduced velocity until it reached the reward location. Interestingly, the mouse seemed to replicate that behavior in the S2R2 condition, at least for some trials, until it returned to the same behavior it was showing in that condition. However, a reduced velocity at the stimulus location that emerges on these trials seems to persist past them.

Collectively, these figures show that this system is capable of recording fine aspects of spatial behavior as mice engage in the OVR experience. Some of the high velocity values reported here are on the higher end of the spectrum of velocities mice naturally run at; however, the relevancy of this data in studying spatial learning and navigation is not related to the absolute velocity values mice run at. Rather, its the dynamics of the velocity trace in each trial, and across trials during the session, that are useful for interpretation of the spatial behavior. This behavioral data is fundamental for evaluating the spatial performance of animals and, when analyzed with the accompanying neural activity, should provide insights about the neural mechanisms mediating olfactory-cued spatial learning processes.

3.3 Mouse neural activity: electrophysiology

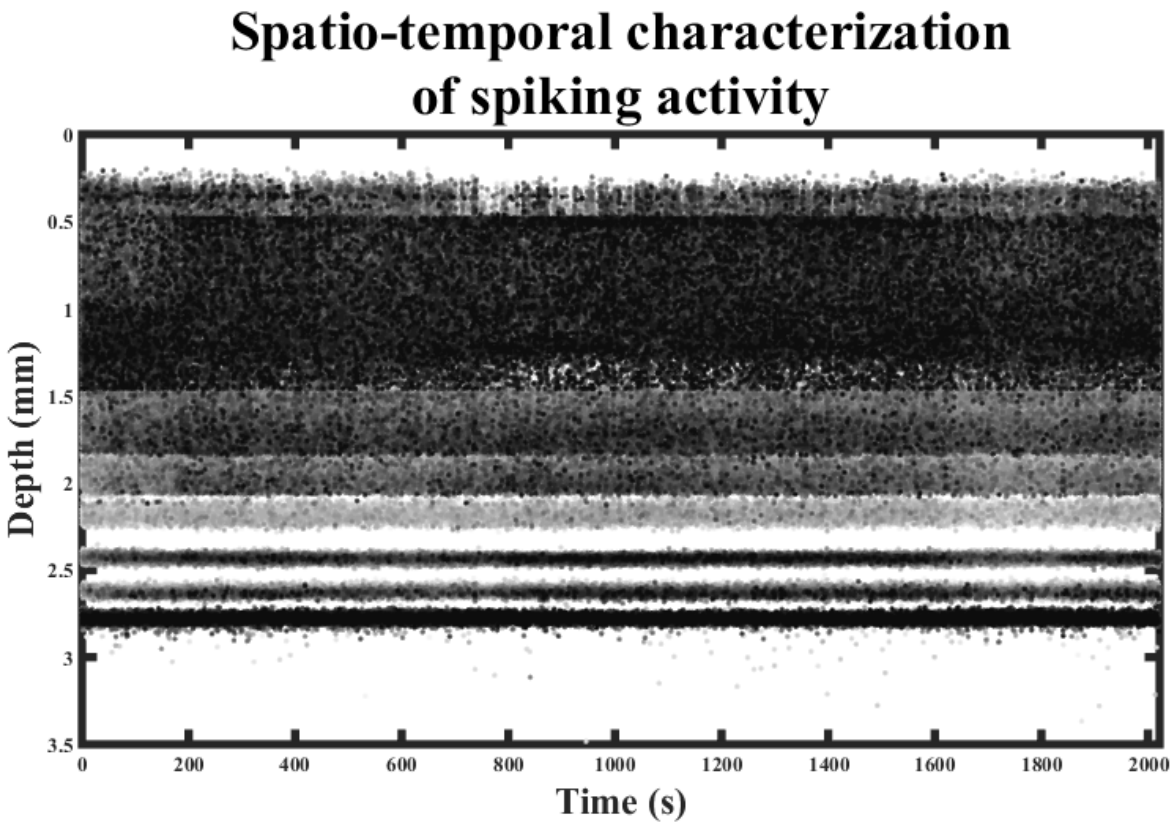

Figure 3.12: Characterization of spiking activity. Each dot represents the depth position (mm) and time (s) of each recorded spike (action potential) during the session.

The viability of this system in recording neural activity from behaving animals was assessed by recording from an anesthetized mouse head-fixed in the experimental rig. Thousands of individual spiking events were recorded at multiple depths of the mouse's brain without any apparent drifting of the probe (Figure 3.12). The system provides enough stability and low-enough levels of electrical noise that it enables the simultaneous recording of the spiking activity of many individual neurons when the animal is performing in the OVR task.

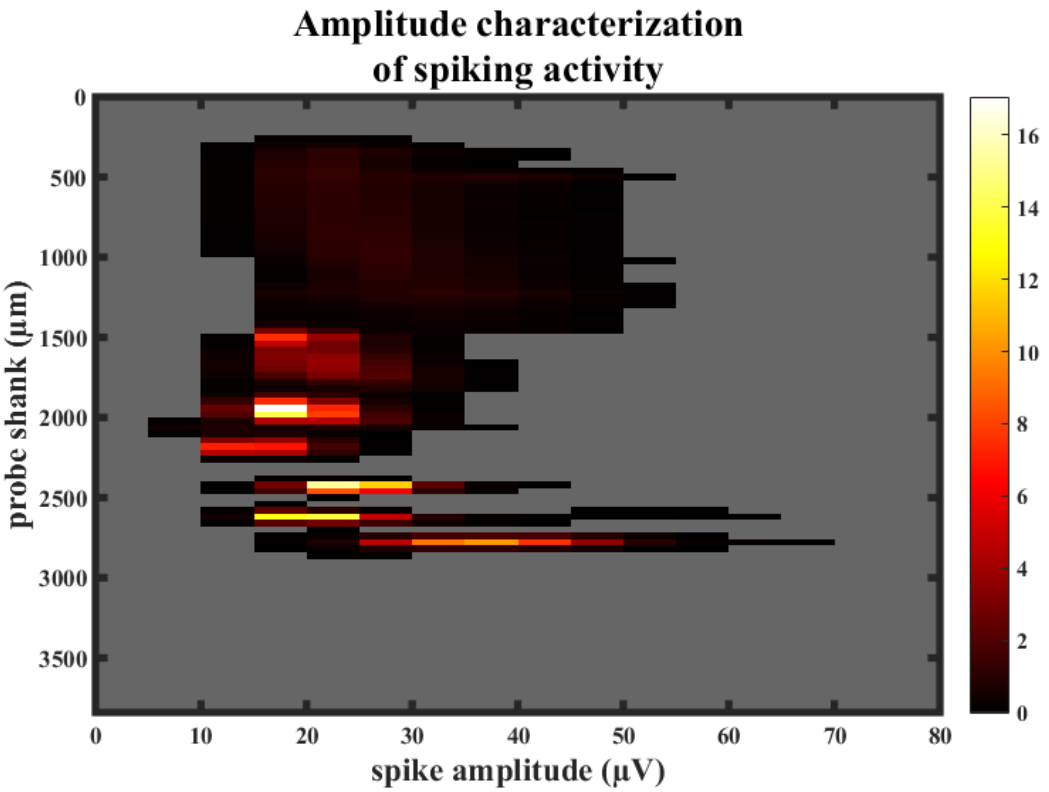

Figure 3.13: Characterization of spiking amplitude. Color represents the number of spikes recorded of a given amplitude along the length of the probe shank.

As expected due to the positioning of the recording probe (Figure 2.12), the majority of the recorded spikes lie within the expected range of positions that the Hipp would span along the probe shank (Figure 3.13). The actual positioning of the probe in the mouse's brain could unfortunately not be verified in the histology analysis of the brain. Despites that, this result suggests that the probe was indeed recording from the Hipp. In any case, the aim of this experiment was to show that the system enables stable and sufficiently noise-free recordings of neural activity regardless of the target brain area.

3.4 Mouse neural activity: photometry

The photometry system's output signal is a time series containing the light intensity value recorded at the implanted optic fiber tip for each time point in the acquisition. In order to generate a time visualization where this signal is aligned to individual stimulus events (Figure 3.14) that allows for the comparison of the neural activity dynamics across trials, the photometry signal is baseline corrected for each stimulus presentation (Appendix .3.4).

A systematic increase in the neuron population activity can be observed in response to the stimuli, suggesting that the targeted brain region is involved in the representation of unexpected events as the stimuli were not cued and provided to the mouse at random moments during the experimental session.

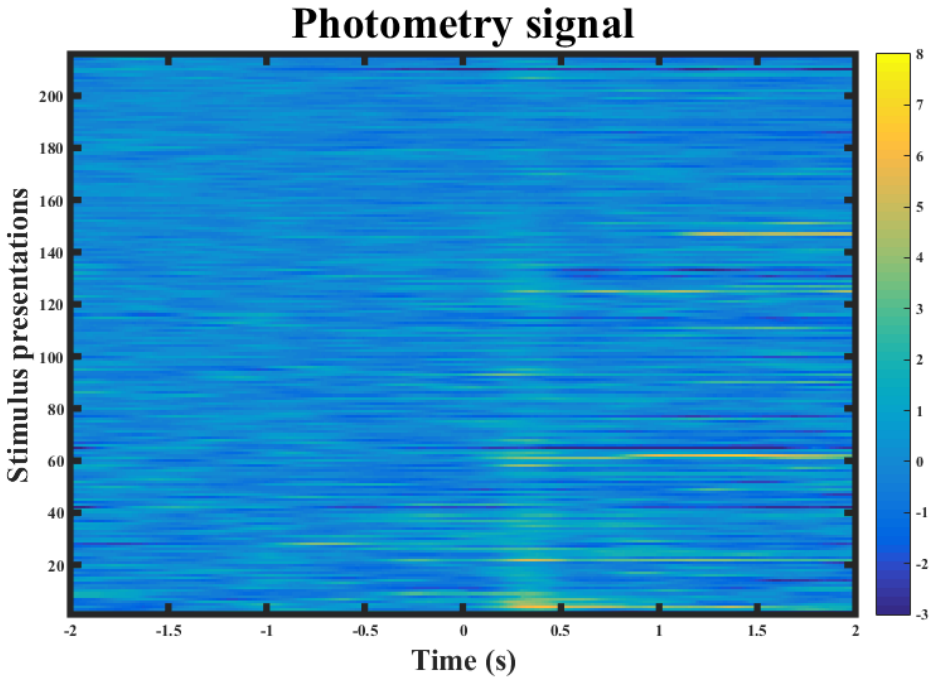

Figure 3.14: Photometry signal of a neuron population recorded in a mouse operating the OVR system. Olfactory stimuli are presented at $Time = 0$ (zero).

This additional experiment confirmed that the OVR system is apt for both electrical and optic techniques of recording neural activity in behaving animals in tasks of different nature, showing that multiple domains of research within neuroscience could profit from this kind of system.

Chapter 4

Conclusion

In summary, the mice are able to navigate in virtual environments on the OVR system, and it can be used to record diverse sources of behavioral and neural data from animals operating it, as shown. They voluntarily engage in the OVR task to collect water rewards and display a wide range of running speeds and naturalistic breathing rates during the course of many virtual corridor transversals. Olfactory stimuli and reward events are generated in a temporally precise manner and their delivery is controlled only by the movement of the animal as required by the closed-loop condition.

The fact that animals are trained in non olfactory-cued and olfactory-cued VR corridors on the same system allows fair comparisons of the behavior and neural activity of the animals in those sessions, potentially revealing differences in non olfactory-cued and olfactory-cued navigation, as well as comparisons of the neural activity across individual animals that show diverse behaviors, possibly reflecting different learning rates or navigation strategies, which is of great importance for the study of spatial learning specifically.

Additional avenues of research within olfactory-cued spatial navigation can already be implemented on this system, as it has built-in capabilities for using multiple odorants (or mixtures of odorants) as the olfactory stimuli, as these are limited by the olfactometer capabilities, or using air 'puffs' (an intense, short duration blow of air to the mouse's face), which are commonly used as aversive stimuli. 'On-the-fly' manipulations to the visual aspect of the VR are also possible, for example by spatially shifting a visual landmark, allowing to segregate mice that learn to navigate relying mostly on egocentric information from those who rely mostly on allocentric information.

Not only, as shown, the system allows recording neural signals of different nature from the whole brain, opening many research avenues as any behavioral task that requires running by the animal can be implemented on this system. It allows for studies of sensorimotor integration without any changes to hardware as the OVR experience by itself is able to engage with the sensorimotor system more than the sample stimuli that are commonly used in labs in such experiments. It can also be easily modifiable/expandable to include other sensory modalities, enabling studies of sensory perception and multisensory integration, for example by including an audio speaker to provide auditory stimuli, or to control for and potentially manipulate other environmental variables such as the air temperature or oxygenation levels inside the training box. In an analogous manner to neural recording tools, optogenetic or electric neural stimulation tools can also be easily accommodated in the system and controlled in a closed-loop manner by the VR engine.

Collectively, these methodological possibilities enable using this system in a wide range of behavioral tasks, including ones that are not about spatial navigation *per se*, but just require running by the animal. For example, neural mechanisms of decision-making can be studied by designing a T-shaped corridor,

where the mouse must navigate towards the left or right arm of the corridor depending on some learned cue. The additional dimension of the VR can be introduced by tracking the body posture of the mouse in order to infer its intended turning direction, or by physically replacing the running wheel with a running ball and adjusting the processing pipeline that generates the movement signal to account for the new dimension. Sensorimotor integration can be studied in this system as it makes it simple to manipulate the movement signal in both an open and closed-loop fashion, thus enabling disentangling the optic flow signal from proprioceptive signals. The fact that the animal's experience is generated by a VR engine also makes it easy to produce unrealistic/unnaturalistic stimuli, introducing a conflict with an animal's previous experience of the world, which enables experiments in the domain of cognition and expectation.

Naturally, one cannot quantitatively determine to what degree the animals perceive the virtual reality experience as actual reality. It is possible that the animals regard the VR task as a kind of game where they can run and collect rewards, however, the similarities in behavior and spatially modulated neural activity between animals freely navigating and animals navigating in VR that can be observed here and in the existing literature qualitatively suggests that they indeed feel immersed in the virtual environment (Chen et al., 2018; Aronov & Tank, 2014; Gray et al., 2002). The addition of other sensory modalities should contribute to the sensation of immersion by adding new dimensions of sensory feedback from the environment, namely a tactile dimension as mice are nocturnal animals that use their whiskers to 'touch' and feel objects in the environment (Sofroniew et al., 2014).

Improvements in the animal's sensation of immersiveness may be possible in the future. In what gives respect to VE design, increasing knowledge about animal visual perception should inform an improved design of the visual aspect of the environment to seem more naturalistic to the mouse, as the goal with research using VR is to generate behavior and accompanying neural activity that resembles what occurs in the real world, regardless of how realistic the VEs appear to humans. Head and body-fixation certainly disrupts the vestibular system and possibly other mechanisms of idiothetic information (Thurley & Ayaz, 2017), so new insights about how this kind of information is processed in the brain and affects behavior should lead to the design of less disrupting restraint methods that still enable the use of recording techniques that are sensitive to motion artifacts. Improvements in animal handling and training protocols should make the animals more apt to feel immersed in the VE by diminishing states of stress, anxiety or discomfort, and facilitating states of attention and motivation.

Finally, the system's modular nature and reliance on open-source or commercially available tools potentiates its generalized use by different research groups as that facilitates implementing modifications to the hardware or the olfactory virtual reality task previously described. For example, any running wheel geometry can be used as it is defined as a parameter within the Bonsai script that processes the rotary encoder signal and generates the virtual position signal. Not only, as there is only a single call to this script within the main Bonsai routine running the OVR experience, one can define a new, custom Bonsai routine to generate a virtual position signal from any kind of device measuring movement of the animal.

The final photometry recording experiment demonstrates precisely that the modular aspect of the system can greatly contribute not only to standardization of methodologies across domains of neuroscience and ethology research, therefore also contributing to replicability of the experiments, it also enables the characterization of similarities in behavior and neural activity of animals performing fundamentally different tasks, and the potential usage of the same animals in parallel experiments as they can take place on the same experimental system.

Bibliography

Aboitiz, F., & Montiel, J. F. (2015). Olfaction, navigation, and the origin of isocortex. *Frontiers in Neuroscience*, *9*.

Ache, B. W., & Young, J. M. (2005). Olfaction: Diverse Species, Conserved Principles. *Neuron*, *48*(3).

Aronov, D., & Tank, D. W. (2014). Engagement of neural circuits underlying 2D spatial navigation in a rodent virtual reality system. *Neuron*, *84*(2).

Astur, R. S., St. Germain, S. A., Baker, E. K., Calhoun, V., Pearlson, G. D., & Constable, R. T. (2005). fMRI Hippocampal Activity During a VirtualRadial Arm Maze. *Applied Psychophysiology and Biofeedback*, *30*(3).

Barnes, D. C., Hofacer, R. D., Zaman, A. R., Rennaker, R. L., & Wilson, D. A. (2008). Olfactory perceptual stability and discrimination. *Nature neuroscience*, *11*(12).

Bianco, I. H., Kampff, A. R., & Engert, F. (2011). Prey Capture Behavior Evoked by Simple Visual Stimuli in Larval Zebrafish. *Frontiers in Systems Neuroscience*, *5*.

Bittner, K. C., Milstein, A. D., Grienberger, C., Romani, S., & Magee, J. C. (2017). Behavioral time scale synaptic plasticity underlies CA1 place fields. *Science*, *357*(6355).

Cazettes, F., Reato, D., Morais, J. P., Renart, A., & Mainen, Z. F. (2021). Phasic Activation of Dorsal Raphe Serotonergic Neurons Increases Pupil Size. *Current Biology*, *31*(1).

Chen, G., King, J. A., Lu, Y., Cacucci, F., & Burgess, N. (2018). Spatial cell firing during virtual navigation of open arenas by head-restrained mice. *eLife*, *7*.

Chen, Y., Chen, X., Baserdem, B., Zhan, H., Li, Y., Davis, M. B., Kebschull, J. M., Zador, A. M., Koulakov, A. A., & Albeanu, D. F. (2021). Wiring logic of the early rodent olfactory system revealed by high-throughput sequencing of single neuron projections. *bioRxiv*.

Chin, S. G., Maguire, S. E., Huoviala, P., Jefferis, G. S. X. E., & Potter, C. J. (2018). Olfactory Neurons and Brain Centers Directing Oviposition Decisions in Drosophila. *Cell Reports*, *24*(6).

DeBose, J. L., & Nevitt, G. A. (2008). The use of odors at different spatial scales: comparing birds with fish. *Journal of Chemical Ecology*, *34*(7).

Dombeck, D. A., & Reiser, M. B. (2012). Real neuroscience in virtual worlds. *Current Opinion in Neurobiology*, *22*(1).

Eichenbaum, H. (2017). The role of the hippocampus in navigation is memory. *Journal of Neurophysiology*, *117*(4).

Etienne, A. S., & Jeffery, K. J. (2004). Path integration in mammals. *Hippocampus*, *14*(2).

Fischler, W. M., Joshi, N. R., Devi-Chou, V., Kitch, L. J., Schnitzer, M. J., Abbott, L. F., & Axel, R. (2021). Olfactory Landmarks and Path Integration Converge to Form a Cognitive Spatial Map. *Neuron*, *109*(24).

Gagliardo, A. (2013). Forty years of olfactory navigation in birds. *Journal of Experimental Biology*, *216*(12).

Gauthier, J. L., & Tank, D. W. (2018). A Dedicated Population for Reward Coding in the Hippocampus. *Neuron*, *99*(1).

Gray, J. R., Pawlowski, V., & Willis, M. A. (2002). A method for recording behavior and multineuronal CNS activity from tethered insects flying in virtual space. *Journal of Neuroscience Methods*, *120*(2).

Grieves, R. M., & Jeffery, K. J. (2017). The representation of space in the brain. *Behavioural Processes*, *135*.

Haberly, L. B. (2001). Parallel-distributed Processing in Olfactory Cortex: New Insights from Morphological and Physiological Analysis of Neuronal Circuitry. *Chemical Senses*, *26*(5).

Haberly, L. B., & Bower, J. M. (1989). Olfactory cortex: model circuit for study of associative memory? *Trends in Neurosciences*, *12*(7).

Hartley, T., Lever, C., Burgess, N., & O'Keefe, J. (2014). Space in the brain: how the hippocampal formation supports spatial cognition. *Philosophical Transactions of the Royal Society B: Biological Sciences*, *369*(1635).

Harvey, C. D., Coen, P., & Tank, D. W. (2012). Choice-specific sequences in parietal cortex during a virtual-navigation decision task. *Nature*, *484*(7392).

Harvey, C. D., Collman, F., Dombeck, D. A., & Tank, D. W. (2009). Intracellular dynamics of hippocampal place cells during virtual navigation. *Nature*, *461*(7266).

Hepper, P. G., & Wells, D. L. (2005). How Many Footsteps Do Dogs Need to Determine the Direction of an Odour Trail? *Chemical Senses*, *30*(4).

Hodgkin, A. L., & Huxley, A. F. (1952). A quantitative description of membrane current and its application to conduction and excitation in nerve. *The Journal of Physiology*, *117*(4).

Huang, K.-H., Rupprecht, P., Frank, T., Kawakami, K., Bouwmeester, T., & Friedrich, R. W. (2020). A virtual reality system to analyze neural activity and behavior in adult zebrafish. *Nature Methods*, *17*(3).

Isaacson, J. S. (2010). Odor representations in mammalian cortical circuits. *Current Opinion in Neurobiology*, *20*(3).

Jacobs, L. F. (2012). From chemotaxis to the cognitive map: The function of olfaction. *Proceedings of the National Academy of Sciences*, *109*(Supplement 1).

Jacobs, L. F., Arter, J., Cook, A., & Sulloway, F. J. (2015). Olfactory Orientation and Navigation in Humans. *PLOS ONE*, *10*(6).

Johnson, B. A., & Leon, M. (2007). Chemotopic Odorant Coding in a Mammalian Olfactory System. *The Journal of comparative neurology*, *503*(1).

Kepecs, A., Uchida, N., & Mainen, Z. F. (2007). Rapid and Precise Control of Sniffing During Olfactory Discrimination in Rats. *Journal of Neurophysiology*, *98*(1).

Knierim, J. J., & Hamilton, D. A. (2011). Framing spatial cognition: Neural representations of proximal and distal frames of reference and their roles in navigation. *Physiological reviews*, *91*(4).

Krakauer, J. W., Ghazanfar, A. A., Gomez-Marin, A., MacIver, M. A., & Poeppel, D. (2017). Neuroscience Needs Behavior: Correcting a Reductionist Bias. *Neuron*, *93*(3).

Leon, M., & Johnson, B. A. (2003). Olfactory coding in the mammalian olfactory bulb. *Brain Research Reviews*, *42*(1).

Li, Y., Liu, Z., Guo, Q., & Luo, M. (2019). Long-term Fiber Photometry for Neuroscience Studies. *Neuroscience Bulletin*, *35*(3).

Litaudon, P., Amat, C., Bertrand, B., Vigouroux, M., & Buonviso, N. (2003). Piriform cortex functional heterogeneity revealed by cellular responses to odours. *European Journal of Neuroscience*, *17*(11).

Liu, A., Papale, A. E., Hengenius, J., Patel, K., Ermentrout, B., & Urban, N. N. (2020). Mouse Navigation Strategies for Odor Source Localization. *Frontiers in Neuroscience*, *14*.

Lopatina, O. L., Morgun, A. V., Gorina, Y. V., Salmin, V. V., & Salmina, A. B. (2020). Current approaches to modeling the virtual reality in rodents for the assessment of brain plasticity and behavior. *Journal of Neuroscience Methods*, *335*.

Lopes, G., Bonacchi, N., Frazão, J., Neto, J. P., Atallah, B. V., Soares, S., Moreira, L., Matias, S., Itskov, P. M., Correia, P. A., Medina, R. E., Calcaterra, L., Dreosti, E., Paton, J. J., & Kampff, A. R. (2015). Bonsai: an event-based framework for processing and controlling data streams. *Frontiers in Neuroinformatics*, *9*.

Lopes, G., Farrell, K., Horrocks, E. A., Lee, C.-Y., Morimoto, M. M., Muzzu, T., Papanikolaou, A., Rodrigues, F. R., Wheatcroft, T., Zucca, S., Solomon, S. G., & Saleem, A. B. (2021). Creating and controlling visual environments using BonVision. *eLife*, *10*.

Mathis, A., Mamidanna, P., Cury, K. M., Abe, T., Murthy, V. N., Mathis, M. W., & Bethge, M. (2018). DeepLabCut: markerless pose estimation of user-defined body parts with deep learning. *Nature Neuroscience*, *21*(9).

Matsumura, N., Nishijo, H., Tamura, R., Eifuku, S., Endo, S., & Ono, T. (1999). Spatial- and Task-Dependent Neuronal Responses during Real and Virtual Translocation in the Monkey Hippocampal Formation. *Journal of Neuroscience*, *19*(6).

Matthews, D. B., & Best, P. J. (1995). Fimbria/fornix lesions facilitate the learning of a nonspatial response task. *Psychonomic Bulletin & Review*, *2*(1).

Minderer, M., Brown, K. D., & Harvey, C. D. (2019). The Spatial Structure of Neural Encoding in Mouse Posterior Cortex during Navigation. *Neuron*, *102*(1).

Moser, M.-B., Rowland, D. C., & Moser, E. I. (2015). Place Cells, Grid Cells, and Memory. *Cold Spring Harbor Perspectives in Biology*, *7*(2).

Nieh, E. H., Schottdorf, M., Freeman, N. W., Low, R. J., Lewallen, S., Koay, S. A., Pinto, L., Gauthier, J. L., Brody, C. D., & Tank, D. W. (2021). Geometry of abstract learned knowledge in the hippocampus. *Nature*, *595*(7865).

O'Keefe, J. (1976). Place units in the hippocampus of the freely moving rat. *Experimental Neurology*, *51*(1).

Pachitariu, M., Steinmetz, N., Kadir, S., Carandini, M., & Harris, K. (2016). Fast and accurate spike sorting of high-channel count probes with KiloSort. *Advances in Neural Information Processing Systems*, *29*.

Poo, C., Agarwal, G., Bonacchi, N., & Mainen, Z. F. (2022). Spatial maps in piriform cortex during olfactory navigation. *Nature*, *601*(7894).

Priestley, J. B., Bowler, J. C., Rolotti, S. V., Fusi, S., & Losonczy, A. (2022). Signatures of rapid plasticity in hippocampal CA1 representations during novel experiences. *Neuron*, *12*.

Radvansky, B. A., & Dombeck, D. A. (2018). An olfactory virtual reality system for mice. *Nature Communications*, *9*(1).

Radvansky, B. A., Oh, J. Y., Climer, J. R., & Dombeck, D. A. (2021). Behavior determines the hippocampal spatial mapping of a multisensory environment. *Cell Reports*, *36*(5).

Reiser, M. B., & Dickinson, M. H. (2008). A modular display system for insect behavioral neuroscience. *Journal of Neuroscience Methods*, *167*(2).

Sato, M., Kawano, M., Mizuta, K., Islam, T., Lee, M. G., & Hayashi, Y. (2017). Hippocampus-Dependent Goal Localization by Head-Fixed Mice in Virtual Reality. *eNeuro*, *4*(3).

Savelli, F., & Knierim, J. J. (2019). Origin and role of path integration in the cognitive representations of the hippocampus: computational insights into open questions. *The Journal of Experimental Biology*, *222*(Suppl 1).

Sherman, W. R., & Craig, A. B. (2003). *Understanding Virtual Reality: Interface, Application, and Design*. San Francisco, California, USA: Elsevier Science, 1 ed.

Sofroniew, N. J., Cohen, J. D., Lee, A. K., & Svoboda, K. (2014). Natural Whisker-Guided Behavior by Head-Fixed Mice in Tactile Virtual Reality. *Journal of Neuroscience*, *34*(29).

Squire, L., Berg, D., Bloom, F., du Lac, S., Ghosh, A., & Spitzer, N. (2008). *Fundamental Neuroscience*. Elsevier Academic Press, 3rd ed.

Steck, K. (2012). Just follow your nose: homing by olfactory cues in ants. *Current Opinion in Neurobiology*, *22*(2).

Stettler, D. D., & Axel, R. (2009). Representations of Odor in the Piriform Cortex. *Neuron*, *63*(6).

Thurley, K., & Ayaz, A. (2017). Virtual reality systems for rodents. *Current Zoology*, *63*(1).

Vorhees, C. V., & Williams, M. T. (2014). Assessing Spatial Learning and Memory in Rodents. *ILAR Journal*, *55*(2).

Wadhams, G. H., & Armitage, J. P. (2004). Making sense of it all: bacterial chemotaxis. *Nature Reviews Molecular Cell Biology*, *5*(12).

White, J. G., Southgate, E., Thomson, J. N., & Brenner, S. (1986). The structure of the nervous system of the nematode Caenorhabditis elegans. *Philosophical Transactions of the Royal Society of London. B, Biological Sciences*, *314*(1165).

Appendices

In this section, supplementary details about the development and applications of the presented OVR system are shown. Included here are a list of the materials used to build the OVR system and figures of behavioral analysis for all the trained mice.

.1 OVR system design

.1.1 Behavioral interface

Wheel design

The wheel that is used in the presented OVR system was designed by the Champalimaud Hardware Platform and was 3D printed in-house (Ultimaker) in CPE filament, weighing $\sim$170 g. Its dimensions are r = 10 cm, width = 10 cm.

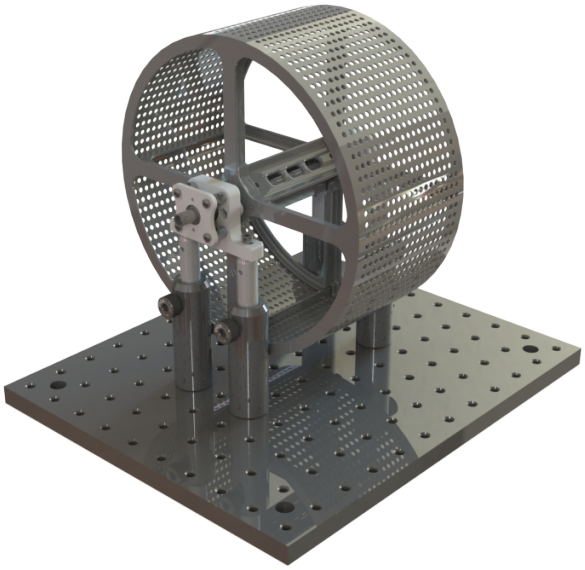

Figure 1: 3D render of the running wheel mounted on a breadboard (Thorlabs) using metal posts (Thorlabs). Image courtesy of Champalimaud Hardware Platform.

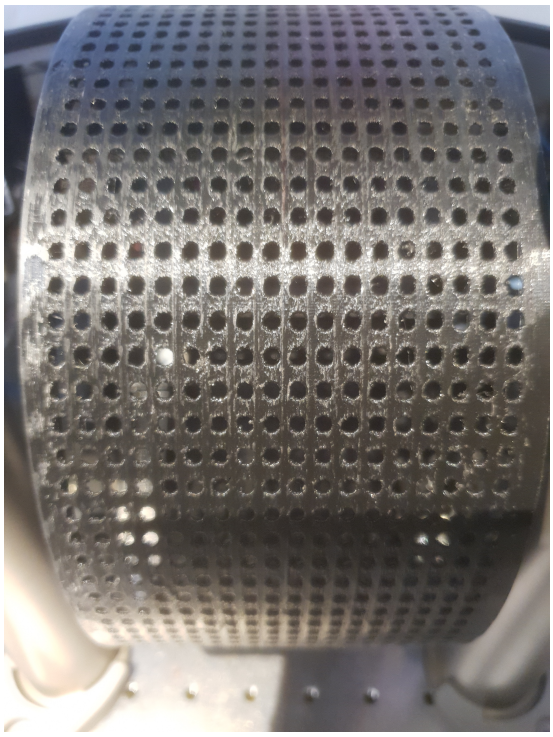

Figure 2: Picture detailing the 3D printed wheel surface.

Camera positioning

The camera is positioned laterally to the mouse in order to capture relevant behaviors such as licking and casting (Figure .1.1, Appendix .2.1).

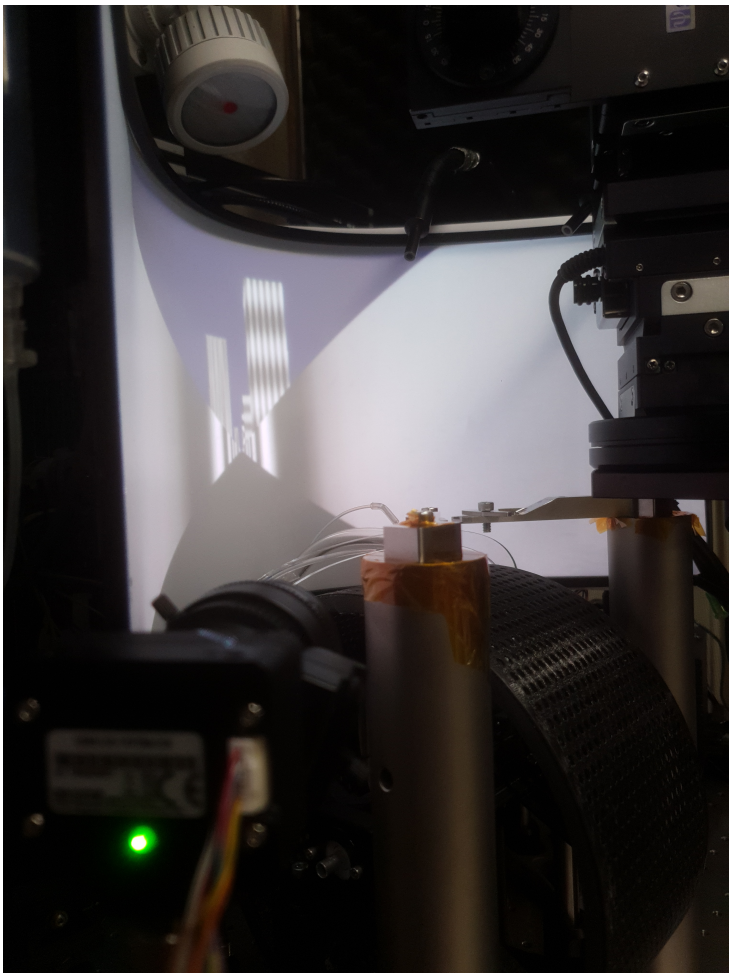

Figure 3: Picture showing the camera positioning in the OVR system. Note that this is the same system used for the electrophysiological recordings.

Reward volume calibration

A reservoir containing liquid water is secured to the outisde of each training box with velcro adhesive tape (Velcro Brand), and thin tubing (Cole-Parmer) is used to connect the reservoir, the solenoid valve (NResearch), and the reward spout located in the acrylic holder (.1.1). The used solenoid valve (NResearch) is passive and normally-closed, meaning that a signal must be provided in order for it to open and flow of water through it cannot be controlled. In this way, by installing the reservoir on a location above the animal, water flow through the open valve is imposed solely by gravity, with flow velocity linearly proportional to the height difference between the mouse and the reservoir (assuming constant water density and gravitational pull - Bernoulli's Equation). Thus, for each reward event, that reward's volume is determined by the amount of time the valve is open.

Considering the previously mentioned daily water intake of $0.7\,\mathrm{mL}$ for mice in the training and experimental regimes, and that the power of statistical analyses increases with the number of samples (*ie*, trials), the volume of each reward event is therefore set such that an animal has to run for hundreds of trials in order for its accumulated reward volume to match the prescribed daily amount.

This 'calibration' process is done in the following way:

1. Weigh an empty eppendorf tube
2. Set the duration of the valve's opening period to a an arbitrary value Δt

3. Trigger multiple (N) repetitions of reward presentation and collect that water in the eppendorf tube
4. Weigh the eppendorf tube loaded with the collected water
5. Calculate the mass of the collected water M (difference in the weightings of the eppendorf tube)
6. Calculate the volume of each individual reward event V_r by dividing the mass of water by the number of collected rewards and dividing the result by the density of water ρ, as depicted in Equation 1.

$$V_r = \frac{M}{N}\frac{1}{\rho}, \qquad \rho = 1\,\mathrm{g\,L^{-1}} \tag{1}$$

As the relationship between reward volume V_r and the amount of time the valve stays open Δt is approximately linear, one can use this result to estimate the Δt that provides the desired value of V_r using a simple rule of three calculation. This estimate can then be verified and optimized by repeating the described calibration process. On the presented experiments, a water volume of $20\,\mu\mathrm{L}$ was provided on each reward event, corresponding to a valve opening duration of $0.14\,\mathrm{s}$.

Acrylic holder design

All animals are head-fixed in the same location in the OVR system as previously described (Figure 2.5). However, variability in mouse anatomy due to age, sex or other natural factors could introduce differences in stimulus perception or reward consumption between individual mice, which would introduce confounding factors when comparing behavior across individuals.

In order to minimize the effects of anatomical variability across mice - thus improving the system's reproducibility - , a custom acrylic holder was designed (Appendix figure 4). It consists of a symmetrical 'inverse U' shape with several (lateral and central) apertures. The lateral apertures (three on each side) are of size M3 and allow for the bilateral installation of the holder in manual or electronic manipulators, hence enabling its repositioning between individuals. The three central apertures hold in place the reward spout, the breathing sensor tube, and the olfactometer output tube (Figure 2.8).

Acrylic was the material selected as it's lightweight but sturdy, relatively cheap, and laser cutting equipment was available in-house, allowing to quickly prototype or replicate any design. Its transparency is fundamental to reduce obstruction of the screen.

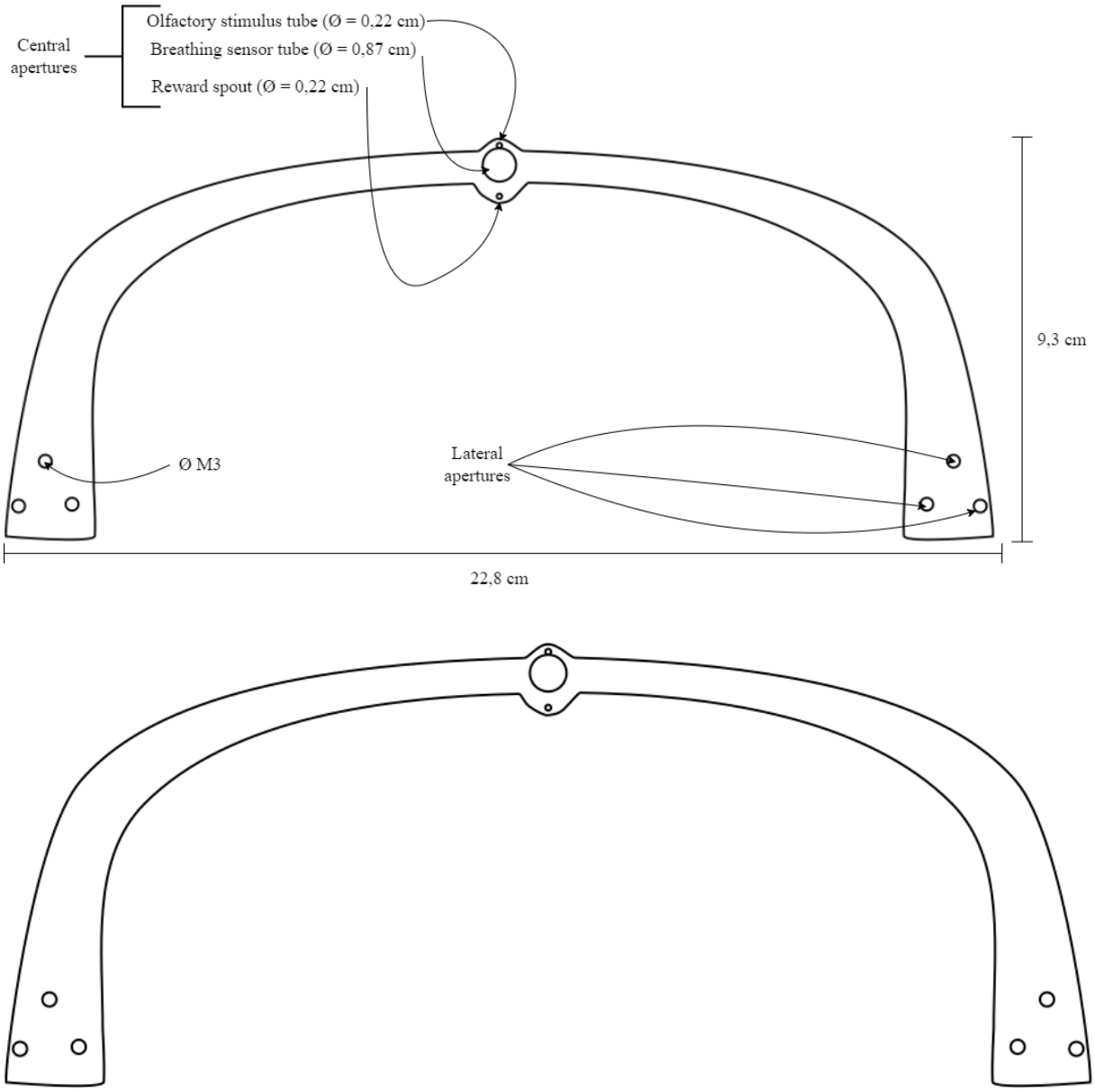

Figure 4: (**Top**) Annotated and (**Bottom**) simple visualizations of the acrylic holder design.

Odorized filter preparation

Pure odorants (Sigma-Aldrich) are individually dissolved in mineral oil (Sigma-Aldrich) at a concentration of $1 : 100$. Each preparation is hermetically sealed to avoid contamination. Before each experimental session, this solution is homogenized by means of an electronic shaker and a volume of $12\,\mu L$ is drawn from it and applied to a new syringe filter (Whatman) that is placed on the corresponding output of the olfactometer. This volume is used as it is enough to saturate the paper filter, allowing for producing hundreds of individual olfactory stimulus events that have similar amplitude and temporal properties.

.1.2 Enclosure assembly design

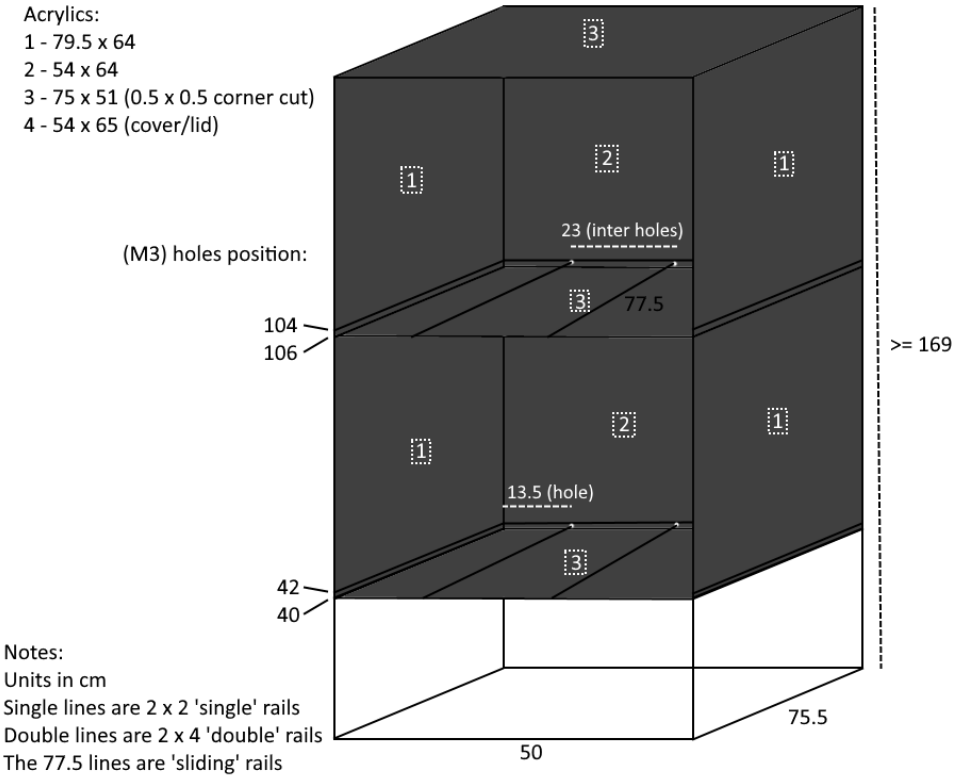

Figure 5: The developed enclosure assembly. (**Top**) Photograph of an enclosure assembly installed with two OVR systems; (**Bottom**) Schematic showing the geometry of the enclosure assembly.

Each OVR rig is fitted in a retractable system that allows sliding it in and out of the training box for convenience in head-fixation of the animals, replacement of components (*eg* the odorized paper filters), or troubleshooting purposes (Figure 6).

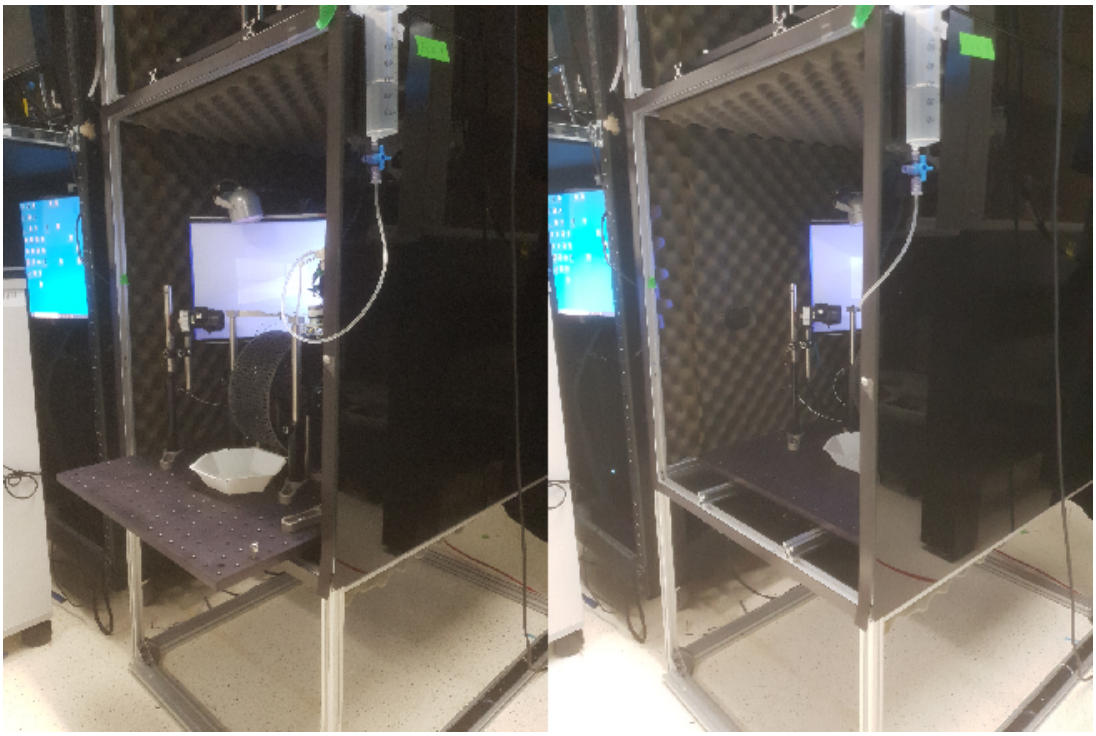

Figure 6: Demonstration of system retraction in the training box.

Each of the training boxes is also equipped with magnetic strips that allow to easily open or close the box while an animal runs in an experimental session in order to promote concentration of the animals (Figure 7).

Figure 7: A closed training box. The acrylic doors are magnetically mounted on the frame of the enclosure assembly.

.2 Mouse behavior

.2.1 Natural behaviors

As animals run in the OVR experience in a closed-loop manner, they are allowed to engage in a wide range of natural behaviors without punishment regarding trial completion, reward availability or overall performance in the task, being only limited by head-fixation in the kinds of behavior they can produce. For example, they are able to run and stop on the 3D printed wheel (Appendix figure 8) at will.

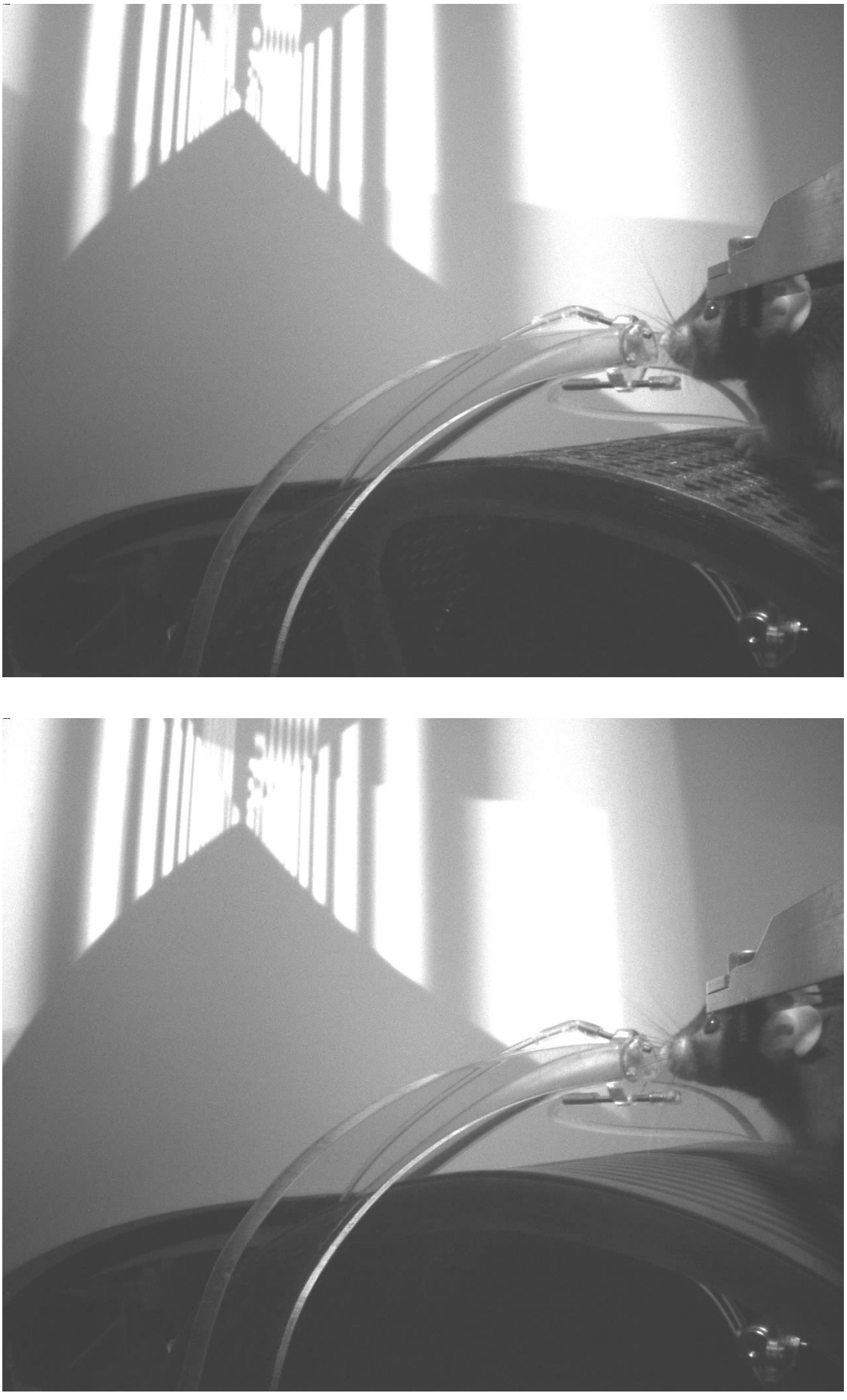

Figure 8: Mouse behaving in OVR. (**Top**) Mouse stopped on the wheel; (**Bottom**) Mouse running.

The increasing adoption of GPU boards in data science has led to the development of automatic or semiautomatic methods for body part tracking such as DeepLabCut (Mathis et al., 2018) and, more specifically in mouse ethology, Facemap (https://github.com/MouseLand/facemap/blob/main/README.md), which is optimized for tracking elements of the mouse's rostrum, (*eg* eye and pupil, nostril, whiskers, tongue, etc.). These allow the quantification of movement of the identified body features, hence enabling characterization of behavior in a reproducible way that relies less on the experimenter's heuristics of what body part movements constitute which kinds of behavior.

The presented OVR system supports usage of these class of methods in an optimal setting for reducing errors or imprecision in the automated body tracking processes, as both the experimental animals and the used video camera are fixed in the system and camera and acquisition settings (namely lighting and focus) are optimised for the expected mouse position in the system. These methods can be used to detect when the mouse reaches for the reward spout with its tongue (Appendix figure 9), generating in this way a licking signal that is automatically aligned in time with the rest of the behavioral signals.

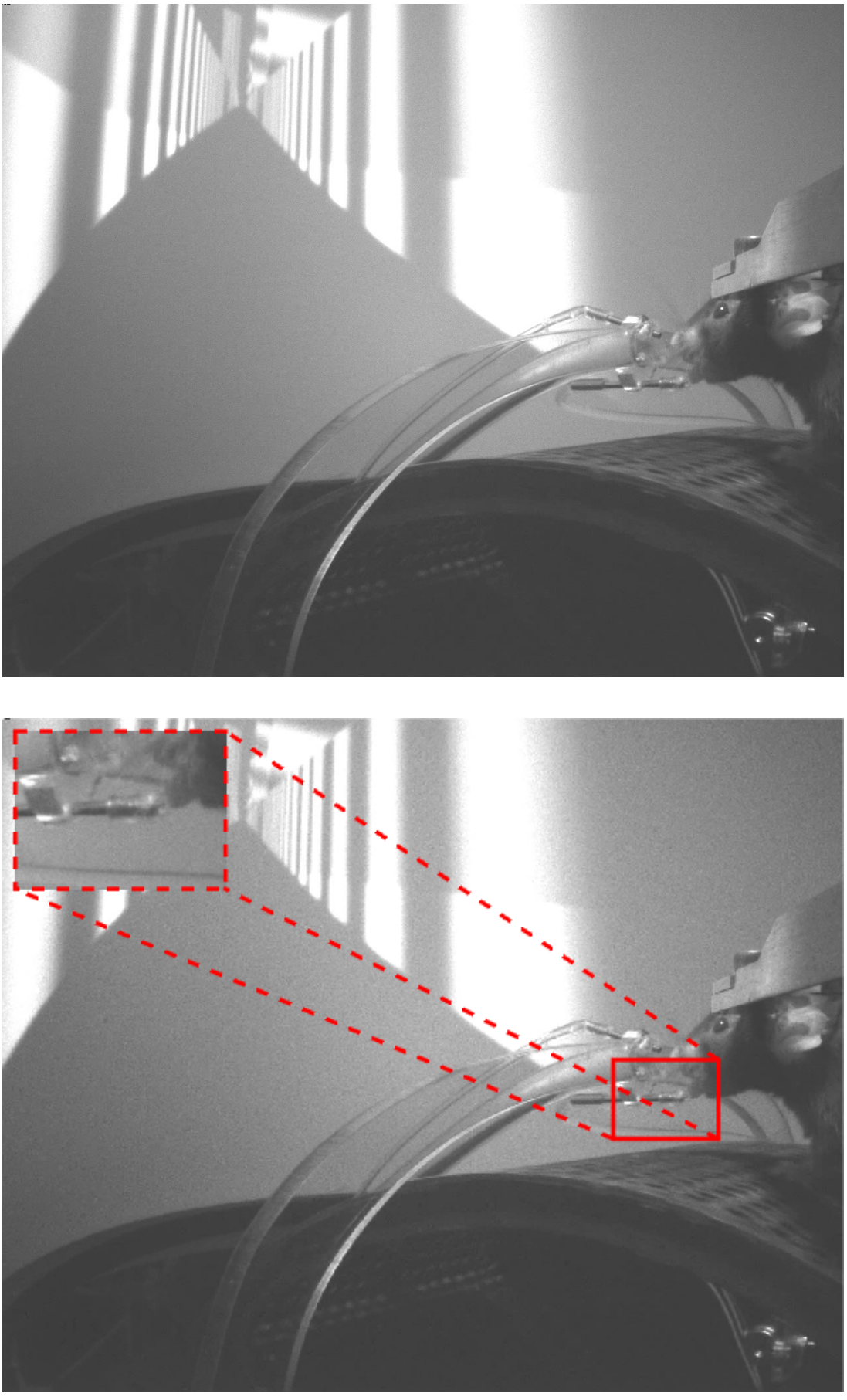

Figure 9: Mouse licking for reward in the OVR system. (**Top**) Raw image; (**Bottom**) Image with inset shows zoom-in of the marked area.

In addition, precisely because of the fixed spatial relationship between the camera and the mouse, traditional approaches for image fusion can be used to reveal small movements of the animal's rostrum. This is particularly useful for the quantification of casting behavior. Casting is a behavior conserved across many species that consists on the lateral back-and-forth movement of the olfactory receptors (nostrils, in the case of rodents) and that is involved in odor source localization (Liu et al., 2020), hence it plays an important role in olfactory-cued spatial navigation. In Appendix figure 10, two different pictures from the same mouse in the same session were fused using MatLAB's $imfuse()$ method. The color of each pixel reflects the intensity difference of that pixel across the two images (gray means there is no difference, red and green reflect greater intensity in one image or the other).

As can be observed in that figure, this method can detect and quantify the movement of the animal's nose, as can be seen by the differently colored regions in the inset on the bottom image. The original pictures used to produce this fused image are shown in Apendix figure 11.

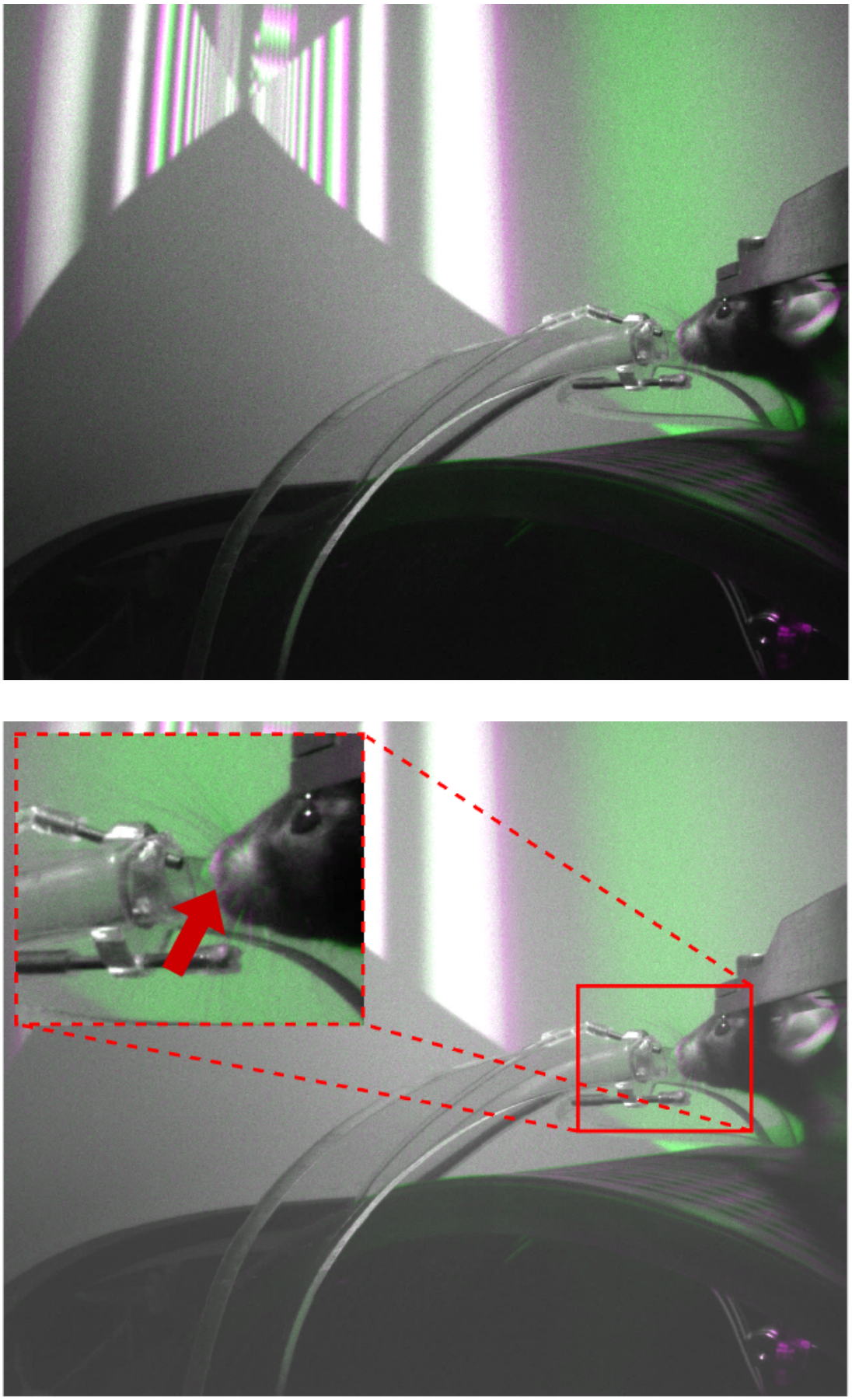

Figure 10: Characterization of casting behavior. (**Top**) Fused image; (**Bottom**) Image with inset shows zoom-in of the marked area. Red arrow points to the tip of the nose.

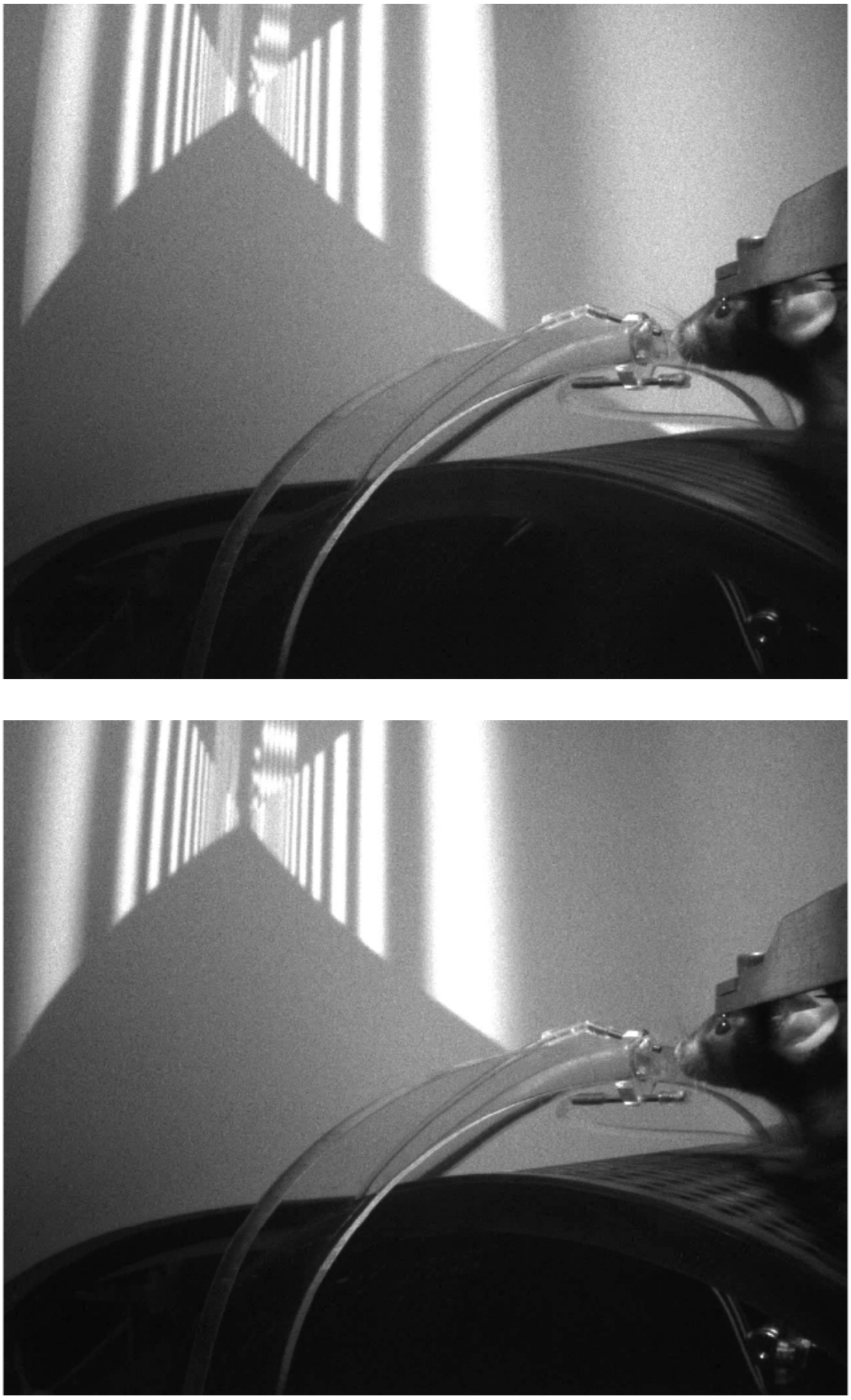

Figure 11: Montage of the images used to produce the fused image in Appendix figure 10. Note the different positions of the mouse's nose.

.2.2 Additional analyses

In a manner analogous to the visualizations of mouse velocity aligned to events of interest (Figures 3.8 and 3.9), visualizations of the behavior respective to omission events (Appendix figure 12) could be useful to reveal potential errors in the implementation of both velocity calculation or the velocity threshold criterion used to enable reward presentation.

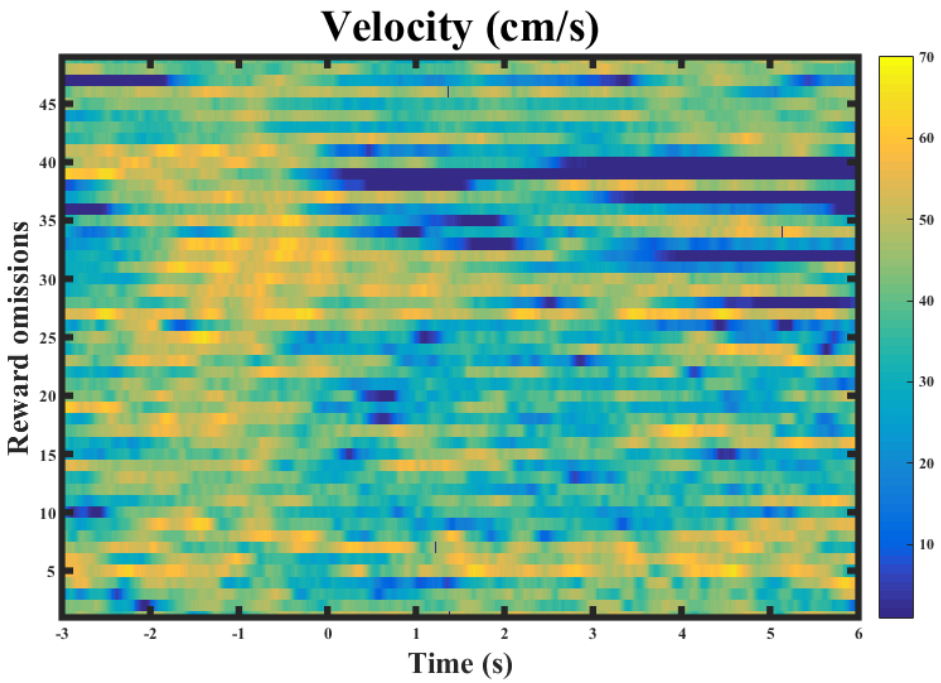

Figure 12: Velocity of mouse #2 aligned in time to individual omission events. Omissons occur at $Time = 0$ (zero), *ie*, the animal would have received a reward at that time if the velocity threshold criterion had been met.

.3 Mouse neural activity

.3.1 Recording rig

In order to reduce sources of noise in the recording of neural activity by means of electrical probes, an OVR system was mounted in a faraday cage and illumination and probe positioning instrumentation was installed (Appendix figure 13).

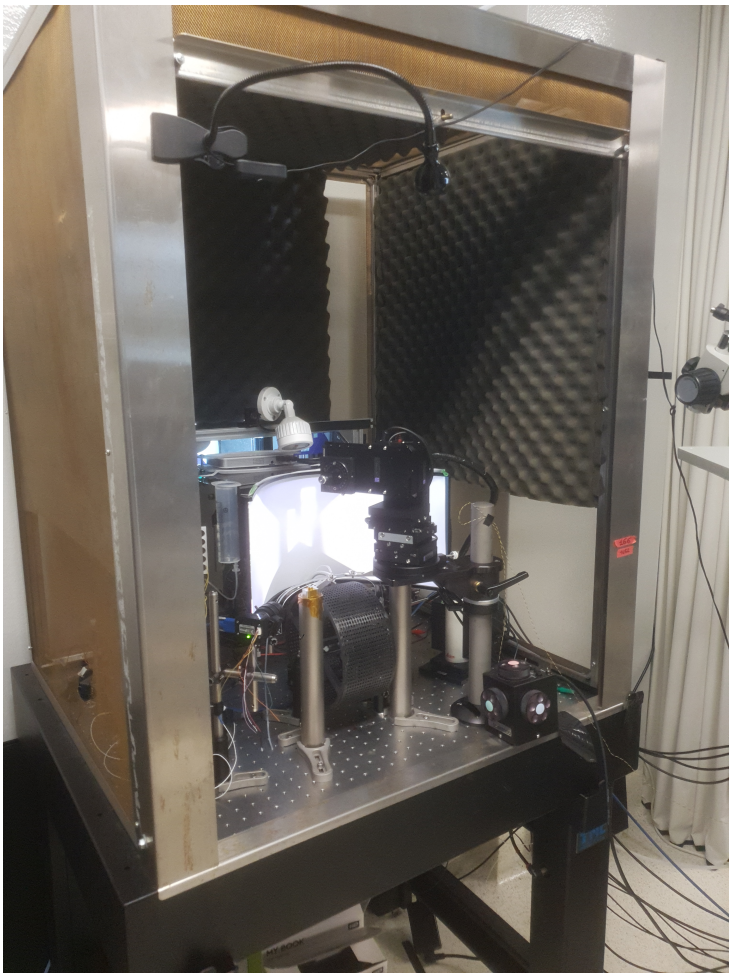

Figure 13: Picture of the recording rig used for electrophysiology recordings.

.3.2 Neuropixels probe implantation

As mentioned, the neuropixels probe was acutely implanted with its tip targeting the coordinate (relative to Bregma) $2.1\,\mathrm{mm}$ posterior, $1.5\,\mathrm{mm}$ lateral, $2.5\,\mathrm{mm}$ ventral in order to ensure recording of hippocampal neurons along the length of the probe's shank. In Appendix figure 14, an additional, sagittal view of the target coordinate is shown.

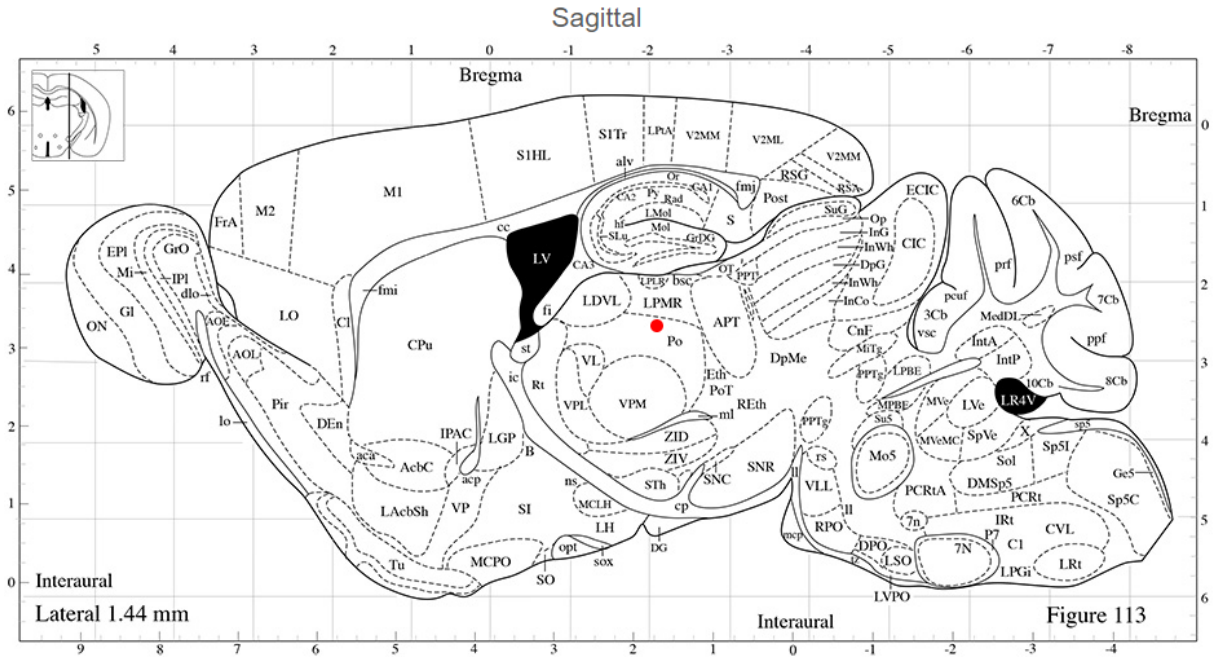

Figure 14: Sagittal view of the approximate recording coordinate. The probe was implanted vertically from the dorsal side of the mouse's head. This figure was generated using `http://labs.gaidi.ca/mouse-brain-atlas/`

.3.3 Electrophysiology signal analysis

An automatic spike clustering algorithm, KiloSort (Pachitariu et al., 2016), was applied to the neuropixels probe recording. This algorithm assigns each recorded action potential to individual, putative neurons according to that action potential's spatio-temporal signature on the probe's many channels. The parameters used to run the algorithm on this data are included in Table 1, below. The MatLAB library *spikes* (https://github.com/cortex-lab/spikes) was used *out-of-the-box* to generate Figure 3.12.

.3.4 Photometry signal analysis

In order to allow a fair comparison of the neural activity across trials, the photometry signal is baseline adjusted for each stimulus presentation. This correction involves, for each stimulus event, calculating the average of the signal on the three seconds preceding that stimulus, and then subtracting that value to the portion of the signal surrounding the stimulus presentation (a time window of $[-3, 2]$ seconds around the stimulus presentation. In this way, the baseline neural activities preceding each stimulus are matched for all the stimuli presentations in the session.

This process is effectively similar to *detrending*, a popular technique used in analog signal analysis,

Parameter	Value
Number of channels	385
Sampling Frequency (Hz)	30000
Time range	$[0, \infty]$
Min. firing rate per channel	0.1
Threshold	$[10, 4]$
Lambda	10
AUC for splits	0.9

Table 1: Parameters used for running the KiloSort algorithm on the electrophysiology data.

Component	Specification	Manufacturer
CPU	Core i7 7700 (3.6 GHz)	Intel
Motherboard	Z270 Gaming M5	MSI
RAM	G.Skill DDR4 2400MHz (2 x 8 GB)	Aegis
Graphic card	GeForce GTX 1060 DUAL 6GB	Asus
Disk	Barracuda 2TB SATA III 64 MB	Seagate
OS	Windows 10 Professional	Windows

Table 2: OVR computer specifications.

but is more robust to drift of the baseline in longer timescales, such as the duration of the recording session ($\sim$1 h).

.4 List of equipment

Component	Specification	Manufacturer
Breadboard	MB4545/M	ThorLabs
Projector	LaserBeamPro	LaserBeamPro
Screen film	24 x 48 inch matte white	AbleDIY
Small Mirror	2.95 x 15.5 x 1/4 inch	First Surface Mirror
Large mirror	5.95 x 15.5 x 1/4 inch	First Surface Mirror
Construction rail	XE25L18 (x4)	ThorLabs
Construction rail	XE25L15 (x2)	ThorLabs
Acrylic panels*	60 x 40 x 6 mm	Custom order
Running wheel	r = 10 cm, w = 10 cm	Champalimaud Hardware Platform
Rotary encoder	MAE3	US Digital
Metal posts	TR100/M (x6)	ThorLabs
Post holders	PH1 (x6)	ThorLabs
Post clamps	SWC/M	ThorLabs
Headfixation	Custom design (CHP)	Hubs
Manual microcontroller	DT12/M	ThorLabs
Acrylic holder	30 x 20 x 0.3 cm transparent	Custom order
Air flow sensor	AWM3100V	Honeywell
Breathing tube	95702-09	Cole-Parmer
Solenoid valve	2-way normally closed 161K012	NResearch
Water tube	95702-00	Cole-Parmer
Reward spout	HTX-19R-24	Small Parts Inc.
Olfactometer	109-024	Island Motion
Syringe filters	6823-1327	Whatman
Air tubes	06422-02	Cole-Parmer
HARP		Champalimaud Hardware Platform
Infrared illuminator	CM-IR30	CMVision
Video camera	Chameleon 3	FLIR Systems
Camera lens	MVL16M23	ThorLabs
Infrared-pass filter	Polyester 87 670 nm	LEE Filters

Table 3: OVR system components. The acrylic panels composing the screen 'box' are laser-cut from the acrylic sheets according to `https://github.com/HarveyLab/mouseVR/blob/master/README.md`

Component	Specification	Manufacturer
Construction rail	0.0.370.03 (x6)	Item24
Construction rail	0.0.370.04 (x4)	Item25
V-Slot linear rail	280-LP (x4)	OpenBuilds
Mini V Gantry Kit	(x6)	OpenBuilds
Acrylic panel	795 x 640 x 4 mm black matte 2 faces (x6)	Custom order
Acrylic panel	640 x 550 x 5 mm black matte 2 faces (x2)	Custom order
Acrylic panel	610 x 550 x 4 mm black matte 2 faces (x4)	Custom order
Magnetic strips	19 x 2.5 mm self adhesive (x10)	Magflex
Sound-absorbing sheets	Contoured, adhesive backing (x8)	McMaster
Air flowmeter	32460-42 (x2)	Masterflex
Water reservoir	SS-60C (x2)	Terumo

Table 4: Enclosure assembly components. Note that the enclosure assembly consists of two training boxes, each fitting an OVR system.

.5 Supplementary visualizations of behavior

.5.1 Behavioral summaries of the mice not shown in the main text

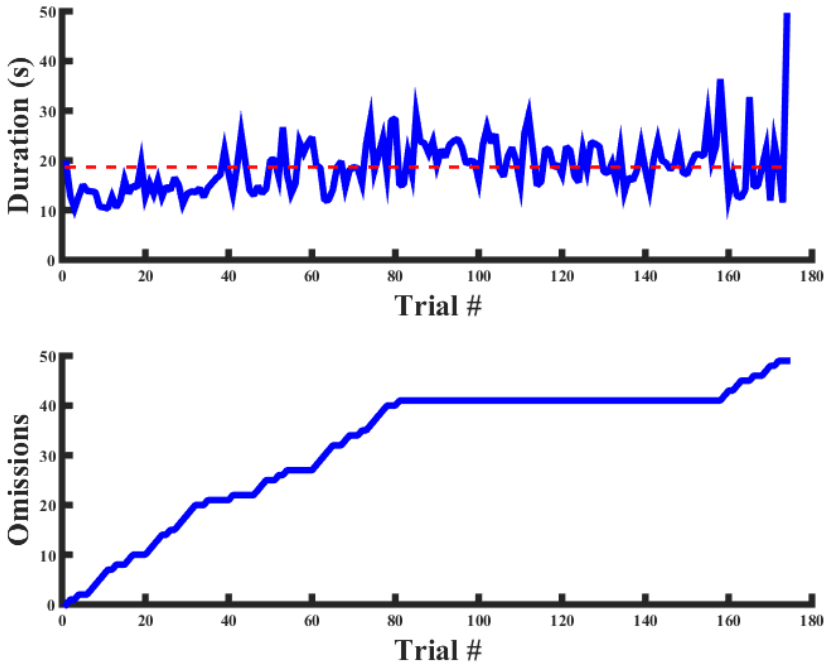

(a) (**Top**) Trial durations (blue solid trace) and average trial duration (red dashed line), in seconds. (**Bottom**) Number of reward omissions during the session.

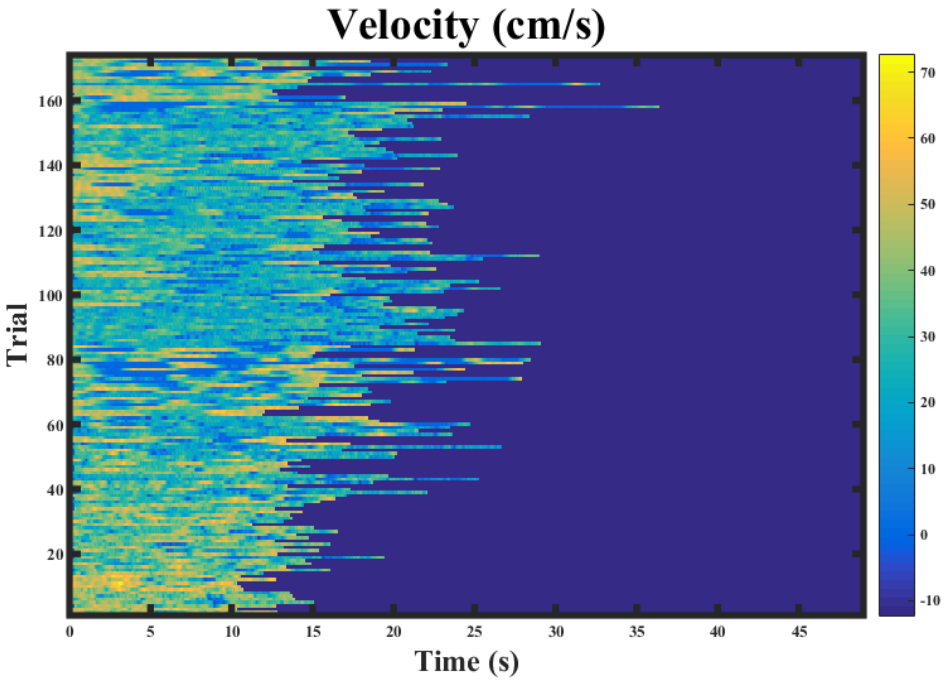

(b) Duration and mouse velocity for each trial. Shorter trials are associated with higher average velocities or less periods of immobility during the session.

Figure 15: Behavioral summary of the first session of mouse #3 in the experimental regime.

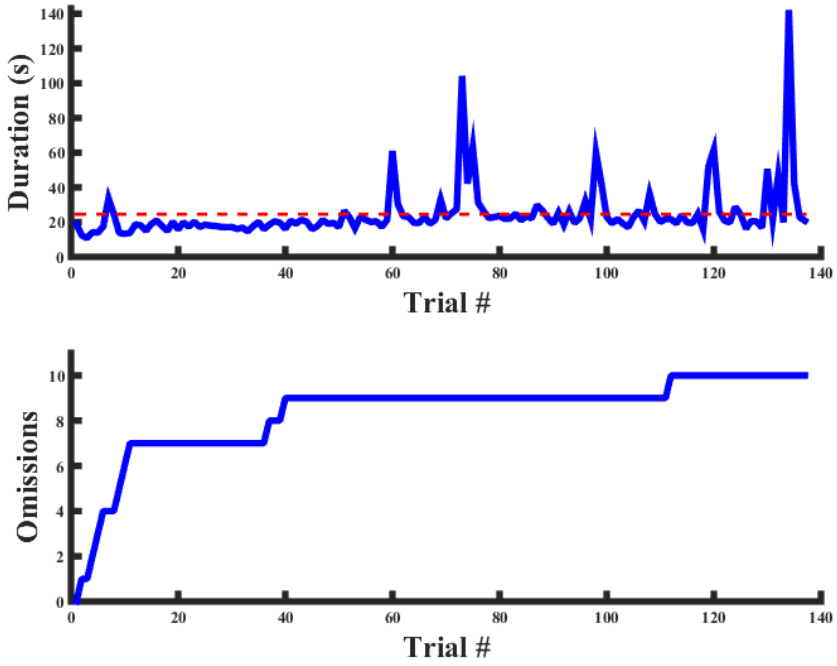

(a) (**Top**) Trial durations (blue solid trace) and average trial duration (red dashed line), in seconds. (**Bottom**) Number of reward omissions during the session.

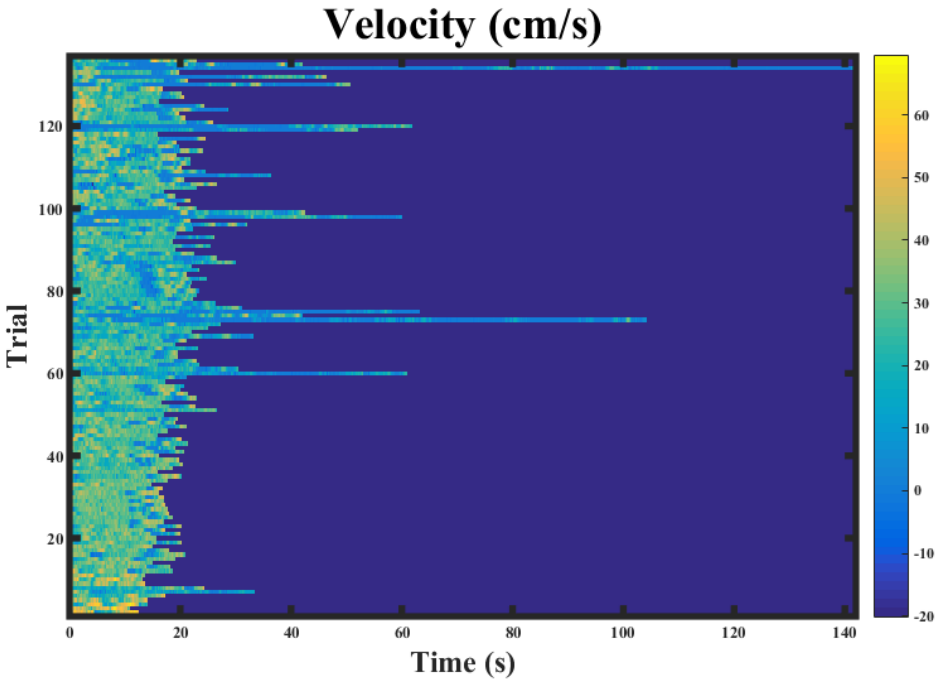

(b) Duration and mouse velocity for each trial. Shorter trials are associated with higher average velocities or less periods of immobility during the session.

Figure 16: Behavioral summary of the first session of mouse #4 in the experimental regime.

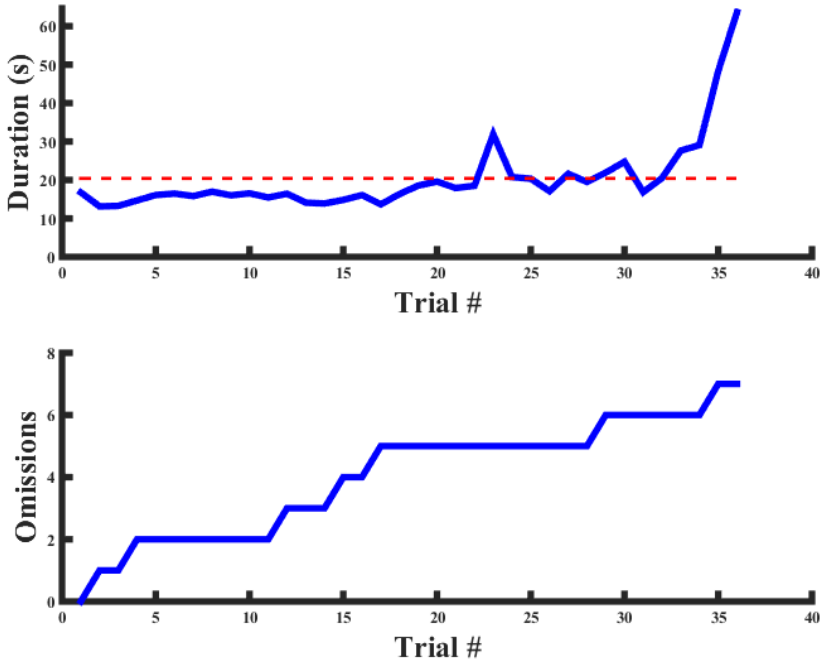

(a) (**Top**) Trial durations (blue solid trace) and average trial duration (red dashed line), in seconds. (**Bottom**) Number of reward omissions during the session.

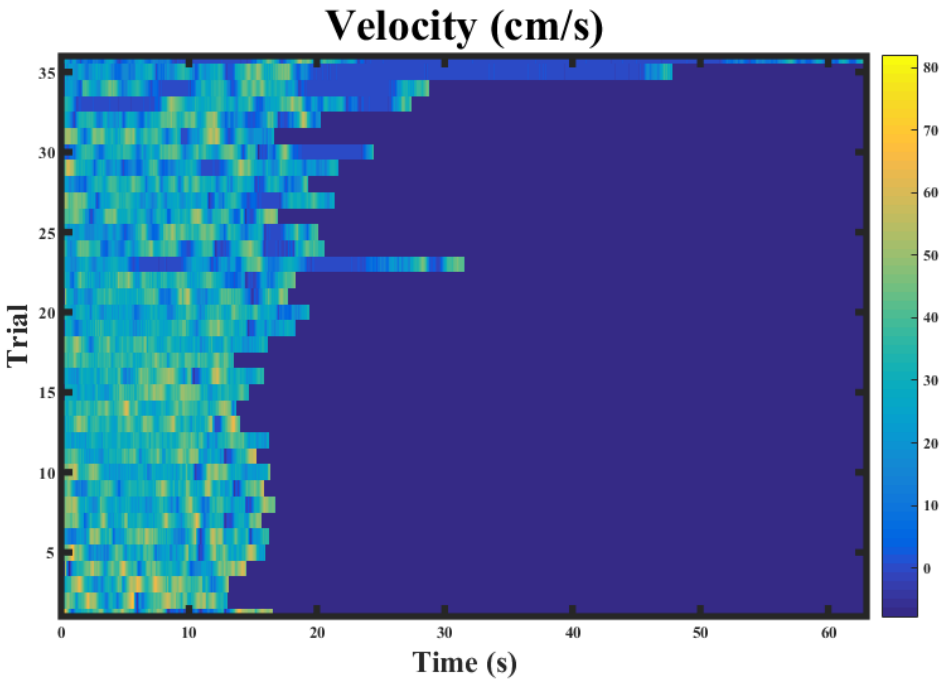

(b) Duration and mouse velocity for each trial. Shorter trials are associated with higher average velocities or less periods of immobility during the session.

Figure 17: Behavioral summary of the first session of mouse #5 in the experimental regime.

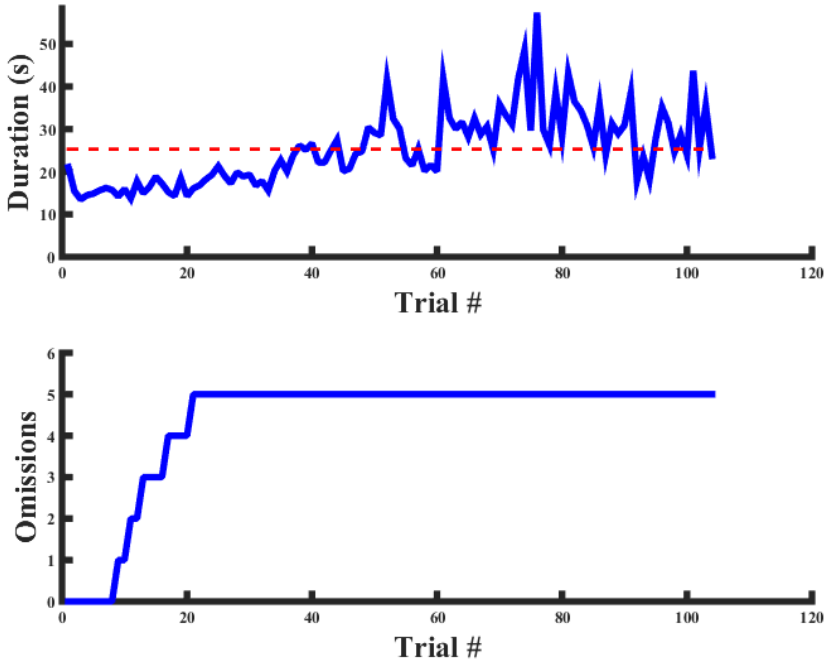

(a) (**Top**) Trial durations (blue solid trace) and average trial duration (red dashed line), in seconds. (**Bottom**) Number of reward omissions during the session.

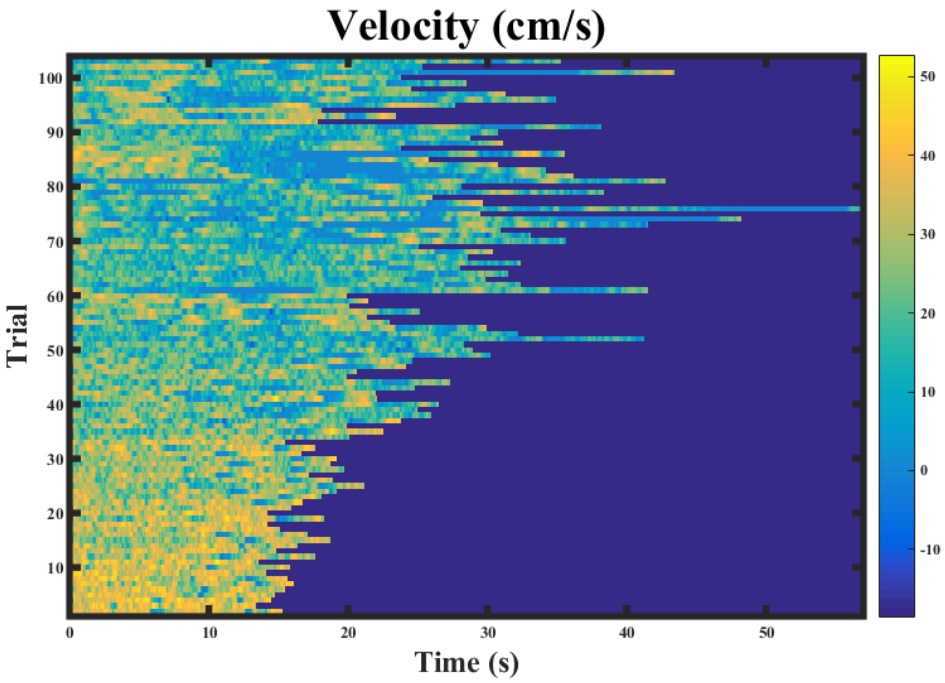

(b) Duration and mouse velocity for each trial. Shorter trials are associated with higher average velocities or less periods of immobility during the session.

Figure 18: Behavioral summary of the first session of mouse #6 in the experimental regime.

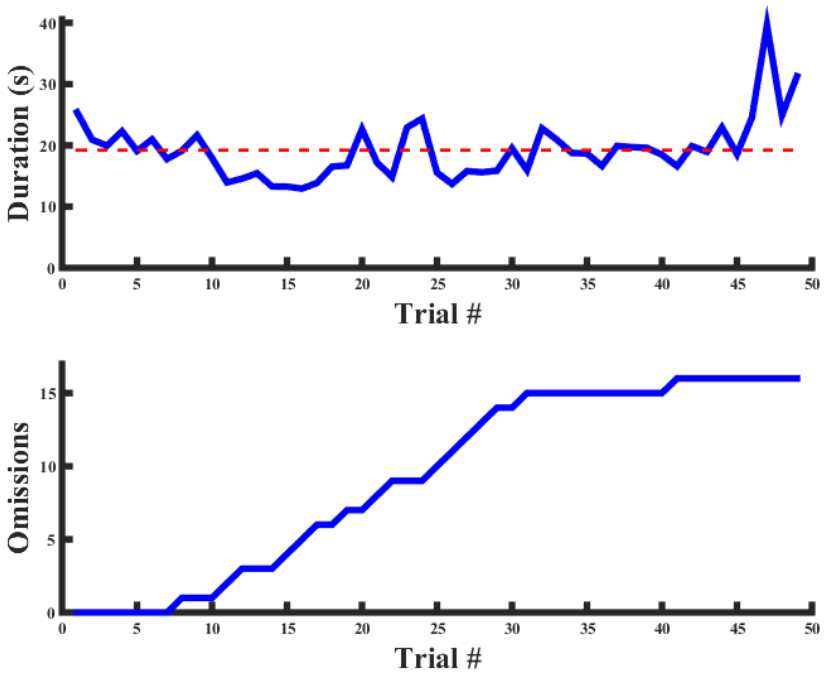

(a) (**Top**) Trial durations (blue solid trace) and average trial duration (red dashed line), in seconds. (**Bottom**) Number of reward omissions during the session.

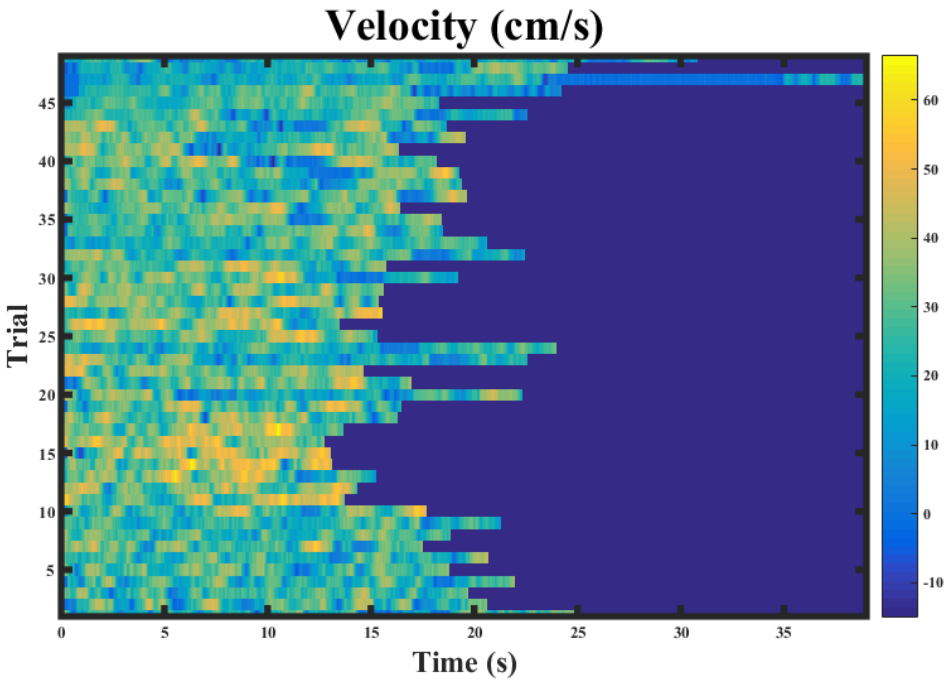

(b) Duration and mouse velocity for each trial. Shorter trials are associated with higher average velocities or less periods of immobility during the session.

Figure 19: Behavioral summary of the first session of mouse #7 in the experimental regime.

.5.2 Running behaviors of the mice not shown in the main text

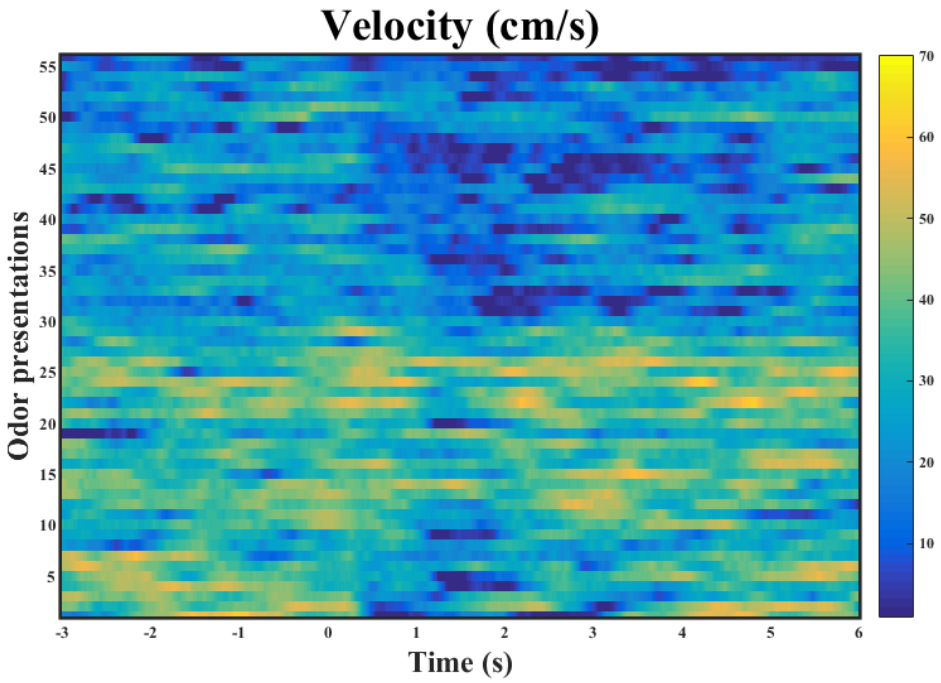

Figure 20: Velocity of mouse #1 aligned in time to individual odor presentations (stimuli). Odors are presented at $Time = 0$ (zero).

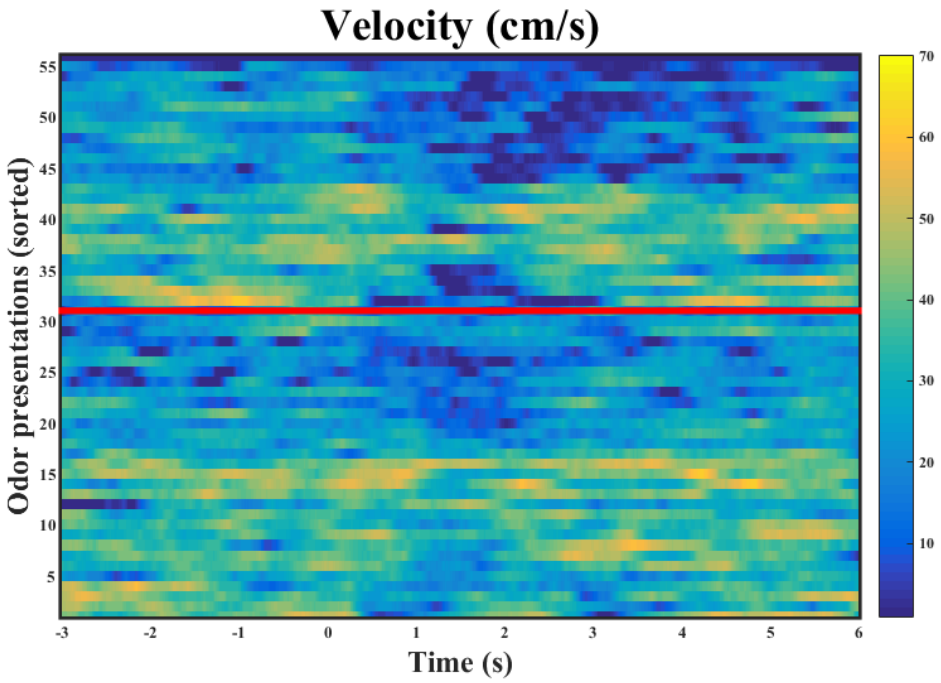

Figure 21: Velocity of mouse #1 aligned in time to individual odor presentations (stimuli), sorted by trial type. Odors are presented at $Time = 0$ (zero).

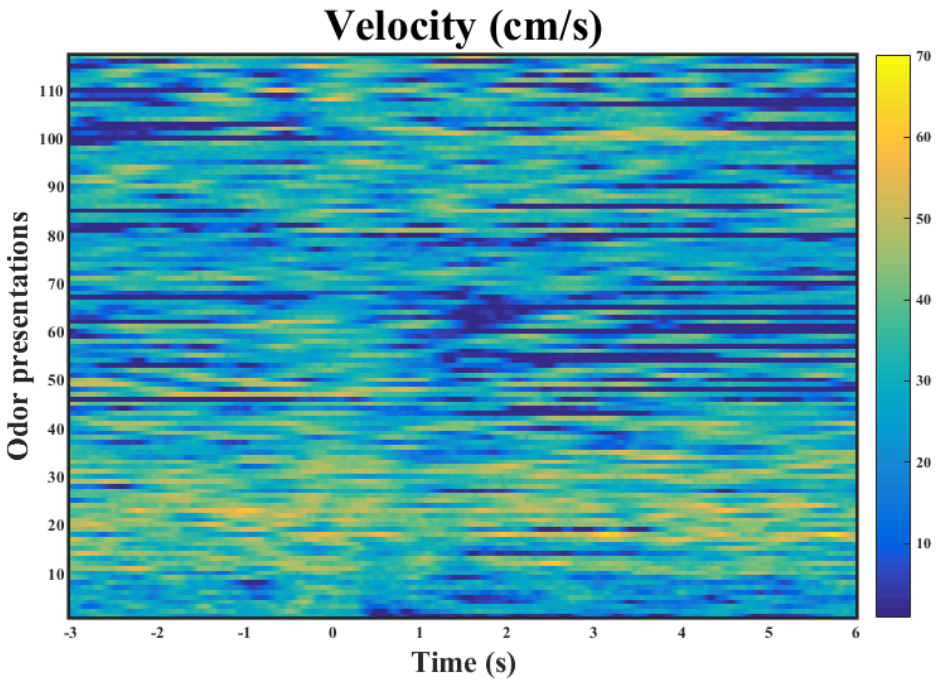

Figure 22: Velocity of mouse #3 aligned in time to individual odor presentations (stimuli). Odors are presented at $Time = 0$ (zero).

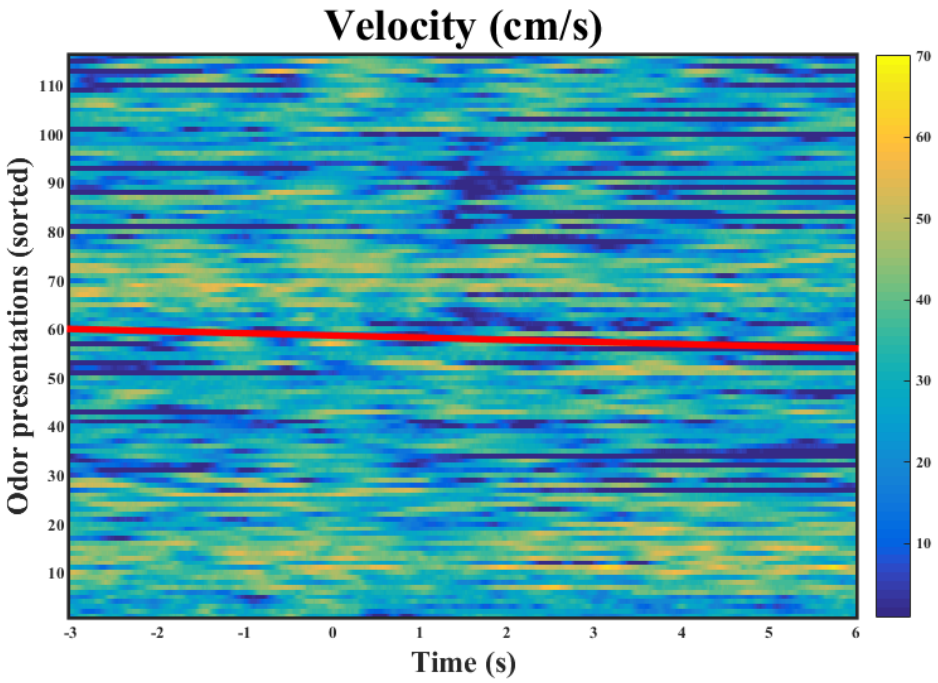

Figure 23: Velocity of mouse #3 aligned in time to individual odor presentations (stimuli), sorted by trial type. Odors are presented at $Time = 0$ (zero).

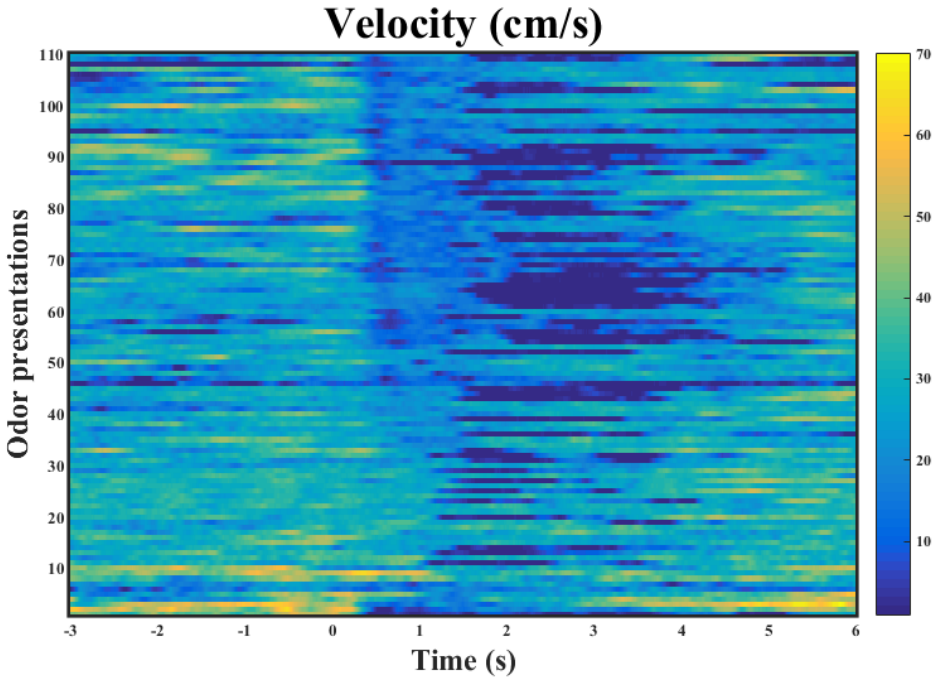

Figure 24: Velocity of mouse #4 aligned in time to individual odor presentations (stimuli). Odors are presented at $Time = 0$ (zero).

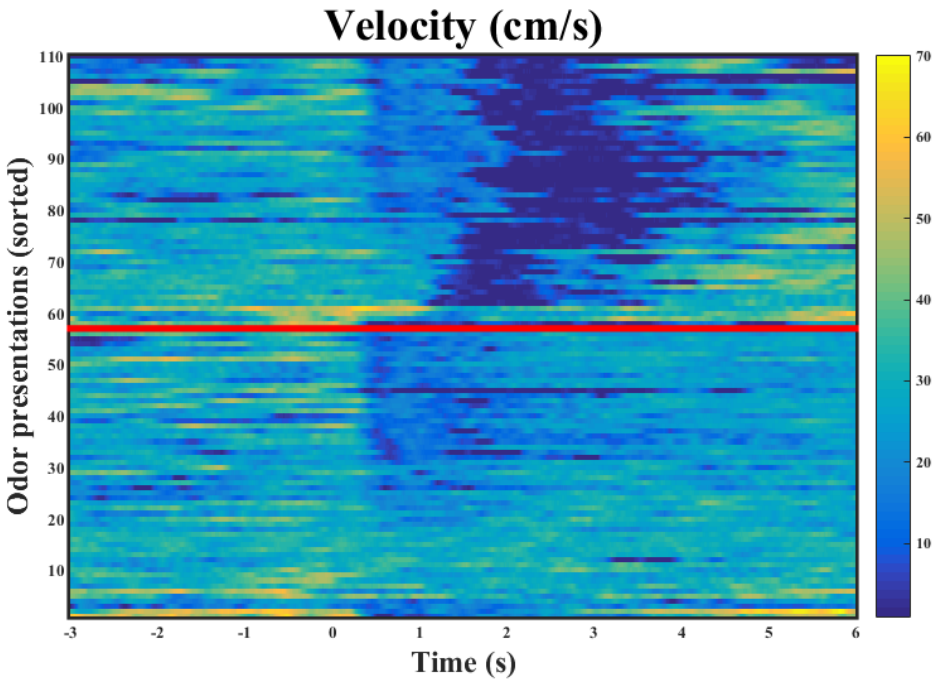

Figure 25: Velocity of mouse #4 aligned in time to individual odor presentations (stimuli), sorted by trial type. Odors are presented at $Time = 0$ (zero).

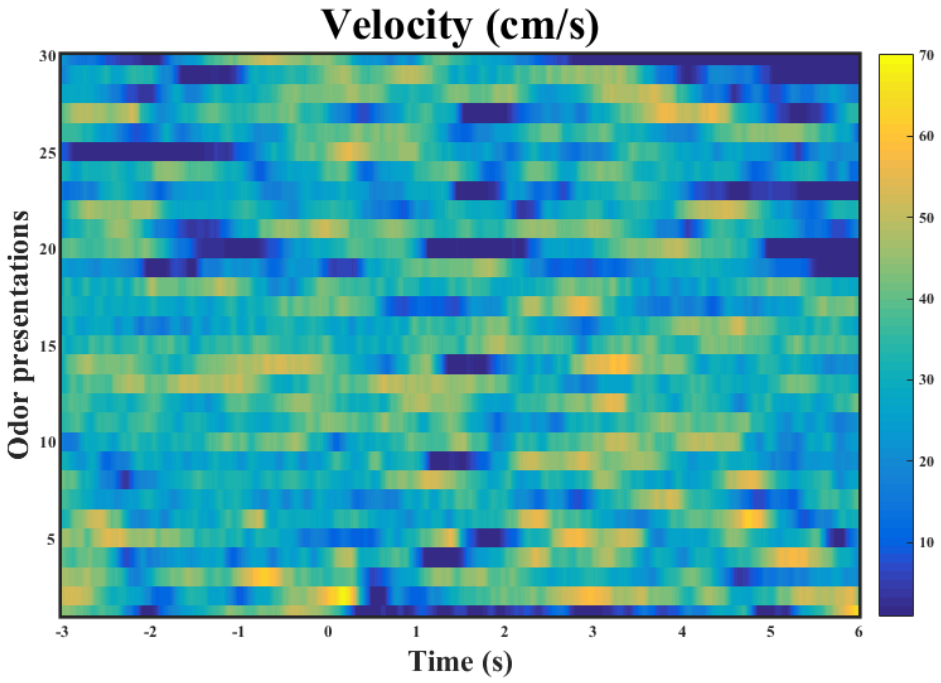

Figure 26: Velocity of mouse #5 aligned in time to individual odor presentations (stimuli). Odors are presented at $Time = 0$ (zero).

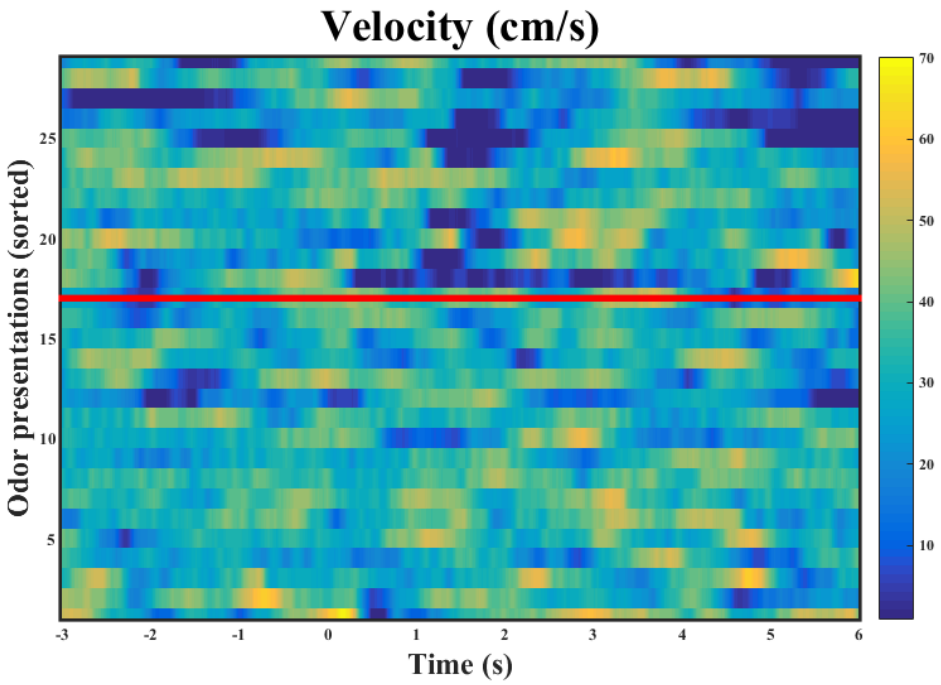

Figure 27: Velocity of mouse #5 aligned in time to individual odor presentations (stimuli), sorted by trial type. Odors are presented at $Time = 0$ (zero).

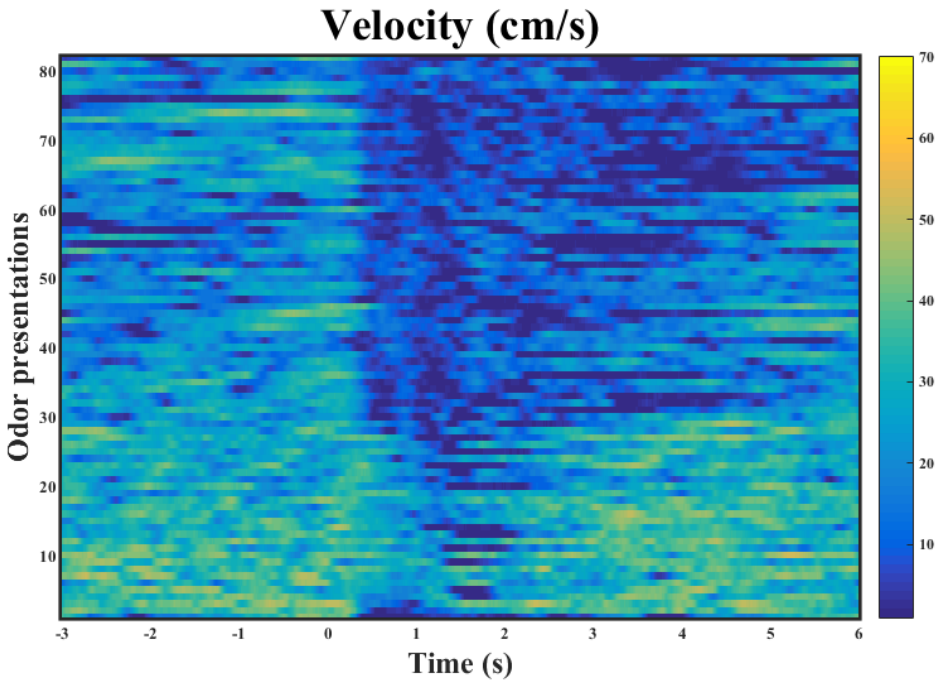

Figure 28: Velocity of mouse #6 aligned in time to individual odor presentations (stimuli). Odors are presented at $Time = 0$ (zero).

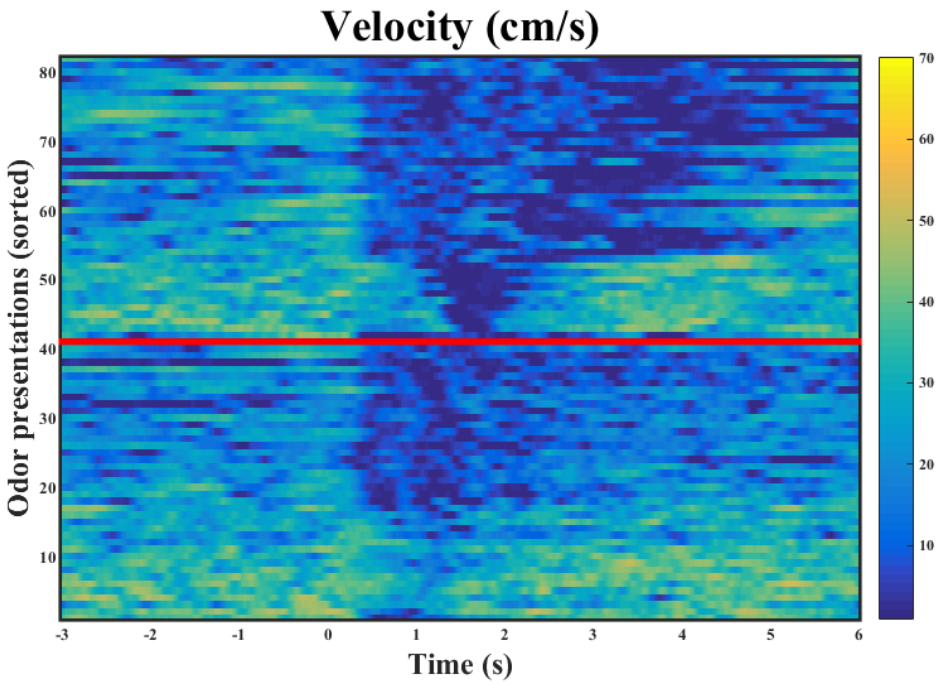

Figure 29: Velocity of mouse #6 aligned in time to individual odor presentations (stimuli), sorted by trial type. Odors are presented at $Time = 0$ (zero).

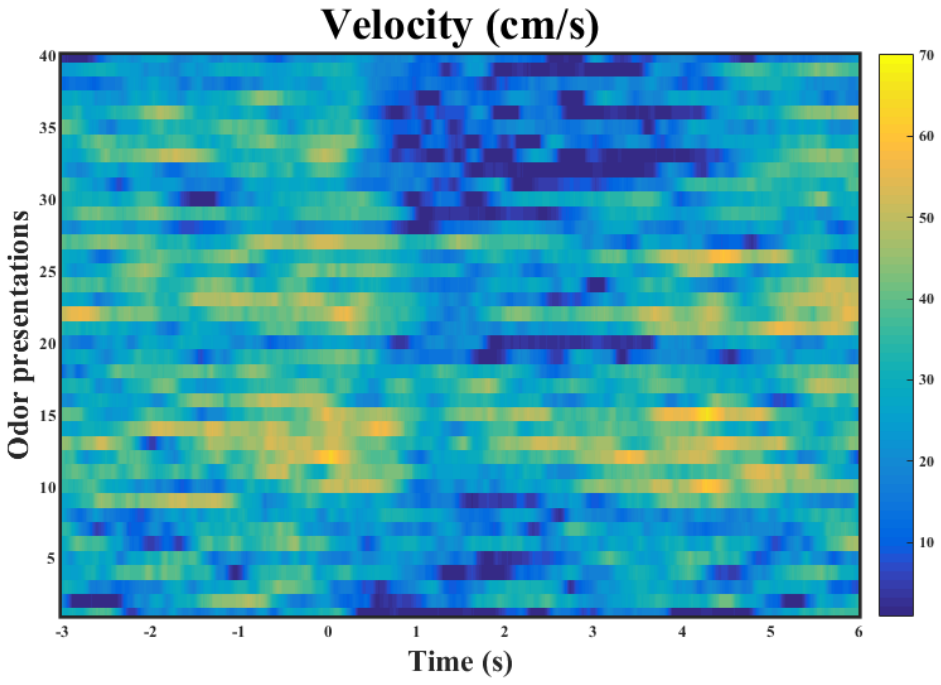

Figure 30: Velocity of mouse #7 aligned in time to individual odor presentations (stimuli). Odors are presented at $Time = 0$ (zero).

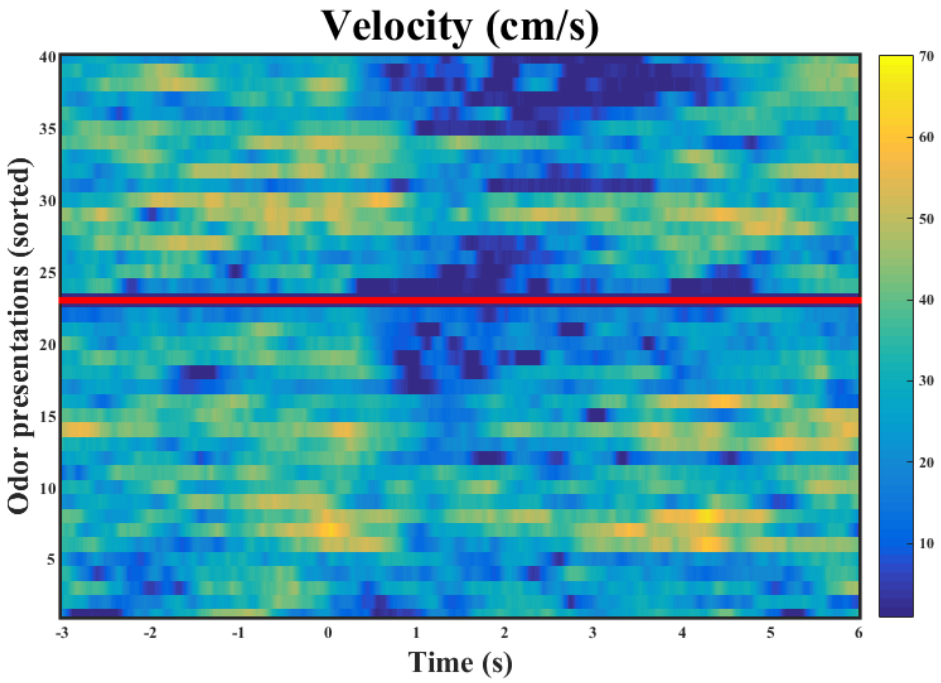

Figure 31: Velocity of mouse #7 aligned in time to individual odor presentations (stimuli), sorted by trial type. Odors are presented at $Time = 0$ (zero).

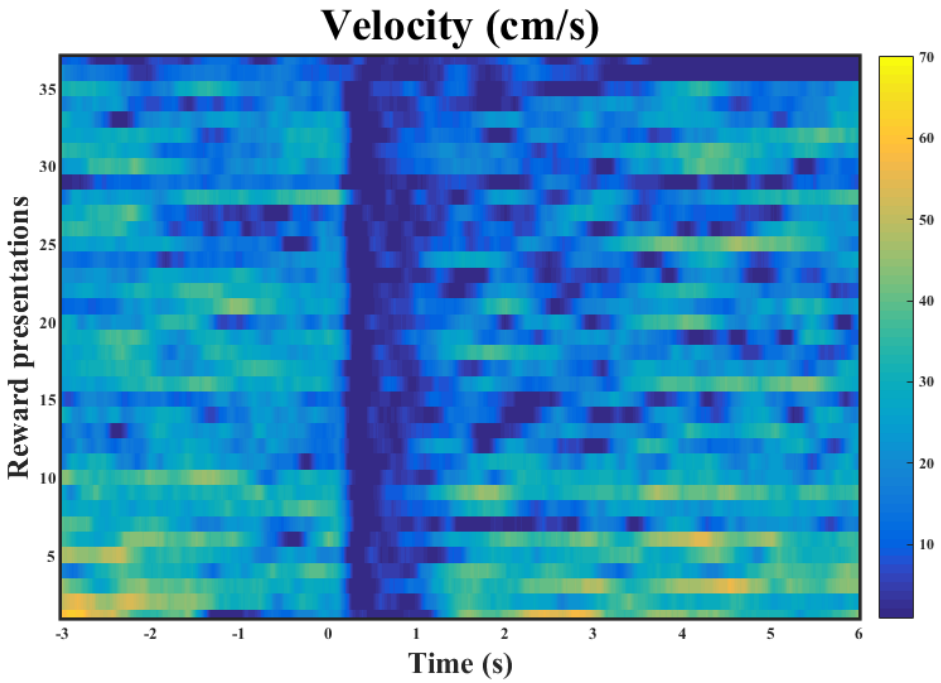

Figure 32: Velocity of mouse #1 aligned in time to individual reward presentations. Rewards are presented at $Time = 0$ (zero).

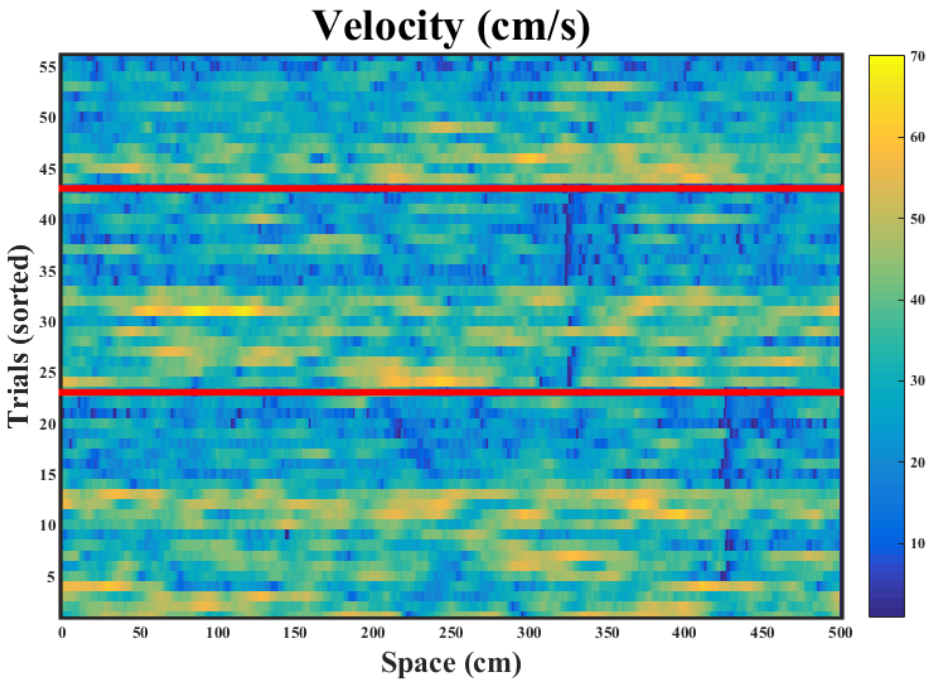

Figure 33: Velocity profile of mouse #1 on the length of the VR corridor.

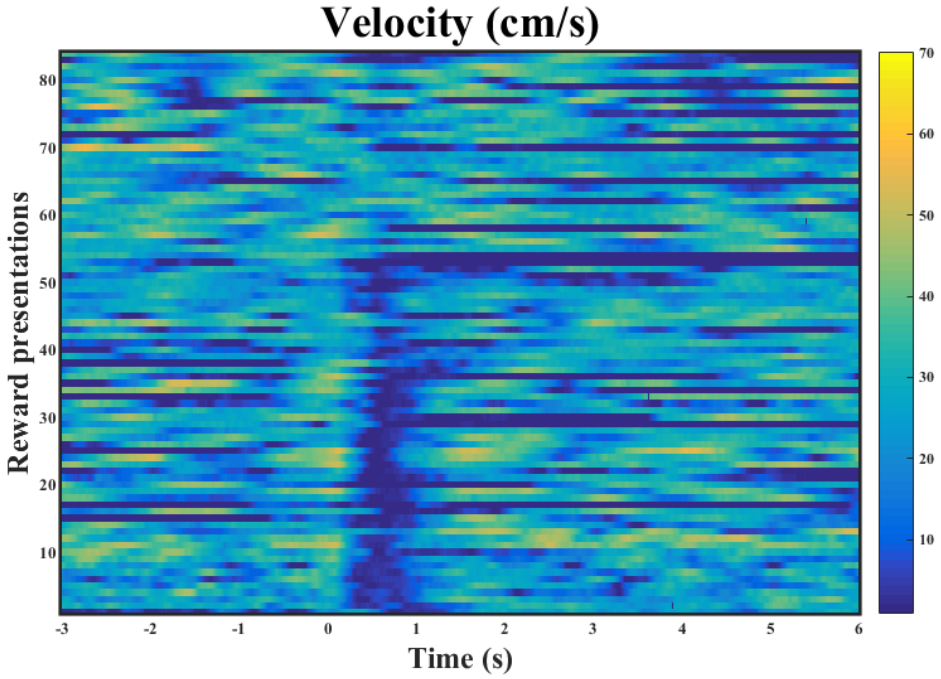

Figure 34: Velocity of mouse #3 aligned in time to individual reward presentations. Rewards are presented at $Time = 0$ (zero).

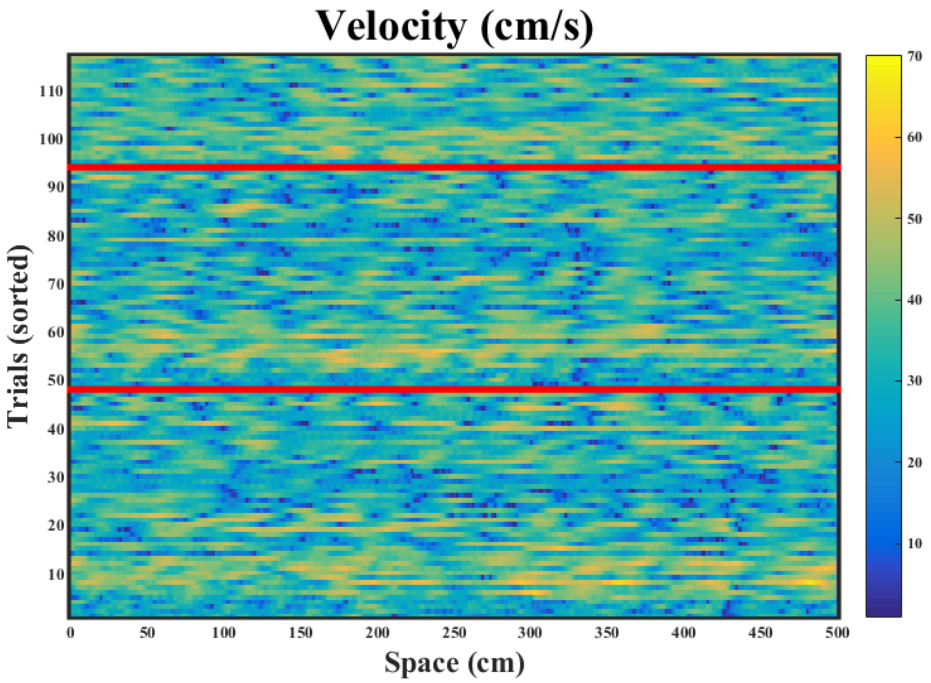

Figure 35: Velocity profile of mouse #3 on the length of the VR corridor.

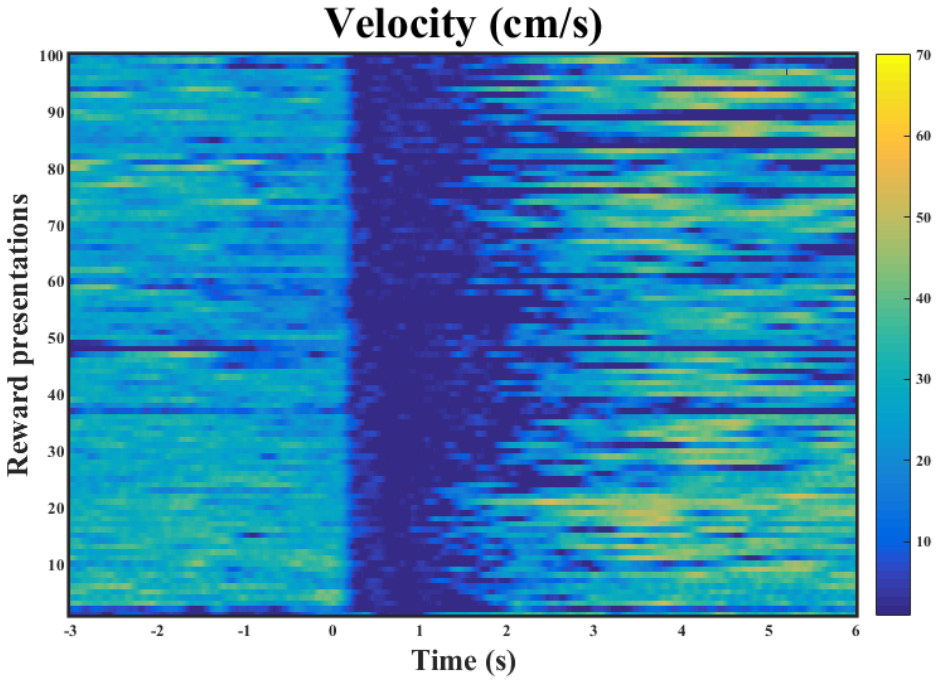

Figure 36: Velocity of mouse #4 aligned in time to individual reward presentations. Rewards are presented at $Time = 0$ (zero).

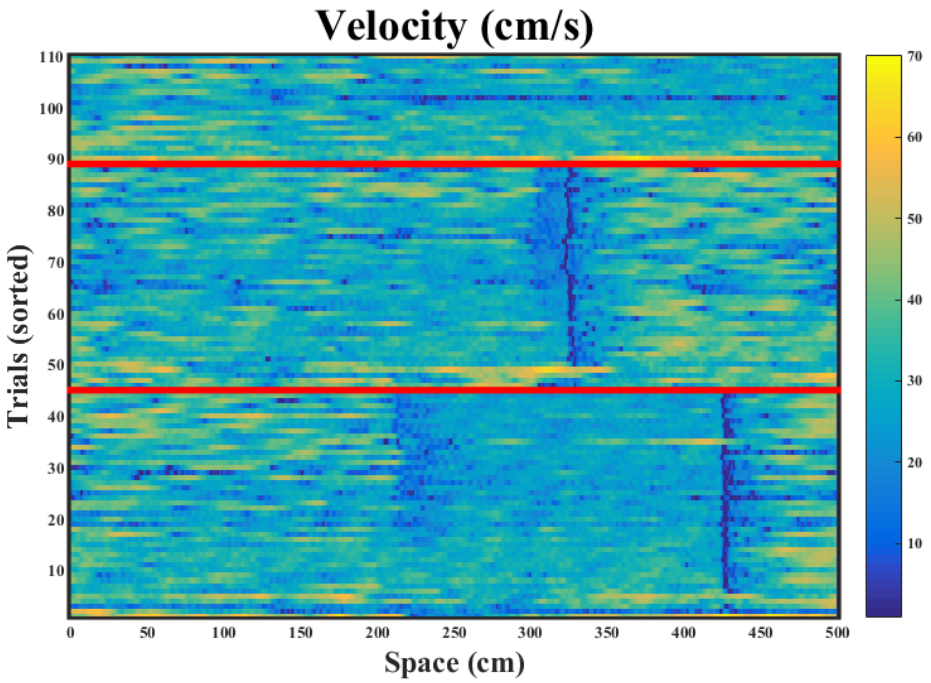

Figure 37: Velocity profile of mouse #4 on the length of the VR corridor.

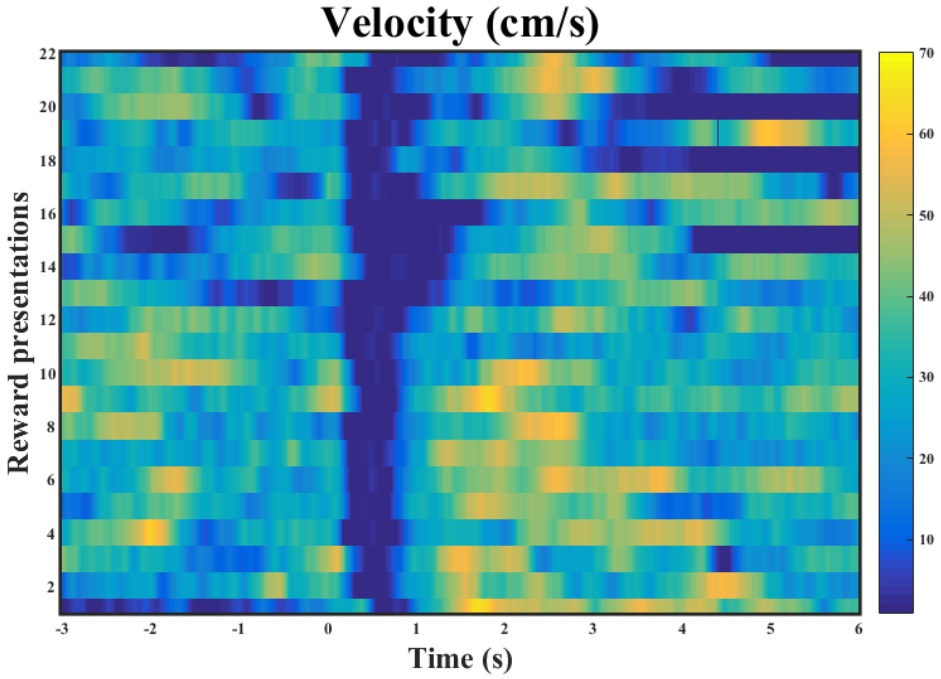

Figure 38: Velocity of mouse #5 aligned in time to individual reward presentations. Rewards are presented at $Time = 0$ (zero).

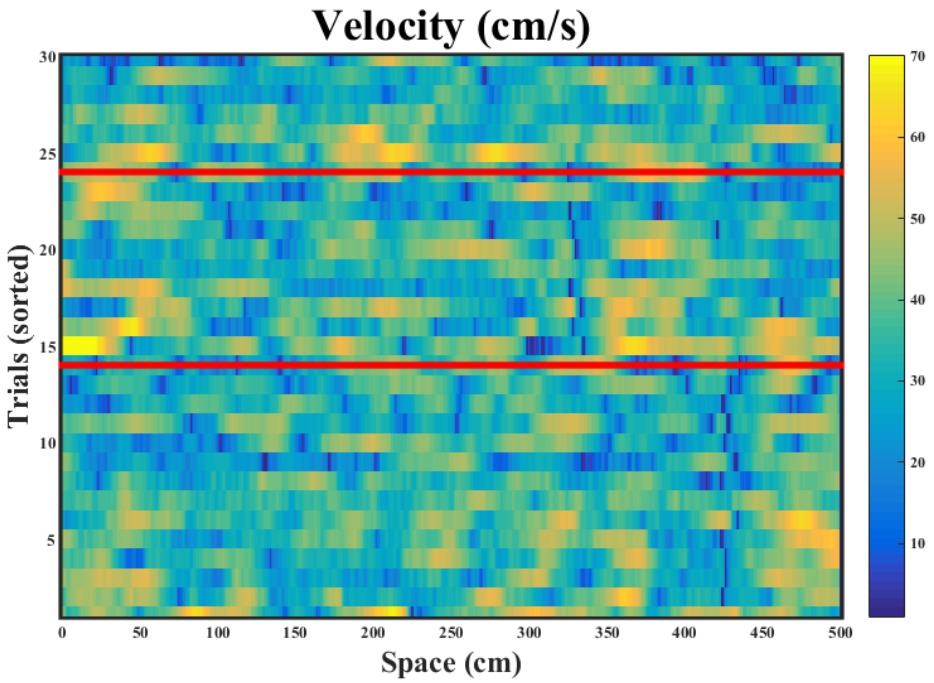

Figure 39: Velocity profile of mouse #5 on the length of the VR corridor.

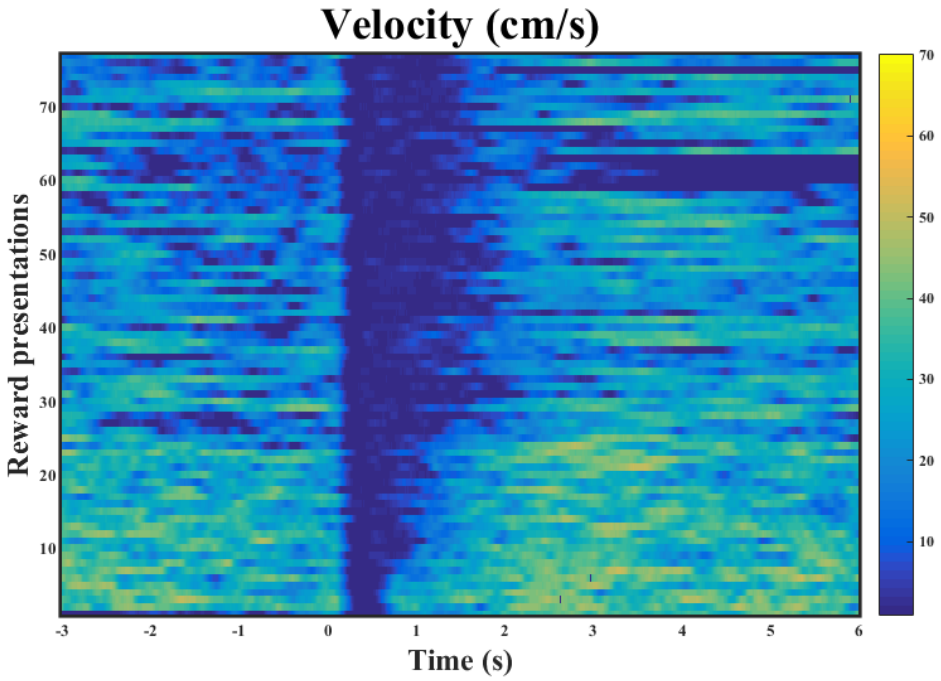

Figure 40: Velocity of mouse #6 aligned in time to individual reward presentations. Rewards are presented at $Time = 0$ (zero).

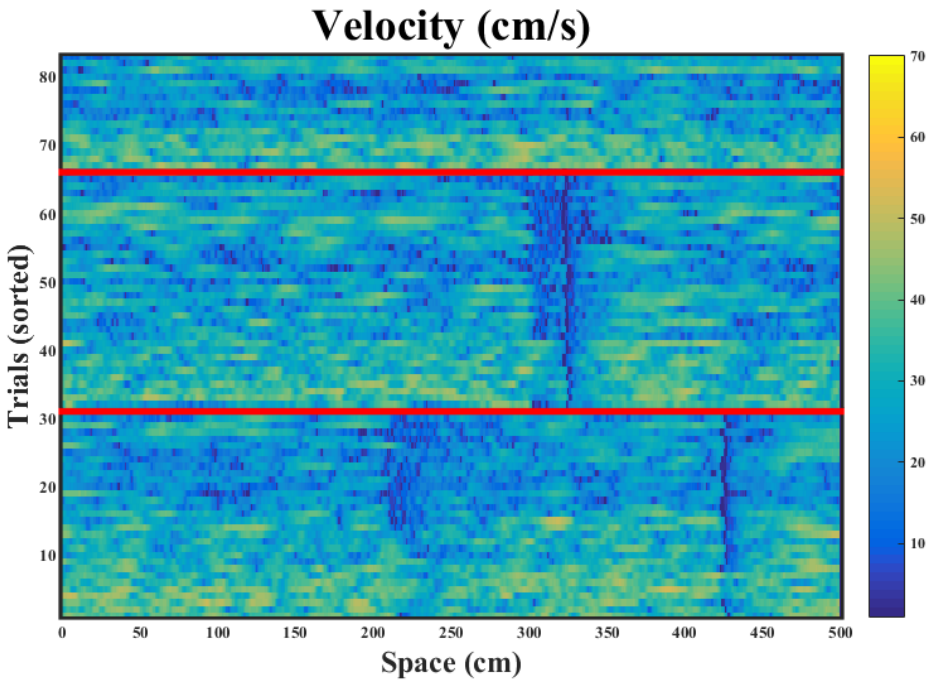

Figure 41: Velocity profile of mouse #6 on the length of the VR corridor.

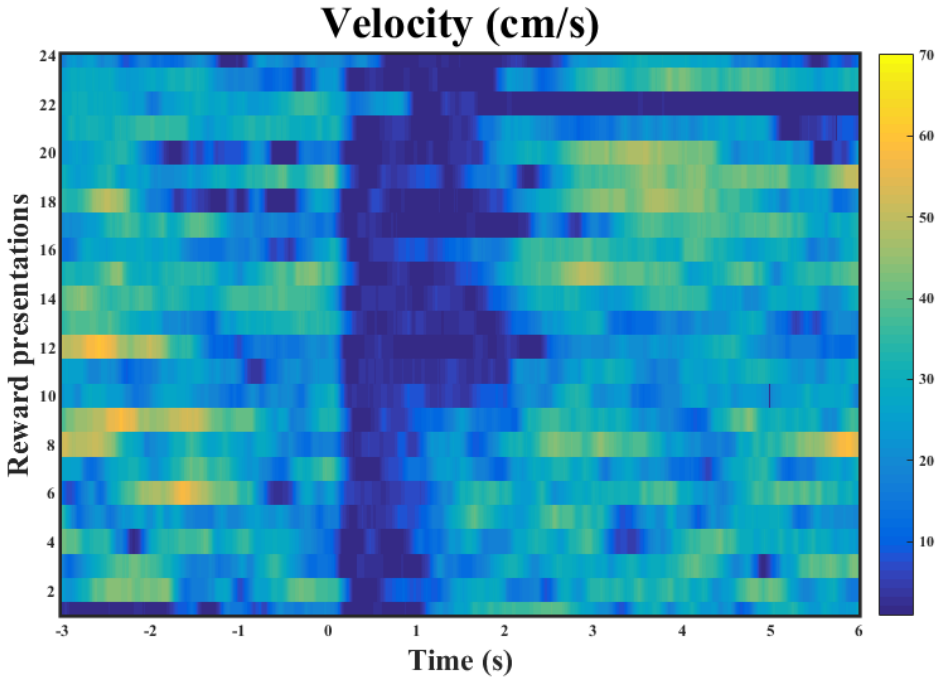

Figure 42: Velocity of mouse #7 aligned in time to individual reward presentations. Rewards are presented at $Time = 0$ (zero).

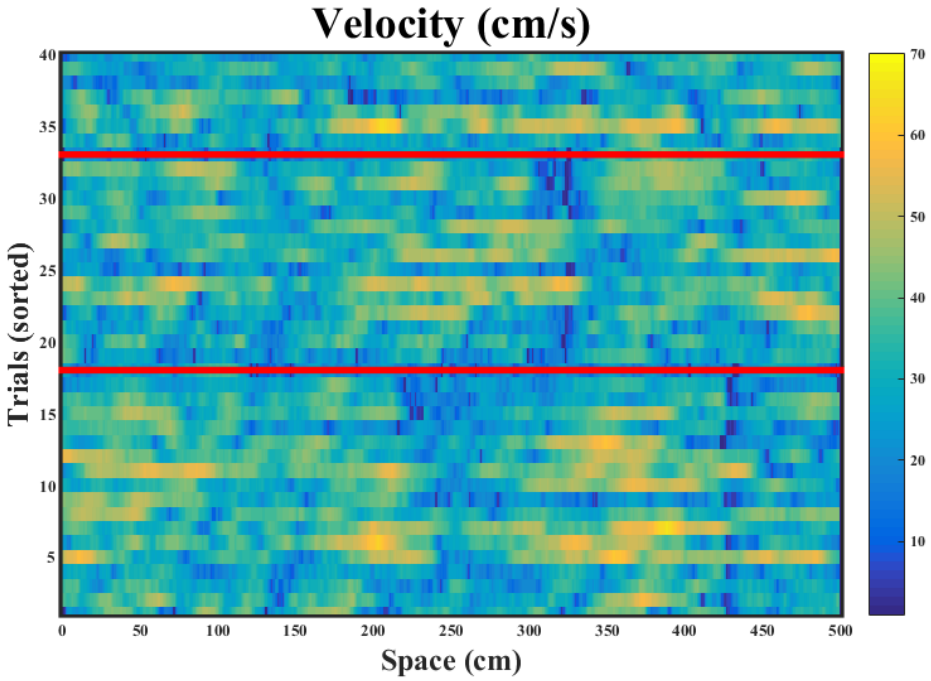

Figure 43: Velocity profile of mouse #7 on the length of the VR corridor.